NASA-CR-198041

A Progress Report

July 1, 1994 to December 31, 1994

NASA-UVA LIGHT AEROSPACE ALLOY AND STRUCTURES TECHNOLOGY PROGRAM (LA²ST)

NASA-LaRC Grant NAG-1-745

Submitted to:

National Aeronautics and Space Administration
Langley Research Center
Hampton, Virginia 23681-0001

Attention:

Mr. Neil Price
Grants Officer
MS 126

For Review by:

Mr. Dennis L. Dicus
Grant Monitor
Metallic Materials Branch, MS 188A

Submitted by:

Edgar A. Starke, Jr.
University Professor

and

Richard P. Gangloff
Professor

Department of Materials Science and Engineering
School of Engineering and Applied Science
University of Virginia

Report No. UVA/528266/MS94/117
March 1995

SCHOOL OF
ENGINEERING
& APPLIED SCIENCE

University of Virginia
Thornton Hall
Charlottesville, VA 22903

UNIVERSITY OF VIRGINIA
School of Engineering and Applied Science

The University of Virginia's School of Engineering and Applied Science has an undergraduate enrollment of approximately 1,500 students with a graduate enrollment of approximately 600. There are 160 faculty members, a majority of whom conduct research in addition to teaching.

Research is a vital part of the educational program and interests parallel academic specialties. These range from the classical engineering disciplines of Chemical, Civil, Electrical, and Mechanical and Aerospace to newer, more specialized fields of Applied Mechanics, Biomedical Engineering, Systems Engineering, Materials Science, Nuclear Engineering and Engineering Physics, Applied Mathematics and Computer Science. Within these disciplines there are well equipped laboratories for conducting highly specialized research. All departments offer the doctorate; Biomedical and Materials Science grant only graduate degrees. In addition, courses in the humanities are offered within the School.

The University of Virginia (which includes approximately 2,000 faculty and a total of full-time student enrollment of about 17,000), also offers professional degrees under the schools of Architecture, Law, Medicine, Nursing, Commerce, Business Administration, and Education. In addition, the College of Arts and Sciences houses departments of Mathematics, Physics, Chemistry and others relevant to the engineering research program. The School of Engineering and Applied Science is an integral part of this University community which provides opportunities for interdisciplinary work in pursuit of the basic goals of education, research, and public service.

NASA-UVA LIGHT AEROSPACE ALLOY AND STRUCTURES TECHNOLOGY PROGRAM

LA^{2}ST

Program Directors:

Edgar A. Starke, Jr.
Richard P. Gangloff

Co-principal Investigators:

Carl T. Herakovich
John R. Scully
Gary J. Shiflet
Glenn E. Stoner
John A. Wert

NASA-LaRC Grant Monitor:

Dennis L. Dicus

Report No. UVA/528266/MSE94/117
March 1995

Copy No. ____

TABLE OF CONTENTS

TABLE OF CONTENTS (continued)

NASA-UVa LIGHT AEROSPACE ALLOY AND
STRUCTURES TECHNOLOGY PROGRAM

(LA²ST)

EXECUTIVE SUMMARY

The NASA-UVa Light Aerospace Alloy and Structures Technology (LA2ST) Program was initiated in 1986 and continues with a high level of activity. Projects are being conducted by graduate students and faculty advisors in the Department of Materials Science and Engineering, as well as in the Department of Civil Engineering and Applied Mechanics, at the University of Virginia. This work is funded by the NASA-Langley Research Center under Grant NAG-1-745. Here, we report on progress achieved between July 1 and December 31, 1994.

The objective of the LA2ST Program is to conduct interdisciplinary graduate student research on the performance of next generation, light-weight aerospace alloys, composites and thermal gradient structures in collaboration with NASA-Langley researchers. Specific technical objectives are presented for each research project. We generally aim to produce relevant data and basic understanding of material mechanical response, environmental/corrosion behavior, and microstructure; new monolithic and composite alloys; advanced processing methods; new solid and fluid mechanics analyses; measurement and modeling advances; and a pool of educated graduate students for aerospace technologies.

The accomplishments presented in this report are summarized as follows.

- oo Three research areas are being actively investigated, including: (1) Mechanical and Environmental Degradation Mechanisms in Advanced Light Metals and Composites, (2)

Aerospace Materials Science, and (3) Mechanics of Materials and Composites for Light Aerospace Structures.

- Twelve research projects are being conducted by 8 PhD and 5 MS level graduate students, with 7 faculty members from 2 departments in the School of Engineering and Applied Science at UVa. Each project is planned and executed in conjunction with a specific branch and technical monitor at NASA-LaRC.

- Two undergraduates are conducting research in the Metallic Materials Branch at NASA-LaRC during the Summer of 1994. No undergraduates are currently participating in LA2ST research at UVa.

- Collective accomplishments between July and December of 1994 include: 16 journal or proceedings publications, 2 NASA progress reports, 10 presentations at national technical meetings, and 1 MS thesis. One student graduated during this reporting period with the Masters of Science Degree in Materials Science and Engineering at UVa. The LA^{2}ST totals since 1986 are 96 publications (53 archival journal or book publications), 18 PhD dissertations or MS theses, 100 external technical presentations, 16 NASA progress reports, and 4 NASA Contractor Reports. Since 1986, 32 graduate students, including 30 citizens of the United States, have been involved with LA2ST research; 18 have received the MS or PhD degree. Four post-doctoral research associates have participated in LA2ST research. A total of 12 different faculty have worked on the LA2ST program.

- ***Research on mechanisms of localized corrosion and environmental fracture in Al-Cu-Li-Mg-Ag alloy X2095 and compositional variations*** experimental technique which allows the propagation and monitoring of environmental cracks in Al-Cu-Li alloys under conditions of constant immersion, monotonic loading and controlled mechanical and electrochemical stresses. This technique has been used to assess crack growth rates in several tempers of AA alloys 2090 and 2095. Under the studied experimental conditions, plateau cracking velocities in these materials have been observed to decrease by a factor of 1000 as temper progresses from severely under-aged to peak-aged. (Project 4)

- ***Research on hydrogen interactions with Al-Li alloys and hydrogen embrittlement of AA2090*** determined that absorbed hydrogen affects the fracture toughness of AA2090 in several ways. Hydrogen promotes additional slip localization in underaged tempers (T3 and UA) and this lowers fracture toughness when fracture initiation is transgranular. Hydrogen trapping occurs at high angle boundaries and T type particles and this lowers fracture toughness when fracture initiation can proceed intergranularly such as when fine grains are favorably oriented in the stress field. Hydrogen uptake and partitioning to dislocations occurs preferentially within the plastic zone of AA2090 fracture toughness specimens. (Project 5)

- ***Research on the deformation and fracture of high strength titanium alloys demonstrated*** that the plane strain fracture toughness of peak-aged Beta 21S plate is not degraded by elevated temperature (150°C) and slow loading. An alloy relevant to the High Speed

Civil Transport (Low Cost Beta sheet) has been offered by TIMET. Experiments will characterize the interactive effects of temperature, slow loading rate and predissolved hydrogen concentration on the fracture toughness of this alloy processed to a high strength level. Specimens will be hydrogen charged prior to deformation by an electrochemical procedure using cathodic polarization in an acid electrolyte for 7 days at 90°C. (Project 6a)

- ***Research on the cryogenic fracture of Al-Cu-Li-In alloys*** focused on the toughness and fracture behavior of 2090-T81 plate at intermediate temperatures between 25°C and -185°C. Delamination fracture had the greatest influence on toughness at -185°C. The Electron Backscattered Pattern (EBSP) technique was employed to investigate microtexture in the region of delamination fracture. (Project 2)

- ***Research on the fracture toughness of several Weldalite™ alloys*** demonstrates that elastic modulus, yield strength and work hardening increase with decreasing temperature between +135°C and -185°C for AA2095 and AA2195, but intrinsic ductility decreases to a plateau for AA2195. The ductility of AA2095 increases with both decreasing and increasing temperatures from ambient. These data are sufficient to model the temperature (in)-dependence of the plane strain initiation fracture toughness of AA2095 and AA2195. Chemical analyses of three alloy variants of Al-Li-Cu-Ag suggest copper segregation, as indicated by the consistently low Cu content at the mid-plane location for each plate. (Project 3)

- ***Research on the elevated temperature fracture toughness of advanced aluminum alloys*** demonstrates that the intrinsic fracture resistance ($\bar{\varepsilon}_f^*$) of ingot metallurgy 2519-T87 (+Mg+Ag) increases with temperature because increasing strain rate hardening and declining dislocation damage accumulation at dispersoids are sufficient to retard plastic instability and coalescence between growing microvoids. In contrast $\bar{\varepsilon}_f^*$ for ultra fine grain-size cryogenically milled aluminum is degraded by elevated temperature-reduced work and strain rate hardening which promotes plastic instability between growing microvoids. Fracture toughness experiments with a spray formed Al-Cu-Mg-Zr alloy (N203) are beginning. Micromechanical modeling continues to yield accurate predictions of the temperature dependence of fracture toughness for several aluminum alloys. (Project 1)

- ***Research on the precipitation hardening and microstructural stability of Al-Si-Ge-Cu alloys*** determined the SiGe precipitate volume fraction in Al-0.55Si-2.02Ge (wt.%) as a function of aging time using TEM and electrical conductivity measurements. This result, as well as lattice parameter measurements led to a significant improvement of the theoretical yield strength prediction for this ternary alloy as a function of aging time. (Project 8)

- ***Research to evaluate wide-panel aluminum alloy extrusions*** demonstrated experimentally yield strength anisotropy due to grain morphology for 2090 near net shape extrusions. Models have been constructed which

predict the expected anisotropy resulting from varying textures, precipitate characteristics and grain shapes. (Project 7)

oo ***Research to incorporate environmental effects into fracture mechanics fatigue life prediction codes such as NASA FLAGRO*** is progressing in two directions.

++Significant environmental fatigue cracking in the 7075-T6 (S-L)/NaCl system is described by linear superposition modeling for slow loading frequencies (< about 0.001 Hz), coupled with analysis of the time-cycle-dependence of da/dN vs K based on the critical growth rate concept. Da/dN_{CRIT} depends on the square root of a critical frequency through a proportionality constant, γ_{CRIT}, supporting hydrogen embrittlement-governed cracking. The diffusivity of hydrogen in aluminum, the critical concentration of hydrogen in the crack tip process zone, and the hydrogen level at the crack tip surface are incorporated into γ_{CRIT}, but are not independently known, hindering predictions. This research was completed and Mr. Mason successfully defended his MS thesis. (Project 10a)

++ A Fortran computer program that employs three methods to estimate environmental effects on time-cycle-dependent fatigue crack propagation kinetics was enhanced with a memory-intensive compiler and by the inclusion of a multiple power-law fitting routine to characterize the complex dependence of da/dN on ΔK. Corrosion fatigue experiments with Ti-6Al-4V (ELI) in aqueous NaCl are providing data to exercise the empirical crack growth rate models and to estimate

environmental effects on crack closure. This alloy exhibits an unexpectedly high threshold stress intensity for static load environmental cracking; linear superposition will not describe environmental fatigue crack propagation rates. (Project 10b)

- ***Research on damage evolution in polymeric composites shows that*** IM7/K3B graphite/polyimide is a very damage tolerant material with a $[\pm 45]_s$ laminate exhibiting strains as high as 18% prior to tensile failure. The large strains are accompanied by extensive fiber rotations (~20°), room temperature creep at high stress levels and extensive fiber/matrix interfacial damage. Acoustic emissions associated with the damage do not follow the well-known Kaiser effect. Modelling the damage evolution using the Ladeveze damage model is progressing well. (Project 9)

INTRODUCTION

Background

In 1986 the Metallic Materials Branch in the Materials Division of the NASA-Langley Research Center initiated sponsorship of graduate student engineering and scientific research in the Department of Materials Science and Engineering at the University of Virginia[1]. This work emphasized the mechanical and corrosion behavior of light aerospace alloys, particularly Al-Li- Cu based compositions, in aggressive aerospace environments[2-4].

In the Fall of 1988, the scope of this program increased to incorporate research on the development and processing of advanced aerospace materials[5]. Additional funding was provided by the Metallic Materials and Mechanics of Materials Branches at NASA-LaRC. In early 1989 the program was further enhanced to include interdisciplinary work on solid mechanics and thermal structures, with funding from several Divisions within the Structures Directorate at NASA-LaRC[6]. The Departments of Civil Engineering (Applied Mechanics Program) and of Mechanical and Aerospace Engineering participated in this expanded program. With this growth, the NASA-UVa **L**ight **A**erospace **A**lloy and **S**tructures **T**echnology **P**rogram (or LA2ST Program) was formed within the School of Engineering and Applied Science at UVa.

Since 1989, the LA2ST program has operated with full participation from 6 to 12 faculty and 10 to 15 graduate students, yearly, as outlined in the last ten progress reports[7-17] and five grant renewal proposals[18-23]. Five 2-day Grant Review Meetings have been held in July at the Langley Research Center, with over 25 faculty and graduate students from UVa participating at each meeting[9,11,13,15,17]. Since 1990, undergraduate engineering students have been involved in research projects at both NASA-LaRC and UVa.

In October of 1991, E.A. Starke proposed a substantial enhancement to the base LA2ST Program[24,25]. The objective of this supplement was to involve UVa faculty with engineering scientists from aluminum alloy producers and airframe manufacturers in a

broad research program to develop aluminum alloys and composites for elevated temperature High Speed Civil Transport applications. This research began in January of 1992 and the results are separately reported. The LA²ST and HSCT activities were merged in 1995[23].

Problem and Needs

Future aerospace structures require high performance light alloys and metal matrix composites with associated processing and fabrication techniques; new structural design methods and concepts with experimental evaluations; component reliability/ durability/damage tolerance prediction procedures; and a pool of masters and doctoral level engineers and scientists. Work on advanced materials and structures must be interdisciplinary and integrated. The thermal and chemical effects of aerospace environments on light metals and composites are particularly important to material performance. Nationally, academic efforts in these areas are limited. The NASA-UVa LA²ST Program addresses these needs.

LA²ST Program

As detailed in the original proposal[6] and affirmed in the most recent renewal[23], faculty from the Departments of Materials Science and Engineering, Mechanical and Aerospace Engineering, and Civil Engineering and Applied Mechanics at UVa are participating in the LA²ST research and education program focused on high performance, light weight, aerospace alloys and structures. We aim to develop long term and interdisciplinary collaborations between graduate students, UVa faculty, and NASA-Langley researchers.

Our research efforts are producing basic understanding of materials performance, new monolithic and composite alloys, advanced processing methods, solid and fluid mechanics analyses, and measurement advances. A major product of the LA²ST program is graduate students with interdisciplinary education and research experience in materials science, mechanics and mathematics. These

advances should enable various NASA technologies.

The scope of the LA²ST Program is broad. Four research areas are being investigated, including:

- oo Mechanical and Environmental Degradation Mechanisms in Advanced Light Metals and Composites,
- oo Aerospace Materials Science,
- oo Mechanics of Materials and Composites for Light Aerospace Structures,
- oo Thermal Gradient Structures.

Twelve research projects are currently ongoing within three of these four areas, and are reported here. These projects involve seven faculty, and thirteen graduate students. Over 60% of the graduate students are currently at the doctoral level (8 of 13), all but one are citizens of the United States, two are cosponsored by private industry, and two are conducting all research at the Langley Research Center. In each case the research provides the basis for the thesis or dissertation requirement of graduate studies at the University of Virginia. Each project is developed in conjunction with a specific LaRC researcher. Research is conducted at either UVa or LaRC, and under the guidance of UVa faculty and NASA staff. Participating students and faculty are closely identified with a NASA-LaRC branch.

Organization of Progress Report

This progress report first provides LA²ST Program administrative information including statistics on the productivity of faculty and graduate student participants, a history of current and graduated students, refereed or archival publications, and a list of ongoing projects with NASA and UVa advisors.

Ten sections summarize the technical accomplishments of each research project, emphasizing the period from July 1 to December 31, 1994. Each section contains a brief narrative of objective, recent progress, conclusions and immediate milestones. Appendices I through III document grant-sponsored publications, conference participation and citations of all LA²ST Progress Reports produced since 1986.

References

1. R.P. Gangloff, G.E. Stoner and M.R. Louthan, Jr., "Environment Assisted Degradation Mechanisms in Al-Li Alloys", University of Virginia, Proposal No. MS-NASA/LaRC-3545-87, October, 1986.

2. R.P. Gangloff, G.E. Stoner and R.E. Swanson, "Environment Assisted Degradation Mechanisms in Al-Li Alloys", University of Virginia, Report No. UVA/528266/MS88/101, January, 1988.

3. R.P. Gangloff, G.E. Stoner and R.E. Swanson, "Environment Assisted Degradation Mechanisms in Advanced Light Metals", University of Virginia, Report No. UVA/528266/MS88/102, June, 1988.

4. R.P. Gangloff, G.E. Stoner and R.E. Swanson, "Environment Assisted Degradation Mechanisms in Advanced Light Metals", University of Virginia, Report No. UVA/528266/MS89/103, January, 1989.

5. T.H. Courtney, R.P. Gangloff, G.E. Stoner and H.G.F. Wilsdorf, "The NASA-UVa Light Alloy Technology Program", University of Virginia, Proposal No. MS NASA/LaRC-3937-88, March, 1988.

6. R.P. Gangloff, "NASA-UVa Light Aerospace Alloy and Structures Technology Program", University of Virginia, Proposal No. MS NASA/LaRC-4278-89, January, 1989.

7. R.P. Gangloff, "NASA-UVa Light Aerospace Alloy and Structures Technology Program", University of Virginia, Report No. UVA/528266/MS90/104, August, 1989.

8. R.P. Gangloff, "NASA-UVa Light Aerospace Alloy and Structures Technology Program", University of Virginia, Report No. UVA/528266/MS90/105, December, 1989.

9. R.P. Gangloff, "NASA-UVa Light Aerospace Alloy and Structures Technology Program", UVa Report No. UVA/528266/MS90/106, June, 1990.

10. R.P. Gangloff, "NASA-UVa Light Aerospace Alloy and Structures Technology Program", UVa Report No. UVA/528266/MS91/107, January, 1991.

11. R.P. Gangloff, "NASA-UVa Light Aerospace Alloy and Structures Technology Program", UVa Report No. UVA/528266/MS91/108, July, 1991.

12. R.P. Gangloff, "NASA-UVa Light Aerospace Alloy and Structures Technology Program", UVa Report No. UVA/528266/MS92/109, January, 1992.

13. R.P. Gangloff, "NASA-UVa Light Aerospace Alloy and Structures Technology Program", UVa Report No. UVA/528266/MS93/111, July, 1992.

14. R.P. Gangloff, "NASA-UVa Light Aerospace Alloy and Structures Technology Program", UVa Report No. UVA/528266/MSE93/112, March, 1993.

15. R.P. Gangloff, "NASA-UVa Light Aerospace Alloy and Structures Technology Program", UVa Report No. UVA/528266/MSE93/113, July, 1993.

16. R.P. Gangloff, "NASA-UVa Light Aerospace Alloy and Structures Technology Program", UVa Report No. UVA/528266/MSE93/114, March, 1994.

17. R. P. Gangloff, "NASA-UVa Light Aerospace Alloy and Structures Technology Program," UVA Report No. UVA/528266/MSE94/116, July 1994.

18. R.P. Gangloff, "NASA-UVa Light Aerospace Alloy and Structures Technology Program", University of Virginia, Proposal No. MS-NASA/LaRC-4512-90, November, 1989.

19. R.P. Gangloff, "NASA-UVa Light Aerospace Alloy and Structures Technology Program", University of Virginia, Proposal No. MS-NASA/LaRC-4841-91, September, 1990.

20. R.P. Gangloff, "NASA-UVa Light Aerospace Alloy and Structures Technology Program", University of Virginia, Proposal No. MS-NASA/LaRC-5219-92, October, 1991.

21. R.P. Gangloff, "NASA-UVa Light Aerospace Alloy and Structures Technology Program", University of Virginia, Proposal No. MSE- NASA/LaRC-5691-93, November, 1992.

22. R.P. Gangloff, "NASA-UVa Light Aerospace Alloy and Structures Technology Program", Proposal No. MSE-NASA/LaRC-6074-94, University of Virginia, Charlottesville, VA, November, 1993.

23. R. P. Gangloff and E. A. Starke, Jr., "NASA-UVa Light Aerospace Alloy and Structures Technology Program," Proposal No. MSE-NASA/LaRC-6478-95, University of Virginia, Charlottesville, VA, November 1994.

24. R.P. Gangloff, E.A. Starke, Jr., J.M. Howe and F.E. Wawner, "NASA-UVa Light Aerospace Alloy and Structures Technology Program: Supplement on Aluminum Based Materials for High Speed Aircraft", University of Virginia, Proposal No. MS NASA/LaRC-5215-92, October, 1991.

25. R.P. Gangloff, E.A. Starke, Jr., J.M. Howe and F.E. Wawner, "NASA-UVa Light Aerospace Alloy and Structures Technology Program: Supplement on Aluminum Based Materials for High Speed Aircraft", University of Virginia, Proposal No. MSE NASA/LaRC-5691-93, November, 1992.

SUMMARY STATISTICS

Table I documents the numbers of students and faculty who have participated in the LA²ST Program, both during this reporting period and since the program inception in 1986. Academic and research accomplishments are indicated by the degrees awarded, publications and presentations. Graduate students and research associates who participated in the LA²ST Program are named in Tables II and III, respectively.

TABLE I: LA²ST Program Statistics

	Current 7/1/94 to 12/31/94	Cumulative 1986 to 12/31/94
PhD Students--UVa:	7	20
--NASA-LaRC:	1	1
MS Students--UVa:	4	10
--NASA:	1	1
--VPI:	0	1
Undergraduates--UVa:	0	9
--NASA-LaRC:	2	13
Faculty--UVa:	6	11
--VPI:	0	1
Research Associates--UVa:	0	4
PhD Awarded:	2	12
MS Awarded:	1	6

TABLE I: LA²ST Program Statistics (continued)

	Current 1/1/94 to 6/30/94	Cumulative 1986 to 6/30/94
Employers--NASA:	0	2
--Federal:	1	4
--University:	0	1
--Industry:	1	6
--Next degree:	1	4
Publications:	16	96
Presentations:	10	100
Dissertations/Theses:	1	18
NASA Reports:	2	20

TABLE II
GRADUATE STUDENT PARTICIPATION IN THE NASA-UVa LA^{2}ST PROGRAM
January, 1995

POS #	GRADUATE STUDENT EMPLOYER	ENTERED PROGRAM	DEGREE COMPLETED	LANGLEY RESIDENCY	RESEARCH TOPIC	UVa/NASA-LaRC ADVISORS
1.	R. S. Piascik NASA-Langley	6/86	Ph.D. 10/89		Damage Localization Mechanisms in Corrosion Fatigue of Aluminum-Lithium Alloys	R. P. Gangloff D. L. Dicus
2.	J. P. Moran NIST	9/88	Ph.D. 12/89		An Investigation of the Localized Corrosion and Stress Corrosion Cracking Behavior of Alloy 2090	G. E. Stoner W. B. Lisagor
3.	R. G. Buchheit Sandia National Laboratories	6/87	Ph.D. 12/90		Measurements and Mechanisms of Localized Aqueous Corrosion in Aluminum-Lithium Alloys	G. E. Stoner D. L. Dicus
4.	D. B. Gundel Ph.D.-UVa	9/88	M.S. 12/90		Investigation of the Reaction Kinetics Between SiC Fibers and Titanium Matrix Composites	F. E. Wawner W. B. Brewer
5.	F. Rivet (VPI)	9/88	M.S. 12/90		Deformation and Fracture of Aluminum-Lithium Alloys: The Effect of Dissolved Hydrogen	R. E. Swanson (VPI) D. L. Dicus
6.	C. Copper Ph.D.-UVa	4/89	M.S. 12/90		Design of Cryogenic Tanks for Space Vehicles	W. D. Pilkey J. K. Haviland D. R. Rummler M.J. Shuart
7.	J. A. Wagner NASA-Langley	6/87	Ph.D.	PhD Research @ LaRC	Temperature Effects on the Deformation and Fracture of Al-Li-Cu-In Alloys	R. P. Gangloff W. B. Lisagor J. C. Newman
8.	W. C. Porr, Jr. David Taylor Naval Ship R&DC	1/88	Ph.D. 6/92		Elevated Temperature Facture of an Advanced Powder Metallurgy Aluminum Alloy	R. P. Gangloff C. E. Harris
9.	J. B. Parse Consultant	9/88	Ph.D. 6/92		Quantitative Characterization of the Spatial Distribution of Particles in Materials	J. A. Wert D. R. Tenney
10.	D. C. Slavik Knolls Atomic Power Laboratory	9/89	Ph.D. 6/93		Environment Enhanced Fatigue of Advanced Aluminum Alloys and Composites	R. P. Gangloff D. L. Dicus

TABLE II (continued)
GRADUATE STUDENT PARTICIPATION IN THE NASA-UVa LA^{2}ST PROGRAM
(continued)

POS #	GRADUATE STUDENT EMPLOYER	ENTERED PROGRAM	DEGREE COMPLETED	LANGLEY RESIDENCY	RESEARCH TOPIC	UVa/NASA-LaRC ADVISORS
11.	C. L. Lach NASA-Langley	9/89	M.S.	MS Research @LaRC	Effect of Temperature on the Fracture Toughness of Weldalite™ 049	R. P. Gangloff W. B. Lisagor
12.	R. J. Kilmer General Motors	11/89	Ph.D. 9/93		Effect of Zn Additions on the Environmental Stability of Alloy 8090	G. E. Stoner W. B. Lisagor
13.	M. F. Coyle	12/89	Ph.D.		Visoplastic Response of High Temperature Structures	E. A. Thornton J. H. Starnes, Jr.
14.	C. J. Lissenden University of Kentucky; Engineering Mechanics	9/90	Ph.D. 6/93		Inelastic Response of Metal Matrix Composites Under Biaxial Loading	C. T. Herakovich M. J. Pindera W. S. Johnson
15.	C. Cooper AMP Incorporated	1/91	Ph.D. 6/93		Shell Structures Analytical Modeling	W. D. Pilkey J. K. Haviland M. Shuart J. Stroud
16.	Douglas Wall	4/91	Ph.D.		Measurements and Mechanisms of Localized Corrosion in Al-Li-Cu Alloys	G. E. Stoner D. L. Dicus
17.	S. W. Smith	4/91	Ph.D.		Hydrogen Interactions with Al-Li Alloys	J. R. Scully W. B. Lisagor
18.	D. B. Gundel Wright Laboratories US Air Force	4/91	Ph.D. 9/94		Effect of Thermal Exposure on the Mechanical Properties of Titanium/SiC Composites	F. E. Wawner W. B. Brewer
19.	K. McCarthy	5/91	M.S. 6/93 (Nonthesis)		Shell Structures Analytical Modeling	W. D. Pilkey M. J. Shuart J. Stroud
20.	M. Lyttle	12/91	M.S. 12/93		Superplasticity in Al-Li-Cu Alloys	J. A. Wert T. T. Bales
21.	T. Johnson NASA-LaRC	12/91	Ph.D. 6/93	(NASA Minority Grantee)	Shell Structures Analytical Modeling	W. D. Pilkey M. J. Shuart J. Stroud

TABLE II (continued)
GRADUATE STUDENT PARTICIPATION IN THE NASA-UVa LA^{2}ST PROGRAM
(continued)

POS #	GRADUATE STUDENT EMPLOYER	ENTERED PROGRAM	DEGREE COMPLETED	LANGLEY RESIDENCY	RESEARCH TOPIC	UVa/NASA-LaRC ADVISORS
22.	S. T. Pride Rohm and Haas	12/91	Ph.D. 6/94	(NASA Minority Grantee)	Metastable Pitting of Al Alloys	J. R. Scully D. L. Dicus
23.	M. A. Rowley	1/92	M.S. 12/93	(UVa AEP Sponsored)	Viscoplasticity of Metals	E. A. Thornton J. H. Starnes, Jr.
24.	M. J. Haynes	9/92	M.S./Ph.D.		Elevated Temperature Fracture of Advanced	R. P. Gangloff TBD
25.	M. Mason Allied Signal	9/92	M.S. 11/94		Environmental Effects in Fatigue Life Prediction	R. P. Gangloff R. S. Piascik
26.	H.J. Koenigsmann	6/93	Ph.D.		Precipitation Hardening and Microstructural Stability in Al-Si-Ge-Cu	E.A. Starke, Jr. W.B. Lisagor
27.	E. Richey	9/93	M.S.		Computer Modeling of Environmental Fatigue Crack Propagation	R.P. Gangloff R.S. Piascik
28.	M. Lyttle	1/94	Ph.D.		Wide-Panel Aluminum Alloy Extrusions	J.A. Wert W.B. Lisagor
29.	Z. Gasem	1/94	Ph.D.		Time-Dependent Environmental Fatigue in 7000-Series Al Alloys	R.P. Gangloff R.S. Piascik
30.	S.P. Hayes	9/94	Ph.D.		Temperature and Hydrogen-Effects on Fracture in Ti Alloys	R.P. Gangloff D.L. Dicus
31.	S.M. Kazanjian	12/94	M.S.		Temperature and Microstructure Effects on Fracture in Ti Alloys	E.A. Starke, Jr. D.L. Dicus
32.	R.D. Schroedter, III	6/93	Ph.D.		Damage Evolution in Polymeric Composites	C.T. Herakovich C.E. Harris

TABLE III
Post-Doctoral Research Associate Participation
in NASA-UVA LaRC-ST Program

Pos #	Research Assoc.	Tenure	Research	Supervisor
1.	Yang Leng	3/89 to 12/91	Elevated Temperature Deformation and Fracture of PM AL Alloys and Composites	R. P. Gangloff
2.	Farshad Mizadeh	7/89 to 12/91	Deformation of Metal Matrix Composites	C. T. Herakovich and Marek-Jerzy Pindera
3.	A.K.Mukhopadhyay	6/91 to 6/92	Aluminum Alloy Development	E. A. Starke, Jr.
4.	Sang-Shik Kim	12/91 to 2/94	Environmental Fatigue Life Prediction	R. P. Gangloff

GRANT PUBLICATIONS: (REFEREED JOURNALS, ARCHIVAL VOLUMES AND NASA CONTRACTOR REPORTS)

The following papers are based on research conducted under LA²ST Program support, and are published in the referred or archival literature.

54. S.T. Pride, J.R. Scully and J.L. Hudson, "Analysis of Electrochemical Noise from Metastable Pitting in Al, Aged Al-2%Cu and AA 2024-T3," in Electrochemical Noise Methods in Corrosion ASTM STP, ASTM, Philadelphia, PA, in review (1994).

53. C. J. Lissenden, B. A. Lerch, and C. T. Herakovich, "Response of SiC/Ti Tubes Under Combined Loading - Part III: Microstructural Evaluation", J. Composite Materials, in review (1994).

52. S.S. Kim, M. J. Haynes and R.P. Gangloff, "Localized Deformation Control of Elevated Temperature Fracture in Submicron Grain Aluminum with Dispersoids", Materials Science and Engineering A, in revision (1994).

51. R.G. Buchheit, G.E. Stoner and G.J. Shiflet, "Corrosion Properties of a Rapidly Solidified Al90Fe5Gd5 Alloy", J. Electrochem. Soc., in revision (1994).

50. R. S. Piascik and R. P. Gangloff, "Modeling Environment-Enhanced Fatigue Crack Growth in Al-Li-Cu-Zr," in Hydrogen Effects on Material Behavior, N. R. Moody and A. W. Thompson, eds., TMS-AIME, Warrendale, PA, in press (1994).

49. E.A. Thornton and J.D. Kolenski, "Viscoplastic Response of Structures with Intense Local Heating", Journal of Aerospace Engineering, in press (1994).

48. S. W. Smith and J. R. Scully, "Hydrogen Trapping and Its Correlation to the Hydrogen Embrittlement Susceptibility of Al-Li-Cu-Zr Alloys," in TMS Hydrogen Effects on Materials Behavior, N. R. Moody and A. W. Thompson, eds., TMS-AIME, Warrendale, PA, in press (1994).

47. C. J. Lissenden, C. T. Herakovich, and M-J. Pindera, "Response of SiC/Ti Tubes Under Combined Loading - Part II: Room Temperature Creep Effects", J. Composite Materials, in press (1994).

46. C. J. Lissenden, C. T. Herakovich, and M-J. Pindera, "Response of SiC/Ti Tubes Under Combined Loading - Part I: Theory and Experiment for Imperfect Bonding", J. Composite Materials, in press (1994).

45. J. R. Scully, "Electrochemical Tests," in Manual on Corrosion Tests: Application and Interpretation, R. Baboian, ed., ASTM, Philadelphia, PA, in press (1994).

44. C. J. Lissenden, C. T. Herakovich, and M-J. Pindera, "Inelastic Deformation of TMC Under Multiaxial Loading" in Life Prediction Methodology for Titanium Matrix Composites, ASTM STP, W.S. Johnson, ed., ASTM, Philadelphia, PA, in press (1994).

43. R.P. Gangloff, "Corrosion Fatigue Cracking", in Manual on Corrosion Tests: Application and Interpretation, R. Baboian, ed., ASTM, Philadelphia, PA, in press (1994).

42. E.A. Thornton, M.F. Coyle, and R.N. McLeod, "Experimental Study of Plate Buckling Induced by Spatial Temperature Gradients," Journal of Thermal Stresses, in press (1994).

41. M.E. Mason and R. P. Gangloff, "Modeling Time-Dependent Corrosion Fatigue Crack Propagation in 7000 Series Aluminum Alloys," in FAA/NASA International Symposium on Advanced Structural Integrity Methods for Airframe Durability and Damage Tolerance, C. E. Harris, ed., NASA Conference Publication 3274, Part 1, NASA-Langley Research Center, Hampton, VA, pp. 441-462 (1994).

40. J. M. Duva, J. Aboudi, and C. T. Herakovich, "A Probabilistic Micromechanics Model for Damaged Composites", Damage Mechanics in Composites, D. H. Allen and J. W. Ju, eds., ASME, AMD-Vol. 185, pp. 1-20 (1994).

39. S.T. Pride, J.R. Scully and J.L. Hudson, "Metastable Pitting of Aluminum and Criteria for the Transition to Stable Pit Growth," Journal of the Electrochemical Society, Vol. 141, No. 11, p. 3028 (1994).

38. C. J. Lissenden, C. T. Herakovich, and M-J. Pindera, "Damage Induced Room Temperature Creep of Titanium Matrix Composites", Durability of Composite Materials, R. C. Wetherhold, ed., ASME MD-Vol. 51, pp. 39-50 (1994).

37. H.J. Koenigsmann and E.A. Starke, Jr.,"Microstructural Stability and Fracture Behavior in Al-Si-Ge Alloys", Proceedings of the 4th International Conference on Aluminum Alloys - Their Physical and Mechanical Properties, T.H. Sanders, Jr. and E.A. Starke, Jr., eds., Atlanta, GA, Vol. II, pp. 24-31 (1994).

36. M.T. Lyttle and J.A. Wert, "Modeling of Continuous Recrystallization in Aluminum Alloys," Journal of Materials Science, Vol. 29, pp. 3342-3350 (1994).

35. Edward Richey, III, A.W. Wilson, J.M. Pope, and R.P. Gangloff, "Computer Modeling the Fatigue Crack Growth Rate Behavior of Metals in Corrosive Environments", NASA CR194982, NASA-Langley Research Center, Hampton, VA (1994).

34. R.G. Buchheit, J.P. Moran and G.E. Stoner, "The Electrochemical Behavior of the T1 (Al2CuLi) Intermetallic Compound and Its Role in Localized Corrosion of Al-3Cu-2Li Alloys", Corrosion, Vol. 50, pp. 120-130 (1994).

33. D. Gundel, P. Taylor and F. Wawner, "The Fabrication of Thin Oxide Coatings on Ceramic Fibers by a Sol-Gel Technique", Journal of Materials Science, Vol. 29, pp. 1795-1800 (1994).

32. M.T. Lyttle and J.A. Wert, "Simulative Modeling of Continuous Recrystallization of Aluminum Alloys", in Advances in Hot Deformation Textures and Microstructures, J.J. Jonas, T.R. Bieler and K.J. Bowman, eds., TMS-AIME, Warrendale, PA, pp. 373-383 (1994).

31. R.P. Gangloff, R.S. Piascik, D.L. Dicus and J.C. Newman, "Fatigue Crack Propagation in Aerospace Aluminum Alloys", Journal of Aircraft, Vol. 31, pp. 720-729 (1994).

30. W.C. Porr, Jr. and R.P. Gangloff, "Elevated Temperature Fracture of RS/PM Alloy 8009: Part I-Fracture Mechanics Behavior", Metall. Trans. A, Vol. 25A, pp. 365-379 (1994).

29. J. R. Scully, T. O. Knight, R. G. Buchheit, and D. E. Peebles, "Electrochemical Characteristics of the Al_2Cu, Al_3Ta and Al_3Zr Intermetallic Phases and Their Relevancy to the Localized Corrosion of Al Alloys," Corrosion Science, Vol. 35, pp. 185-195 (1993).

28. E.A. Thornton, "Thermal Buckling of Plates and Shells," Applied Mechanics Reviews, Vol. 46, No. 10, pp. 485-506 (1993).

27. R.P. Gangloff and Sang Shik Kim, "Environment Enhanced Fatigue Crack Propagation in Metals: Inputs to Fracture Mechanics Life Prediction", NASA CR-191538, NASA-Langley Research Center, Hampton, VA (1993).

26. R.S. Piascik and R.P. Gangloff, "Environmental Fatigue of an Al-Li-Cu Alloy: Part II - Microscopic Hydrogen Cracking Processes", Metall. Trans. A, Vol. 24A, pp. 2751-2762 (1993).

25. D.C. Slavik, J.A. Wert and R.P. Gangloff, "Determining Fracture Facet Crystallography Using Electron Back Scatter Patterns and Quantitative Tilt Fractography", Journal of Materials Research, Vol. 8, pp. 2482-2491 (1993).

24. D.C. Slavik, C.P. Blankenship, Jr., E.A. Starke, Jr. and R.P. Gangloff, "Intrinsic Fatigue Crack Growth Rates for Al-Li-Cu-Mg Alloys in Vacuum", Metall. Trans. A, Vol. 24A, pp. 1807-1817 (1993).

23. D. Gundel and F. Wawner, "The Influence of Defects on the Response of Titanium/SiC Fiber Composites to Thermal Exposure", Composites Engineering, Vol. 4, No. 1, pp. 47-65 (1993).

22. J.B. Parse and J.A. Wert, "A Geometrical Description of Particle Distributions in Materials", Modeling and Simulation in Materials Science and Engineering, Vol. 1, pp. 275-296 (1993).

21. D.C. Slavik and R.P. Gangloff, "Microscopic Processes of Environmental Fatigue Crack Propagation in Al-Li-Cu Alloy 2090", in Fatigue '93, Vol. II, J.-P. Bailon and J.I. Dickson, eds., EMAS, West Midlands, UK, pp. 757-765 (1993).

20. C.J. Lissenden, M-J. Pindera and C.T. Herakovich, "Response of SiC/Ti Tubes Under Biaxial Loading in the Presence of Damage," Damage Mechanics in Composites, D.H. Allen and D.C. Lagoudas, Eds., ASME- AMD-Vol. 150, pp. 73-90 (1992).

19. J.A. Wagner and R.P. Gangloff, "Fracture Toughness of Al-Li-Cu-In Alloys", Scripta Metallurgica et Materialia, Vol. 26, pp. 1779-1784 (1992).

18. R.G. Buchheit, Jr., J.P. Moran, F.D. Wall, and G.E. Stoner, "Rapid Anodic Dissolution Based SCC of 2090 (Al-Li-Cu) by Isolated Pit Solutions," Parkins Symposium on Fundamental Aspects of Stress Corrosion Cracking, S.M. Bruemmer, E.I. Meletis, R.H. Jones, W.W. Gerberich, F.P. Ford and R.W. Staehle, eds., TMS-AIME, Warrendale, PA, p. 141 (1992).

17. J.P. Moran, R.G. Buchheit, Jr., and G.E. Stoner, "Mechanisms of SCC of Alloy 2090 (Al-Li-Cu) - A Comparison of Interpretations from Static and Slow Strain Rate Techniques", Parkins Symposium on Fundamental Aspects of Stress Corrosion Cracking, S.M. Bruemmer, E.I. Meletis, R.H. Jones, W.W. Gerberich, F.P. Ford and R.W. Staehle, eds., TMS-AIME, Warrendale, PA, p. 159 (1992).

16. R.J. Kilmer, T.J. Witters and G.E. Stoner, "Effect of Zn Additions on the Precipitation Events and Implications to Stress Corrosion Cracking Behavior in Al-Li-Cu-Mg-Zn Alloys", Proceedings of the Sixth International Al-Li Conference, M. Peters and P.J. Winkler, eds., DGM Informationsgesellschaft, Verlag, pp. 755-760 (1992).

15. C.T. Herakovich and J.S. Hidde, "Response of Metal Matrix Composites with Imperfect Bonding", Ultramicroscopy, Vol. 40, pp. 215-228 (1992).

14. R.G. Buchheit, Jr., F.D. Wall, G.E. Stoner and J.P. Moran, "Stress Corrosion Cracking of Al-Li-Cu-Zr Alloy 2090 in Aqueous Cl- and Mixed Cl-/CO3-2 Environments", CORROSION/91, Paper No. 99, NACE, Houston, TX (1991).

13. R.P. Gangloff, D.C. Slavik, R.S. Piascik and R.H. Van Stone, "Direct Current Electrical Potential Measurement of the Growth of Small Fatigue Cracks", in Small Crack Test Methods, ASTM STP 1149, J.M. Larsen and J.E. Allison, eds., ASTM, Philadelphia, PA, pp. 116-168 (1992).

12. R.J. Kilmer and G.E. Stoner, "The Effect of Trace Additions of Zn on the Precipitation Behavior of Alloy 8090 During Artificial Aging", Proceedings, Light Weight Alloys for Aerospace Applications II, E.W. Lee, ed., TMS-AIME, Warrendale, PA, pp. 3-15, 1991.

11. W.C. Porr, Jr., Anthony Reynolds, Yang Leng and R.P. Gangloff, "Elevated Temperature Cracking of RSP Aluminum Alloy 8009: Characterization of the Environmental Effect", Scripta Metallurgica et Materialia, Vol. 25, pp. 2627-2632 (1991).

10. J. Aboudi, J.S. Hidde and C.T. Herakovich, "Thermo-mechanical Response Predictions for Metal Matrix Composites", in Mechanics of Composites at Elevated and Cryogenic Temperatures, S.N. Singhal, W.F. Jones and C.T. Herakovich, eds., ASME AMD, Vol. 118, pp. 1-18 (1991).

9. R.S. Piascik and R.P. Gangloff, "Environmental Fatigue of an Al-Li-Cu Alloy: Part I - Intrinsic Crack Propagation Kinetics in Hydrogenous Environments", Metallurgical Transactions A, Vol. 22A, pp. 2415-2428 (1991).

8. W.C. Porr, Jr., Y. Leng, and R.P. Gangloff, "Elevated Temperature Fracture Toughness of P/M Al-Fe-V-Si", in Low Density, High Temperature Powder Metallurgy Alloys, W.E. Frazier, M.J. Koczak, and P.W. Lee, eds., TMS- AIME, Warrendale, PA, pp. 129-155 (1991).

7. Yang Leng, William C. Porr, Jr. and Richard P. Gangloff, "Time Dependent Crack Growth in P/M Al-Fe-V-Si at Elevated Temperatures", Scripta Metallurgica et Materialia, Vol. 25, pp. 895-900 (1991).

6. R.J. Kilmer and G.E. Stoner, "Effect of Zn Additions on Precipitation During Aging of Alloy 8090", Scripta Metallurgica et Materialia, Vol. 25, pp. 243-248 (1991).

5. D.B. Gundel and F.E. Wawner, "Interfacial Reaction Kinetics of Coated SiC Fibers", Scripta Metallurgica et Materialia, Vol. 25, pp. 437-441 (1991).

4. R.G. Buchheit, Jr., J.P. Moran and G.E. Stoner, "Localized Corrosion Behavior of Alloy 2090-The Role of Microstructural Heterogeneity", Corrosion, Vol. 46, pp. 610-617 (1990).

3. Y. Leng, W.C. Porr, Jr. and R.P. Gangloff, "Tensile Deformation of 2618 and Al-Fe-Si-V Aluminum Alloys at Elevated Temperatures", Scripta Metallurgica et Materialia, Vol. 24, pp. 2163-2168 (1990).

2. R.P. Gangloff, "Corrosion Fatigue Crack Propagation in Metals", in Environment Induced Cracking of Metals, R.P. Gangloff and M.B. Ives, eds., NACE, Houston, TX, pp. 55-109 (1990).

1. R.S. Piascik and R.P. Gangloff, "Aqueous Environment Effects on Intrinsic Corrosion Fatigue Crack Propagation in an Al-Li-Cu Alloy", in Environment Induced Cracking of Metals, R.P. Gangloff and M.B. Ives, eds., NACE, Houston, TX, pp. 233-239 (1990).

COMPLETED PROJECTS: (1986 to present reporting period)

1. DAMAGE LOCALIZATION MECHANISMS IN CORROSION FATIGUE OF ALUMINUM-LITHIUM ALLOYS
   Faculty Investigator: R.P. Gangloff
   Graduate Student: Robert S. Piascik
   Degree: PhD
   UVa Department: Materials Science and Engineering (MS&E)
   NASA-LaRC Contact: D. L. Dicus (Metallic Materials)
   Start Date: June, 1986
   Completion Date: November, 1989
   Employment: NASA-Langley Research Center

2. AN INVESTIGATION OF THE LOCALIZED CORROSION AND STRESS CORROSION CRACKING BEHAVIOR OF ALLOY 2090 (Al-Li-Cu)
   Faculty Investigator: Glenn E. Stoner
   Graduate Student: James P. Moran
   Degree: PhD
   UVa Department: MS&E
   NASA-LaRC Contact: W.B. Lisagor (Metallic Materials)
   Start Date: September, 1988
   Completion Date: December, 1989
   Co-Sponsor: ALCOA
   Employment: ALCOA Laboratories

3. MECHANISMS OF LOCALIZED CORROSION IN AL-LI-CU ALLOY 2090
   Faculty Investigator: G.E. Stoner
   Graduate Student: R.G. Buchheit
   Degree: PhD
   UVa Department: MS&E
   NASA-LaRC Contact: D.L. Dicus (Metallic Materials)
   Start Date: June, 1987
   Completion Date: December, 1990
   Cosponsor: Alcoa
   Employment: Sandia National Laboratories

4. DEFORMATION AND FRACTURE OF ALUMINUM-LITHIUM ALLOYS: THE EFFECT OF DISSOLVED HYDROGEN
   Faculty Investigator: R.E. Swanson (VPI)
   Graduate Student: Frederic C. Rivet
   Degree: MS
   VPI Department: Materials Engineering
   NASA-LaRC Contact: D.L. Dicus (Metallic Materials)
   Start Date: September, 1988
   Completion Date: December, 1990
   Employment: Not determined

5. INVESTIGATION OF THE REACTION KINETICS BETWEEN SiC FIBERS AND SELECTIVELY ALLOYED TITANIUM MATRIX COMPOSITES AND DETERMINATION OF THEIR MECHANICAL PROPERTIES

Faculty Investigator: F.E. Wawner
Graduate Student: Douglas B. Gundel
Degree: MS
UVa Department: MS&E
NASA-LaRC Contact: D.L. Dicus and W.B. Brewer (Metallic Materials)
Start Date: January, 1989
Completion Date: December, 1990
Employment: Graduate School, University of Virginia; PhD candidate on LA²ST Program; Department of Materials Science

6. DESIGN OF CRYOGENIC TANKS FOR SPACE VEHICLES

Faculty Investigators: W.D. Pilkey and J.K. Haviland
Graduate Student: Charles Copper
Degree: MS
UVa Department: Mechanical and Aerospace Engineering (MAE)
NASA-LaRC Contact: D.R. Rummler (Structural Mechanics Division), R.C. Davis and M.J. Shuart (Aircraft Structures)
Start Date: April, 1989
Completion Date: December, 1990
Employment: Graduate School, University of Virginia; PhD candidate on NASA-Headquarters sponsored program; Department of Mechanical and Aerospace Engineering

7. ELEVATED TEMPERATURE FRACTURE OF AN ADVANCED RAPIDLY SOLIDIFIED, POWDER METALLURGY ALUMINUM ALLOY

Faculty Investigator: R.P. Gangloff
Graduate Student: William C. Porr, Jr.
Degree: PhD
UVa Department: MS&E
NASA-LaRC Contact: C.E. Harris (Mechanics of Materials)
Start Date: January, 1988
Completion Date: June, 1992
Employment: David Taylor Naval Ship R&D Center

8. QUANTITATIVE CHARACTERIZATION OF THE SPATIAL DISTRIBUTION OF PARTICLES IN MATERIALS: APPLICATION TO MATERIALS PROCESSING

Faculty Investigator: John A. Wert
Graduate Student: Joseph Parse
Degree: PhD
UVa Department: MS&E
NASA-LaRC Contact: D.R. Tenney (Materials Division)
Start Date: September, 1988
Completion Date: June, 1992
Employment: Private Consultant

9. ENVIRONMENTAL FATIGUE CRACK GROWTH AND CRACKING MECHANISMS IN Al-Li-Cu Alloy 2090

Faculty Investigator: R.P. Gangloff
Graduate Student: Donald C. Slavik
Degree: PhD
UVa Department: MS&E
NASA-LaRC Contact: D.L. Dicus (Metallic Materials)
Start Date: September, 1989
Completion Date: June, 1993
Employment: Knolls Atomic Power Laboratory

10. INELASTIC DEFORMATION OF METAL MATRIX COMPOSITES UNDER BIAXIAL LOADING

Faculty Investigators: Carl T. Herakovich and Marek-Jerzy Pindera
Graduate Student: Mr. Clifford J. Lissenden
Degree: PhD
UVa Department: Civil Engineering and the Applied Mechanics Program
NASA-LaRC Contact: W.S. Johnson (Mechanics of Materials)
Start Date: September, 1990
Completion Date: June, 1993
Employment: University of Kentucky, Department of Engineering Mechanics

11. EFFECT OF TEMPERATURE ON THE RESPONSE OF METALLIC SHELL STRUCTURES

Faculty Investigators: W.D. Pilkey and J.K. Haviland
Graduate Student: Karen McCarthy
Degree: MS (non-thesis)
Graduate Student: Theodore Johnson (NASA Minority Grantee)
Degree: PhD
Employment: NASA-LaRC

Graduate Student: Charles Copper
Degree: PhD
Employment: AMP Incorporated
UVa Department: MAE
NASA-LaRC Contact: M.J. Shuart and Jeffrey Stroud (Aircraft Structures)
Start Date: April, 1991
Completion Date: May, 1993

12. EFFECTS OF Zn ADDITIONS ON THE PRECIPITATION AND STRESS CORROSION CRACKING BEHAVIOR OF ALLOY 8090
    Faculty Investigator: Glenn E. Stoner
    Graduate Student: Raymond J. Kilmer
    Degree: PhD
    Department: MS&E
    NASA-LaRC Contact: W.B. Lisagor (Metallic Materials)
    Start Date: September, 1989
    Completion Date: September, 1993
    Cosponsor: Alcoa
    Employment: General Motors

13. PROCESSING AND SUPERPLASTIC PROPERTIES OF WELDALITETM SHEET
    Faculty Investigator: John A. Wert
    Graduate Student: Mark Lyttle
    Degree: MS
    Department: MS&E
    NASA-LaRC Contact: T.T. Bales (Metallic Materials)
    Start Date: September, 1991
    Completion Date: December, 1993
    Employment: Graduate School, University of Virginia; PhD Candidate in Materials Science and Engineering

14. METASTABLE PITTING OF Al ALLOYS AND CRITERIA FOR THE TRANSITION TO STABLE PITTING
    Faculty Investigators: John R. Scully and J.L. Hudson
    Graduate Student: Sheldon T. Pride
    Degree: PhD
    Department: Chemical Engineering
    NASA-LaRC Contact: D.L. Dicus (Metallic Materials)
    Start Date: September, 1991
    Completion Date: May, 1994
    Cosponsor: NASA Graduate Student Researchers Program; Under Represented Minority Emphasis
    Employment: Rohm and Haas Chemical Company

15. THE EFFECT OF THERMAL EXPOSURE ON THE MECHANICAL PROPERTIES OF Ti-1100/SCS-6 COMPOSITES
    Faculty Investigator: F.E. Wawner
    Graduate Student: Douglas B. Gundel
    Degree: PhD
    UVa Department: MS&E
    NASA-LaRC Contact: D.L. Dicus and W.B. Brewer (Metallic Materials)
    Start Date: April, 1991
    Completion Date: June, 1994
    Employment: Wright Laboratories (WL/MLLM), US Air Force Materials Laboratory

16. ENVIRONMENTAL EFFECTS IN FATIGUE LIFE PREDICTION: MODELING ENVIRONMENTAL CRACK PROPAGATION IN LIGHT AEROSPACE ALLOYS

Faculty Investigator: R. P. Gangloff
Graduate Student: Mark E. Mason
Degree: MS
UVa Department: MS&E
NASA-LaRC Contact: R. S. Piascik (Mechanics of Materials)
Start Date: January, 1992
Completion Date: November, 1994
Employment: Allied-Signal; Hopewell, VA

ADMINISTRATIVE PROGRESS

Faculty Participation

Professor Herakovich resumed participation in the 1994 program, with a research project examining damage evolution in a polymeric composite under strain. Professor Thornton transferred his research program on thermal structures modeling from the LA²ST Program to individual sponsorship by a NASA-Langley branch.

Graduate Student Recruitment

The LA²ST Program has encountered no problems in recruiting the best graduate students entering the participating Departments at UVa, and in sufficient numbers to achieve our education and research objectives. Professor Starke recently recruited Ms. Susan Kazanjian into the MS program in Materials Science and Engineering at UVa under LA²ST sponsorship. Ms. Kazanjian was previously employed as a Laboratory Manager at a materials testing company and entered UVa in December of 1994. Her LA²ST research will focus on elevated temperature and microstructure effects on the fracture toughness of α/β titanium alloys.

Undergraduate Research Participation

In April of 1990, the LA²ST Program was increased in scope to include undergraduate engineering students. Four students worked at NASA-LaRC during the Summer of 1990, none were recruited for the 1991 program, and seven were successfully recruited to work at NASA-LaRC during the Summer of 1992. Each student was a rising senior in an engineering or science major closely related to aerospace materials and mechanics. Represented universities have included Harvard, Georgia Institute of Technology, Virginia Polytechnic Institute, Duke, the University of Missouri, California Polytechnical Institute, and North Carolina State University.

Professor Glenn E. Stoner assumed responsibility for the 1993 Summer Undergraduate Program. During the 1994 reporting periods, he recruited two undergraduates in Materials Science and Engineering at Duke and North Carolina State University. These students worked at the Langley Research Center during the summer of 1994.

CURRENT PROJECTS

MECHANICAL AND ENVIRONMENTAL DEGRADATION MECHANISMS IN ADVANCED LIGHT METALS AND COMPOSITES

1. TIME-TEMPERATURE DEPENDENT FRACTURE IN ADVANCED WROUGHT INGOT METALLURGY, AND SPRAY DEPOSITED ALUMINUM ALLOYS
   Faculty Investigator: R.P. Gangloff
   Graduate Student: Michael J. Haynes; PhD (direct) candidate
   UVa Department: MS&E
   NASA-LaRC Contact: A. P. Reynolds (Metallic Materials)
   Start Date: September, 1992
   Completion Date: September, 1996
   Project #1

2. CRYOGENIC TEMPERATURE EFFECTS ON THE DEFORMATION AND FRACTURE OF Al-Li-Cu-In ALLOYS
   Faculty Investigator: R.P. Gangloff
   Graduate Student: John A. Wagner; PhD candidate and NASA- LaRC employee
   UVa Department: MS&E
   NASA-LaRC Contacts: W.B. Lisagor (Metallic Materials) and J.C. Newman (Mechanics of Materials)
   Start Date: June, 1987
   Anticipated Completion Date: December, 1995
   Project #2

3. THE EFFECT OF CRYOGENIC TEMPERATURE ON THE FRACTURE TOUGHNESS OF WELDALITE™ X2095
   Faculty Investigator: R.P. Gangloff
   Graduate Student: Cynthia L. Lach; MS candidate and NASA- LaRC employee
   UVa Department: MS&E
   NASA-LaRC Contacts: W.B. Lisagor (Metallic Materials)
   Start Date: August, 1990
   Anticipated Completion Date: December, 1995
   Project #3

4. MECHANISMS OF LOCALIZED CORROSION IN 2090 AND X2095
   Faculty Investigator: G.E. Stoner
   Graduate Student: Douglas Wall; PhD candidate
   UVa Department: MS&E
   NASA-LaRC Contact: M.S. Domack (Metallic Materials)
   Start Date: April, 1991
   Completion Date: December, 1994
   Cosponsor: Reynolds Metals Company (A. Cho)
   Project #4

5. HYDROGEN INTERACTIONS IN ALUMINUM-LITHIUM 2090 AND SELECTED MODEL ALLOYS

Faculty Investigator: John R. Scully
Graduate Student: Stephen W. Smith; PhD Candidate
UVa Department: MS&E
NASA-LaRC Contact: W.B. Lisagor and D.L. Dicus (Metallic Materials)
Start Date: April, 1991
Anticipated Completion Date: May, 1995
Cosponsor: Virginia CIT
Project #5

6a. MECHANISMS OF DEFORMATION AND FRACTURE IN HIGH STRENGTH TITANIUM ALLOYS: EFFECTS OF TEMPERATURE AND DISSOLVED HYDROGEN

Faculty Investigators: R. P. Gangloff
Graduate Student: Sean P. Hayes; PhD Candidate
UVa Department: MS&E
NASA-LaRC Contact: To be determined (Metallic Materials)
Start Date: September, 1994
Completion Date: September, 1997
Project #6

6b. MECHANISMS OF DEFORMATION AND FRACTURE IN HIGH STRENGTH TITANIUM ALLOYS: EFFECTS OF TEMPERATURE AND MICROSTRUCTURE

Faculty Investigators: E. A. Starke, Jr.
Graduate Student:Susan M. Kazanjian, MS Candidate
UVa Department: MS&E
NASA-LaRC Contact: To be determined (Metallic Materials)
Start Date: December, 1994
Completion Date: To be determined
Project #6

AEROSPACE MATERIALS SCIENCE

7. EVALUATION OF WIDE-PANEL ALUMINUM ALLOY EXTRUSIONS

Faculty Investigator: John A. Wert
Graduate Student: Mark T. Lyttle, Ph.D. Candidate
UVa Department: Materials Science and Engineering
NASA-LaRC Contact: T. T. Bales (Metallic Materials)
Start Date: January, 1994
Completion Date: September, 1996
Project #7

8. Al-Si-Ge-Cu ALLOY DEVELOPMENT
   Faculty Investigator: E.A. Starke, Jr.
   Graduate Student: H.J. Koenigsmann, Ph.D. Candidate
   UVa Department: Materials Science and Engineering
   NASA-LaRC Contact: W.B. Lisagor
   Start Date: September, 1993
   Completion Date: To be determined
   Project #8.

MECHANICS OF MATERIALS FOR LIGHT AEROSPACE STRUCTURES

9. DAMAGE EVOLUTION IN POLYMERIC COMPOSITES
   Faculty Investigator: C. T. Herakovich
   Graduate Student: R. D. Schroedter III, MS Candidate
   UVa Department: Civil Engineering & Applied Mechanics
   NASA-LaRC Contact: C. E. Harris & T. Gates
   Start Date: September 1993
   Completion Date: August 1995
   Project #9

10. ENVIRONMENTAL EFFECTS IN FATIGUE LIFE PREDICTION: MODELING ENVIRONMENTAL CRACK PROPAGATION IN LIGHT AEROSPACE ALLOYS
   Faculty Investigator: R.P. Gangloff
   Graduate Students: Mark E. Mason; MS Candidate
   Zuhair Gasem; PhD Candidate
   Edward Richey III; MS Candidate
   (Mechanical and Aerospace Engineering)
   UVa Department: MS&E
   NASA-LaRC Contact: R.S. Piascik (Mechanics of Materials)
   Start Date: January, 1992
   Anticipated Completion Date: September, 1994 (Mason)
   June, 1995 (Richey)
   December, 1996 (Gasem)
   Project #10

THERMAL GRADIENT STRUCTURES

None

RESEARCH PROGRESS AND PLANS (July 1 to December 31, 1994)

Research progress, recorded during the period from July 1, 1994 to December 31, 1994, is summarized for each project in the following sections. The standard format includes the program objective, recent progress, conclusions, and immediate milestones.

Project #1 **Time-Temperature Dependent Fracture in Advanced Wrought Ingot Metallurgy, and Spray Deposited Aluminum Alloys**

Michael J. Haynes and Richard P. Gangloff

Background and Problem Statement

A significant effort is currently aimed at developing advanced aluminum alloys for elevated temperature aerospace applications, particularly for airframes such as the High Speed Civil Transport[1,2]. Since existing precipitation hardened aluminum alloys (e.g., 2024, 7075/7475 and 2090/8090) may not be sufficient to meet microstructural stability combined with strength/toughness requirements, new compositions of wrought ingot metallurgy (IM), spray deposited, and rapidly solidified powder metallurgy (RS/PM) alloys are under development. As promising compositions are determined, it is necessary to characterize the critical effects of loading rate and temperature on fracture toughness, and to establish metallurgical fracture mechanisms and predictive micromechanical models for such properties.

Objectives

The current objective of this PhD research is to characterize the initiation and growth fracture toughnesses of a spray formed and extruded Al-Cu-Mg-Mn-Zr-Ag alloy as a function of temperature,

and to establish the effect of thermomechanical processing to 3.2 sheet. As a second objective, we aim to expand previously reported work on ingot metallurgy 2519 (+Mg+Ag) by characterizing and modeling an improved composition (C416). We aim to better understand fracture at elevated temperatures by considering the microstructural factors that govern the evolution of microvoid damage, including novel plastic instability fracture mechanisms between growing microvoids, for each of these alloy classes and including ultra- fine grain sized aluminum alloys. A critical strain-critical distance micromechanical model of microvoid-based fracture is being tested and improved based on experimental results for each advanced aluminum alloy class.

Technical Approach

Materials

Research is currently focused on spray formed and extruded Al-Cu-Mg-Mn-Zr-Ag alloy N203 (Al-4.9Cu-0.5Mg-0.5Mn-0.4Ag-0.5Zr-0.2Ti-0.2V by wt%) provided by T. Bayha at Lockheed Aerospace. Additional materials include a cryogenically milled aluminum alloy in the submicron grain size class (CM Al: Al-3.0Al2O3 by vol%, provided by M.J. Luton at Exxon Research and Engineering Company) and two alloy sheets from the advanced ingot metallurgy class ([1] IM 2519-T87 (+Mg+Ag): Al-5.75Cu-0.52Mg-0.49Ag-0.3Mn-0.16Zr- 0.09V by wt%, and [2] Peak Aged IM C416: Al-5.4Cu-0.5Mg-0.5Ag-0.3Mn-0.13Zr-0.09V by wt%, provided by L. Angers at the Alcoa Technical Center).

Fracture Methods

The approach was outlined in past renewal proposals[3,4]. In summary, our approach focuses on:

(1) Characterizing microstructures of as-received alloys through optical, scanning electron, and transmission electron microscopy.

(2) Implementing J-Integral fracture mechanics methods and direct current potential drop (DCPD) crack length

measurements to determine crack initiation and propagation resistance at ambient and elevated temperatures.

(3) Establishing microstructural fracture paths and mechanisms through SEM fractography, crack tip profiles, and transmission electron microscopy. Stereofractographic and matching surface methods are being used.

(4) Performing uniaxial compression tests to determine yield strength, strain hardening exponent and strain rate sensitivity.

(5) Employing smooth and notched tensile tests to estimate intrinsic fracture strains.

(6) Evaluating the predictive capabilities of micromechanical models in explaining the temperature dependence of ductile fracture initiation toughness, K_{JICi}.

(7) Interrupting notched tensile tests at various strain levels before failure to determine the onset (using DCPD monitoring) and three dimensional distribution of microvoid damage in the notch root at ambient and elevated temperatures.

Progress During the Reporting Period

The results for this period are divided into three sections for each of the three aluminum alloy classes (ingot metallurgy, spray formed, and cryogenically milled). Section I presents the conclusions from a Metallurgical Transactions A manuscript on elevated temperature fracture of IM AA2519+Mg+Ag. Section II presents the conclusions from a Materials Science and Engineering A manuscript on elevated temperature fracture of cryogenically milled aluminum (CM Al). Section III presents preliminary work on spray formed and extruded N203 received from Lockheed.

Section I: I/M 2519-T87 (+Mg+Ag)

The time-temperature dependent fracture toughness of 2519+Mg+Ag was the subject of previous NASA-LaRC sponsored research, as summarized in past proposals and progress reports[3-7]. A detailed manuscript is currently undergoing final preparations for submittal to Metallurgical Transactions A. The conclusions from the manuscript are listed below, and new findings are discussed.

1. Fracture initiation toughness is high (K_{JICi} > 30 MPa$\sqrt{m}$) for 2519+Mg+Ag with a substantial volume fraction of undissolved Θ (≈1.2%), and decreases slightly with increasing temperature to 175°C. 2519+Mg possesses a significantly lower K_{JICi} than its Ag bearing counterpart at 175°C.
2. Fracture surfaces are characterized by a bimodal distribution of dimples. Fracture evolved by primary void initiation at large undissolved Al_2Cu particles, followed by limited void growth and unstable coalescence through propagation of fine dimpled void sheets nucleated at dispersoids. Void sheeting is less dominant as temperature increases.
3. Yield strength and strain hardening decrease monotonically with temperature in 2519+Mg+Ag, consistent with increasing dynamic recovery.
4. The effective plastic strain to fracture of 2519+Mg+Ag decreases markedly with increasing triaxial constraint and asymptotically approaches an intrinsic fracture strain at high constraint levels. Ductility increases with increasing temperature, independent of triaxial constraint.
5. The critical plastic strain-controlled micromechanical model of initiation toughness accurately predicts the measured temperature dependence of K_{JICi} regardless of whether uniaxial or notched bar reduction in area is employed to estimate the intrinsic fracture resistance, $\bar{\varepsilon}_f^*$.
6. The critical distance (l*), estimated to equal between 1 and

2 undissolved Θ particle spacings, is relevant to the size scale of microvoid fracture processes in 2519+Mg+Ag.

7. The flow stress of I/M 2000 series alloys and pure aluminum shows two regimes when plotted versus the Zener-Hollomon parameter (Z): a relatively temperature/strain rate insensitive region above a Z of 10^{16} s^{-1}, and a temperature/strain rate sensitive region below a Z of 10^{15} s^{-1}. At the standard strain rate employed in this study ($\dot{\varepsilon}$ = 6 x 10^{-5} s^{-1}), Z is within the strain rate sensitive region for temperatures above 100°C.
8. The propensity for strain localization between growing primary microvoids (intravoid strain localization or ISL) is believed to have a major influence on the intrinsic fracture resistance, $\bar{\varepsilon}_f^*$.
9. As temperature is increased from 25°C to 175°C in 2519, the Humphreys-Kalu dislocation climb model predicts a transition from dislocation accumulation at dispersoids to dislocation bypassing of dispersoids. A consequence of dislocation bypassing is a decreased void nucleation rate at dispersoids, a decreased flow softening within an ISL band, decreased void sheeting, and hence increased intrinsic fracture resistance.
10. Strain and strain rate hardening provide strengthening in an ISL band, where strain rate is amplified above the global strain rate. Speculatively, ISL band hardening at elevated temperatures is sufficient to overcome flow softening and delay ISL, consistent with the microscopic evidence of retarded void sheeting at 150°C.
11. $\bar{\varepsilon}_f^*$ was found to increase linearly with strain rate hardening in AA2519-T87 (+Mg+Ag) and AA2618-T851.

Conclusions 7 through 10 have not been previously discussed in LA^{2}ST progress reports. The ensuing sections amplify these conclusions.

Temperature and Strain Rate Dependence of Flow Stress

The temperature and strain rate dependence of flow stress is represented by the Zener-Hollomon parameter[8]:

$$Z = \dot{\varepsilon} \exp\left(\frac{\Delta H}{RT}\right) \qquad [8]$$

where ΔH is the activation energy associated with the temperature dependence of flow stress and is assumed to equal the activation energy for self diffusion in aluminum (140 kJ/mol[9]). R is the universal gas constant and T is temperature in degrees Kelvin. Z represents constant deformation conditions for dislocation recovery processes; at equal Z, the effect of increased temperature or lowered strain rate is the same.

Figure 1 summarizes the temperature and strain rate sensitivity of flow stress for 2519+Mg+Ag, 2219-T851[10], and low solute aluminum alloys[11-13]. For 2219-T851, the flow stress is plotted versus the Z derived from temperature and the time for 1% creep strain under constant stress. Flow stress is uniquely dependent on Z for a given alloy. For a strain rate of 6×10^{-5} s^{-1}, the equivalent temperature is plotted as a second ordinate. At constant temperature, an order of magnitude decrease in Z is equivalent a 10-fold reduction in strain rate. Consequently, the strain rate sensitivity of flow stress (m in the relation $\sigma_0 \alpha \dot{\varepsilon}^m$) is obtained at constant temperature from the slope of the curve.

The flow stresses for each alloy show a similar temperature-strain rate dependence within two regimes. For $Z > 10^{16}$ s^{-1}, the flow stress is relatively insensitive to changes in temperature or strain rate. For $Z < 10^{15}$ s^{-1}, dynamic recovery is enhanced and the flow stress decreases markedly with decreasing Z (decreasing $\dot{\varepsilon}$ or increasing T). These two regimes correspond to changes in the equilibrium dislocation cell size during steady state deformation of pure aluminum[8]. The equilibrium cell size changes from 1.0 μm

at a Z of 10^{30} s^{-1} to 1.5 μm at a Z of 10^{15} s^{-1}, while a further decrease in Z of 5 orders of magnitude increases the equilibrium size to 8 μm. The larger cell size results in the lower flow strength. Of importance to fracture is the result that m increases with increasing temperature and is substantial for Z < 10^{15} s^{-1}, as developed in the next section.

Intravoid Strain Localization (ISL) Controlled Fracture

A general notion is that the intrinsic fracture resistance of aluminum alloys increases with increasing temperature because of a decreasing tendency for ISL and a decreased tendency for the associated plastic shear instability between growing microvoids. As strain accumulates ahead of a crack tip in an aluminum alloy, the critical condition for microscopic ISL is easily attained because of: 1) a high volume fraction of inhomogeneously distributed second phase particles and associated voids, 2) a reduction in cross sectional area between primary microvoids due to void growth, and 3) a highly triaxial stress state. From the embryonic stages of ISL to final separation along the band by void sheet coalescence, the local strain rate ($\dot{\varepsilon}_{ISL}$) is estimated to increase between one and four orders of magnitude above the applied global strain rate[14,15].

The progression or abatement of ISL depends on the competition between flow softening and flow hardening within the ISL band. Softening, arising from void nucleation and growth at dispersoids (which may depend on temperature), promotes continued localization. The accelerated strain rate in the intravoid shear band, coupled with strain and strain rate hardening, produce an increase in local flow strength ($\Delta\sigma_{hardening}$ or ISL band hardening) relative to the flow strength of the surrounding homogeneously deforming material. If the band hardens sufficiently to overcome flow softening, then it becomes an unfavorable location for strain localization and ISL is abated. A finite $\Delta\sigma_{hardening}$ is required to arrest ISL because of flow softening and because stresses are

concentrated in the intravoid region. Hardening processes are governed by time and temperature dependent dynamic recovery.

Temperature/strain rate dependent bypassing of dispersoids controls the rate of dislocation accumulation at the dispersoid/matrix interface, and therefore should control the rate of void nucleation and associated flow softening in the ISL band. Humphreys and Kalu developed a model for two phase aluminum alloys that predicts the critical strain rate for dislocation bypassing of particles by climb, as influenced by bulk and interface diffusion of aluminum, and dependent on temperature and particle size[9]. A temperature-critical strain rate prediction is plotted in Figure 2 for measured dispersoid sizes in 2519+Mg+Ag ranging from 0.1 to 0.3 μm (The average size of 0.2 μm is plotted as a solid line). The plot provides a "microdeformation mechanism map", where dislocation bypassing of dispersoids is predicted to occur at all temperature-strain rate combinations lying below a line and dislocation accumulation is predicted for combinations lying above the line for a given dispersoid size. Superimposed on the plot are the temperature and global strain rate conditions for 2519+Mg+Ag tensile testing. The arrows represent local strain rates in an ISL band ($\dot{\varepsilon}_{ISL}$) due to an assumed 100-times amplification of the global strain rate, and the dashed lines represent strain rate amplifications (γ) of 100, 1000, and 10000 times the global strain rate.

Figure 2 suggests that, during tensile fracture at ambient temperature, dislocations do not bypass dispersoids, even at the relatively slower global strain rate. Dislocation accumulation and void nucleation at dispersoids is abundant, leading to significant flow softening, enhanced ISL and relatively low strain fracture involving void sheeting. Deformation at 75°C to 125°C represents a transition region, where some dispersoids are bypassed and others are not, depending on their size. At 150°C and above, significant strain rate amplifications are needed to enable dislocation accumulation within the ISL band. Flow

softening from void nucleation at dispersoids is greatly reduced, unless very high strain rate amplifications occur.

Increased temperature results in reduced ISL by a second mechanism that operates in addition to reduced dispersoid-void nucleation. When the strain rate is amplified within an ISL band, the level of dynamic recovery is reduced below that of the globally deforming material. The decreased magnitude of dynamic recovery is responsible for flow hardening and abatement of intravoid strain localization. The beneficial effect of dynamic recovery is particularly important at temperatures above about 100°C (Fig. 1). Less dynamic recovery between growing voids decreases the rate of dislocation annihilation, increasing the work hardening rate and flow stress level in the ISL band relative to the global material. The flow strength increase arises from a smaller equilibrium dislocation cell size in the ISL band versus the global material.

With increasing temperature, strain rate hardening (m) increases and strain hardening (n) decreases. At 25°C, and the strain rate employed in this study ($\dot{\epsilon} = 6 \times 10^{-5}$ s^{-1}), the Z value lies within the strain rate insensitive regime (Log Z = 20.6 s^{-1}) and m is determined as 0.020 for 2219-T851. At 150°C, the alloy is within the strain rate sensitive regime (Log Z = 13.3 s^{-1}) and m is 0.035. Conversely, n is estimated to decrease from 0.05 at 25°C to 0.03 at 150°C, based on work hardening data from uniaxial compression of 2519+Mg+Ag, modified to reflect work hardening at the increased strain rate within the ISL band.

As temperature increases, the change in ISL band hardening (the combination of strain and strain rate hardening) is difficult to predict due to uncertainties in strain, strain rate, and the form of the constitutive law within the ISL band. None-the-less, a first order approximation of ISL band hardening determined the combinations of strain and strain rate differentials (between the ISL band and globally deforming material) at which hardening is equal for 25°C and 150°C. (Power law constitutive equations

$(\sigma_o = K\varepsilon^n$ and $\sigma_o = K\dot{\varepsilon}^m)$ are assumed and the incremental increases in σ_o due to increased strain and strain rates within the ISL band are superimposed.) For example, the relative benefit in strain rate hardening between 150°C and 25°C, due to a two-fold strain rate differential and higher m, is counterbalanced by a relative detriment in strain hardening due to a strain differential of 15% and lower n. For three and four-fold strain rate differentials, ISL band hardening is equal at 25°C and 150°C for strain differentials of 30% and 95%, respectively.

Increased intrinsic fracture strain, and reduced void sheeting, with increasing tensile deformation temperature for IM 2519+Mg+Ag is rationalized from the above discussion. At room temperature, dislocations do not bypass dispersoids, void nucleation is abundant within the ISL band, and flow softening is significant. ISL is catalyzed. Void sheeting is prevalent since low strain rate hardening (nil recovery contribution) and low work hardening are not sufficient to overcome flow softening. At elevated temperatures (150°C), dislocations bypass dispersoids, void nucleation within the ISL band decreases, and flow localization is reduced. Speculatively, void sheeting is retarded at 150°C because ISL band hardening overcomes flow softening (mostly due to enhanced strain rate hardening following from reduced recovery between growing microvoids) and delays the progression of ISL. The Zener-Hollomon and Humphries-Kalu descriptions of time-temperature-dependent deformation are consistent with this argument for IM 2519.

Section II: Cryogenically Milled Aluminum (CM Al)

Work was performed on CM Al to extend previous experiments and analysis conducted by Dr. Sang-Shik Kim during his post-doctoral study at UVa. A manuscript was submittal to Materials Science and Engineering A. The conclusions from this paper are listed below, and new findings are discussed.

1. The uniaxial tensile ductility, plane strain crack initiation fracture toughness, and plane strain stable-tearing resistance of CM Al decrease monotonically with increasing temperature between 25°C and 325°C. Delamination does not affect the initiation toughness of CM Al, or the temperature dependence.
2. Continuum micromechanical models of K_{JIC_i} and T_R for CM Al show that temperature-dependent toughness decreases because of declining yield strength, elastic modulus and intrinsic fracture resistance. This latter property is controlling for submicron grain alloys, but increases with increasing temperature for conventional aluminum alloys.
3. Fracture in CM Al is by microvoid processes at all temperatures, however, reductions in fracture resistance correlate with a change in primary void morphology from spherical to faceted.
4. Dynamic strain aging, due to diffusing solute such as iron, is not a necessary element of the elevated temperature reduction in intrinsic tensile ductility and fracture toughness for submicron grain size, dispersion-strengthened aluminum.
5. Speculatively, the intrinsic fracture resistance of alloys such as CM Al is degraded by temperature-reduced work and strain rate hardening which promote plastic instability between growing microvoids to exacerbate low-strain coalescence.
6. Plasticity localizes between primary voids at elevated temperatures due to dynamic recovery, which eliminates work hardening dislocation cell and source structures in submicron grains, coupled with reduced strain-rate hardening or softening. Decreased strength with increasing strain rate is due to increased mobile dislocation density from the emission or detrapping of dislocations from dispersoids in the source deficient microstructure.

The first three conclusions are discussed.

CM Al Flow Properties The temperature dependencies of σ_{YS}, σ_{UTS}, and RA are shown in Fig. 3. Unlike conventional large grain-size aluminum alloys, which exhibit improved tensile ductility at elevated temperatures, the ductility (as well as the modulus and yield strength) of CM Al decrease with increasing temperature to 325°C. RA for CM Al does not exhibit a minimum for temperatures between 25°C and 325°C, similar to the behavior of AA8009.

Micromechanical Modelling of Initiation Fracture Toughness The toughness behavior of CM Al was analyzed by a critical strain-critical distance crack tip modeling approach outlined in a previous LA²ST progress report[7]. Input parameters included temperature dependent elastic modulus (E), work hardening (n), yield strength (σ_{YS}), and the critical plastic strain to nucleate crack tip microvoid damage ($\bar{\varepsilon}_f^*$). Temperature dependent elastic modulus was based on literature data[16]. (E equals 72, 68, 66, 64, 63, 62, and 58 GPa at 25, 80, 125, 175, 215, 250, and 325°C respectively) and $\bar{\varepsilon}_f^*$ was approximated by -ln(1 - pct RA/100) divided by a plane strain constraint factor (r) of 7. Three parameters (C1, C2, and d_n) are necessary in addition to σ_{YS} and E, to describe the crack tip effective plastic strain field (C1 = 0.1256, C2 = 1.228, and d_n = 0.70). The critical distance over which the crack tip damage is produced (1*) was back-calculated to equal 10 μm from the measured K_{JICi} at 25°C. This distance is of the correct order of magnitude and is assumed to be constant with increasing temperature because of the invariant CM Al microstructure and microvoid fracture mode. 1* is not relatable to a specific microstructural feature because of modeling uncertainties.

With these values, the strain-based initiation toughness model reasonably predicted absolute values and the monotonic

decline in K_{JICi} with increasing temperature for CM Al, without a minimum for temperatures between 25°C and 325°C. These model predictions are compared with experimental results in Fig. 4. The model reasonably reproduces the measured toughness trend, with maximum discrepancies of 2.4 MPa$\sqrt{m}$ and 32%. For conventional aluminum alloys, E, n, and σ_{YS} decrease with increasing temperature, tending to reduce K_{JICi}: however, $\bar{\varepsilon}_f^*$ increases with the net effect being a constant toughness. In contrast the adverse effect of temperature on the initiation and growth fracture toughness of CM Al is traced to the temperature-dependent decline in intrinsic $\bar{\varepsilon}_f^*$, analogous to the behavior of RS AA8009.

CM Al Fractography Fracture of CM Al evolves by microvoid coalescence at all deformation temperatures. Figure 5 shows SEM fractographs of CM Al compact tension fracture surfaces produced at a loading rate of 2.5 μm/sec and at (a),(b),(c) 25°C and (d),(e),(f) 175°C. Both fractures show significant surface roughness (Figs. 5a and 5b), and the dimple morphology changes significantly with temperature. At 25°C, dimples are well developed and spherical, as demonstrated in Figs. 5b and 5c. Dimples at 175°C are much less developed; with anisotropic and discontinuous perimeters as well as dimple walls that form triple point junctions (Figs. 5e and 5f). When the dimples are well developed, their perimeters form polygonal shapes (pentagonal or hexagonal) and their surfaces are faceted (Fig. 5f). High magnification matching surface stereo-fractographic analysis of the CM Al compact tension fracture surface produced at 175°C demonstrated that the fracture surface contains dimples on both halves. No evidence of grain boundary fracture was observed, confirming dimpled rupture as the acting fracture mechanism at elevated temperature. The origin of the faceted dimple walls is not understood. Coble creep-type deformation could be important in this submicron grain size alloy; this possibility is being considered, as is a mechanism for ISL due to strain rate softening

due to dispersoid-dislocation interactions between growing microvoids.

Section III - Spray Formed N203 Extrusion

Aging Study The heat treatment of spray formed N203 was optimized to obtain peak hardness and to minimize constituents that do not dissolve during solution heat treatment. Lockheed performed replicate differential scanning calorimetry (DSC) scans on the current lot of N203, at a heating rate of 10°C/min, and determined that localized melting begins between 538°C and 541°C. Based on these results, a sample of N203 was solution heat treated at 530°C for 3 hours, cold water quenched and subsequently mounted and polished for microscopic examination. Figure 6 shows a Nomarski contrast optical micrograph of the resulting N203 microstructure. No evidence of localized melting (incipient or eutectic) was observed. Constituents range in size from 0.5 μm to 7 μm, with an average diameter of 4 μm, and the volume fraction is roughly 3% (determined from image analysis). The small grain size, relative to I/M alloys, is confirmed by the contrasted grain structure in the micrograph.

A second N203 sample was solution heat treated at 530°C for 2 hours, and hardness was measured as a function of aging time for an aging temperature of 190°C (Fig. 7). Peak hardness was achieved for an aging time of 6 to 7 hours. Material for mechanical test specimens was solution heat treat treated at 530°C for 3 hours, cold water quenched, and aged for 6 hours at 190°C. Compact tension and tensile specimens are currently being machined.

Proposed Research for the Next Reporting Period

Work in the first half of 1995 will concentrate on characterizing the elevated temperature fracture toughness of spray formed N203. We will concurrently evaluate the elevated temperature fracture toughness of C416 (low constituent version of

AA2519+Mg+Ag) to determine if toughness is improved and why. Specifically, we propose to:

- Evaluate the changes in K_{JICi} and T_R^{ps} as a function of temperature for C416 sheet, a modified chemistry of 2519+Mg+Ag with lower Cu and constituent content.
- Determine the types, sizes, and distributions of constituent, dispersoid, and precipitate particles in spray formed N203 with optical, scanning electron, and transmission electron microscopy.
- Measure the temperature dependence of J-Δa resistance curves for N203 extrusion (from 25°C to 200°C) and determine initiation (K_{JICi}) and plane stress growth (T_R^{ps}) toughnesses.
- Employ SEM methods, including high-magnification tilt fractography and stereo-pair viewing, to explore the role of microstructure, temperature, and time on void nucleation as well as on localized shear instabilities affecting void growth to coalescence.
- Determine yield strength and work hardening of N203 as a function of temperature from 25°C to 200°C with uniaxial compression tests.
- Based on limited smooth and notched tensile measurements of the effect of temperature on the intrinsic fracture strain for N203 extrusion, we will explain the temperature dependency of K_{JICi} with the existing micromechanical model of ductile fracture.

References

1. W.B. Lisagor, in Thermal Structures and Materials for High-Speed Flight, E.A. Thornton, Ed., Volume 140, Progress in Astronautics and Aeronautics, A.R. Seebass, Editor-in-Chief, AIAA, Washington, DC, pp. 161-179, (1992).

2. R.P. Gangloff, E.A. Starke, Jr., J.M. Howe and F.E. Wawner,Jr., "Aluminum Based Materials for High Speed Aircraft", University of Virginia, Proposal No. MS-NASA/LaRC-5691-93, November (1992).

3. R.P. Gangloff, "NASA-UVa Light Aerospace Alloy and Structures Technology Program", Proposal No. MSE-NASA/LaRC-6074-94, University of Virginia, Charlottesville, VA, November (1993).

4. R.P. Gangloff, "NASA-UVa Light Aerospace Alloy and Structures Technology Program", Proposal No. MSE-NASA/LaRC-6478-95, University of Virginia, Charlottesville, VA, November (1994).

5. E.A. Starke, Jr., "NASA-UVa Light Aerospace Alloy and Structures Technology Program: HSCT Supplement", University of Virginia, Semi-Annual Progress Report, January to June (1993).

6. R.P. Gangloff, "NASA-UVa Light Aerospace Alloy and Structures Technology Program", Proposal No. MSE-NASA/LaRC-5691-93, University of Virginia (1992).

7. R.P. Gangloff, "NASA-UVa Light Aerospace Alloy and Structures Technology Program", University of Virginia Report No. UVA/528266/MSE94/114, March (1994).

8. H.J. McQueen and J.J. Jonas, in Treatise on Materials Science and Technology, Vol. 6, Plastic Deformation of Materials, R.J. Arsenault, ed., Academic Press, New York, NY, 1975, pp. 393-493.

9. F.J. Humphreys and P.N. Kalu, Acta Metall., 1987, vol. 35, pp. 2815-29.

10. Metals Handbook, ASM International, Metals Park, Ohio, 1987, ninth edition, vol. 2, pp. 79-84.

11. P. Olla and P.F. Virdis, Metall. Trans. A, 1987, vol. 18A, pp. 293-301.

12. J.E. Hockett, Transactions of AIME, 1967, vol. 239, pp. 969-76.

13. E.W. Hart and H.D. Solomon, Acta Metall., 1973, vol. 21, pp. 295-307.

14. P.F. Thomason, Ductile Fracture of Metals, Pergamon Press, Oxford, UK, 1990, pp. 105-11.

15. R. Becker and R.E. Smelser, J. Mech. Phys. Solids, 1994, vol. 42, pp. 773-96.

16. L.F. Mondolfo, Aluminum Alloys Structure and Properties, Butterworth and Co., Woburn, MA, 1976, p. 82.

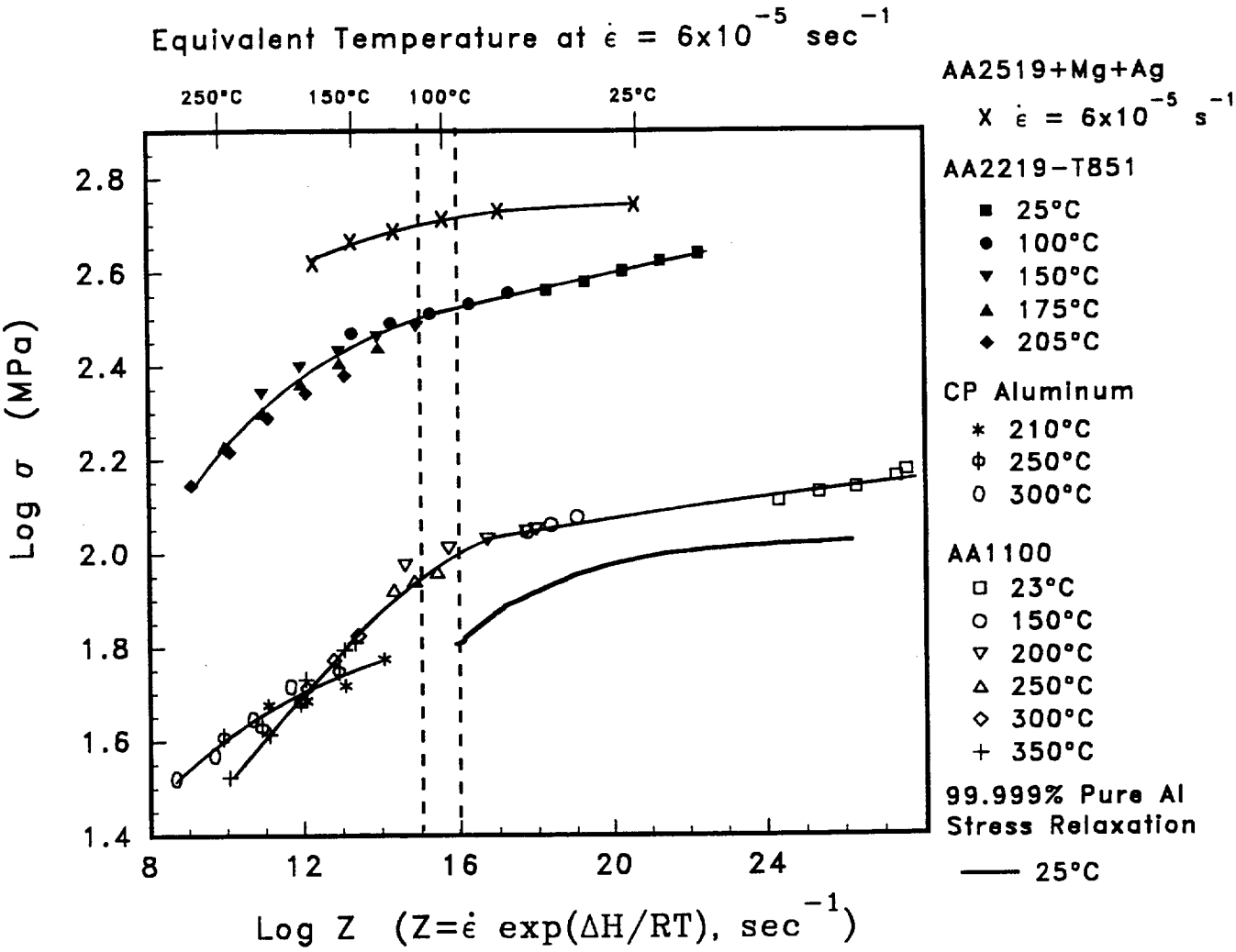

Figure 1 Temperature/strain rate dependence of flow stress for AA2519-T87 (+Mg+Ag), AA2219-T851[10], comercially pure aluminum[11], AA1100[12], and 99.999% pure aluminum[13]. Use of the Zener-Hollomon parameter condenses each data set into one curve.

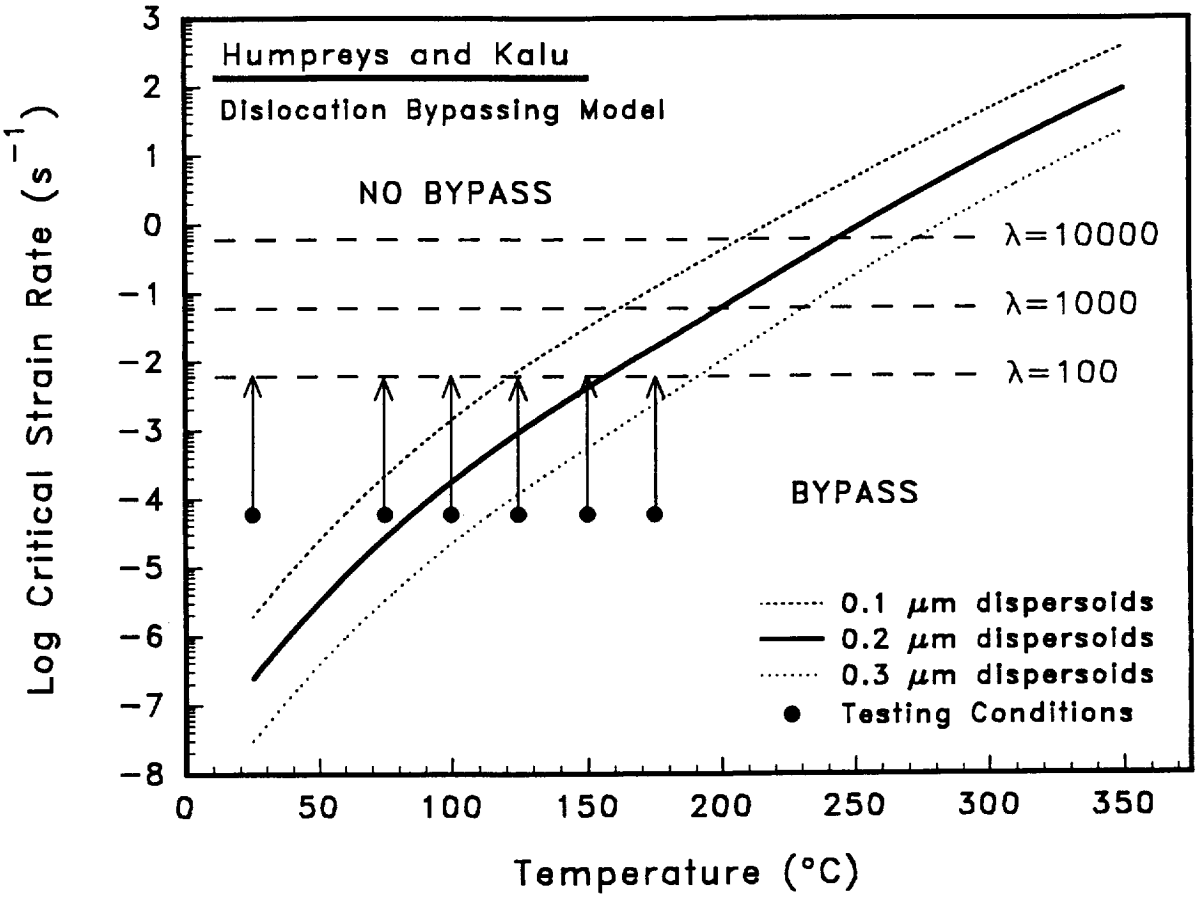

Figure 2 Dislocation bypassing model of submicron dispersoids (after Humphreys and Kalu[9]). The region below the curve represents deformation conditions where dislocations climb around dispersoids, and the region above the curve represents deformation conditions where dislocations pile-up at dispersoids. The solid dots represent deformation conditions for 2519-T87 (+Mg+Ag). The three dashed lines represent strain rate amplifications (λ) of 10^2, 10^3, and 10^4 times the global strain rate.

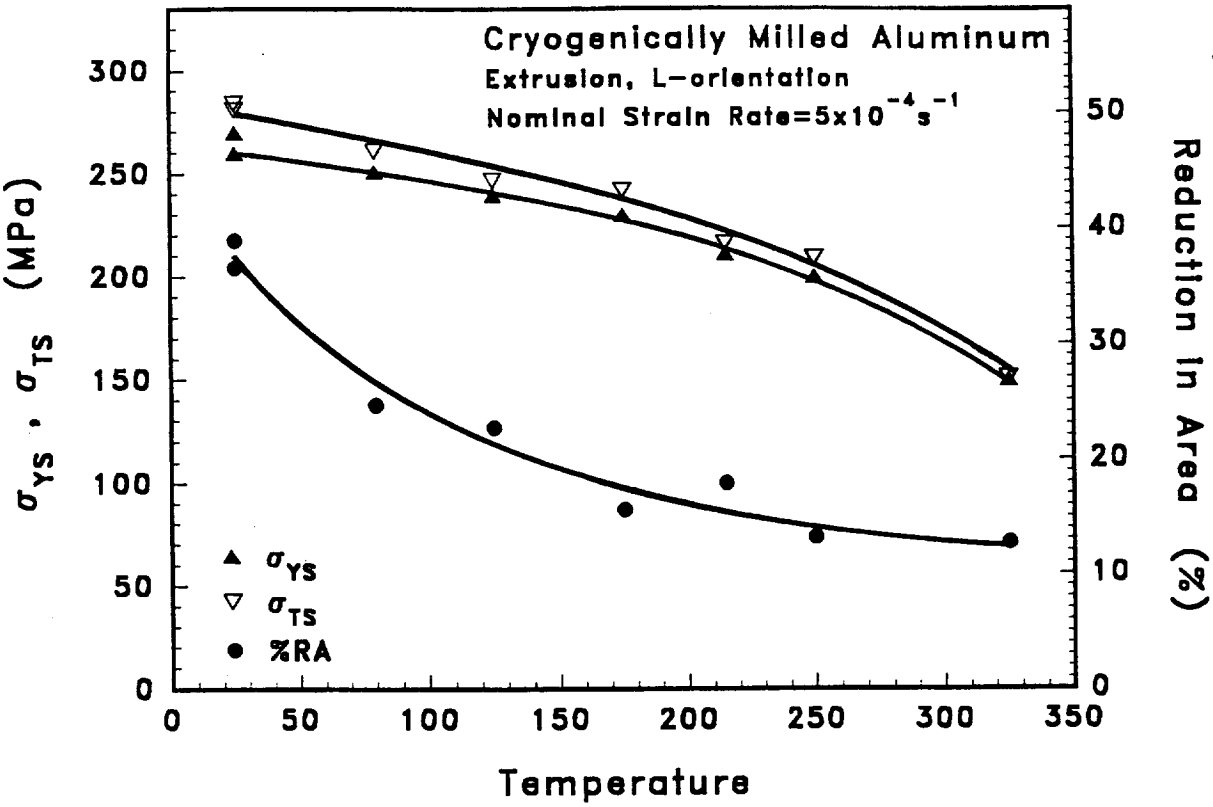

Figure 3 The temperature dependencies of tensile yield strength, ultimate tensile strength and ductility (%RA) of CM Al at a single loading rate.

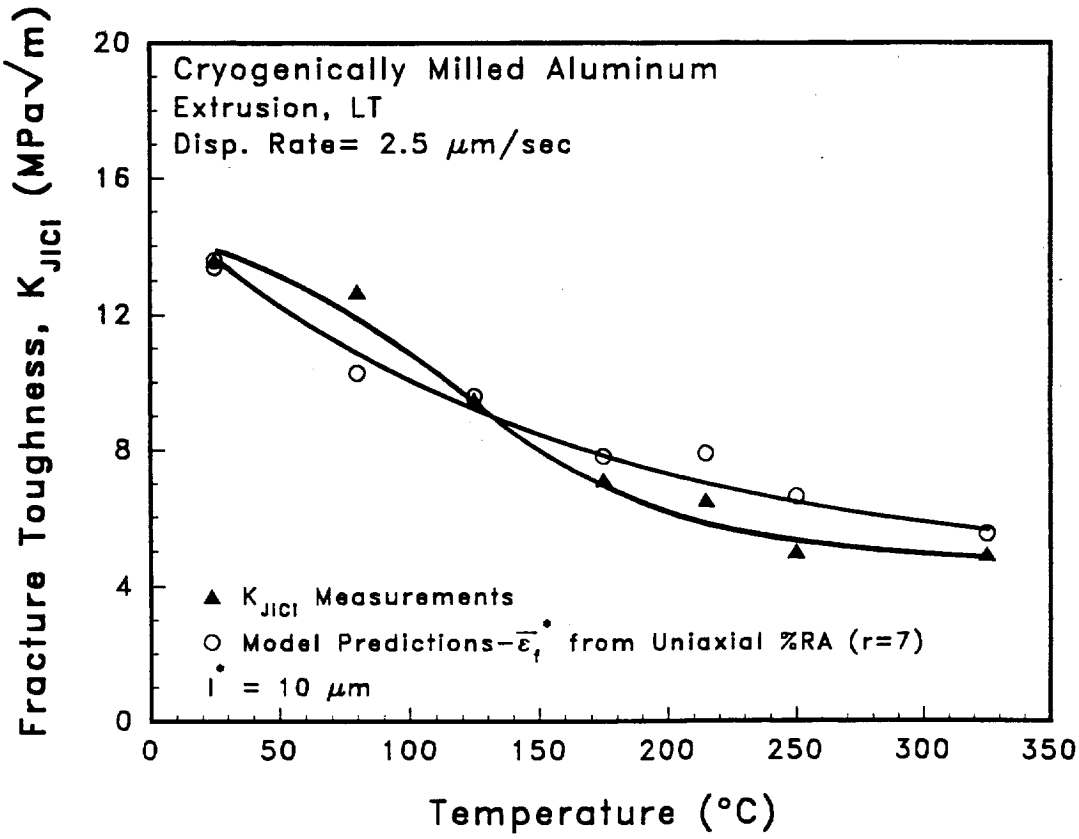

Figure 4. Critical plastic strain-controlled model predictions compared to experimentally measured values of the plane strain crack initiation toughness for CM Al as a function of temperature.

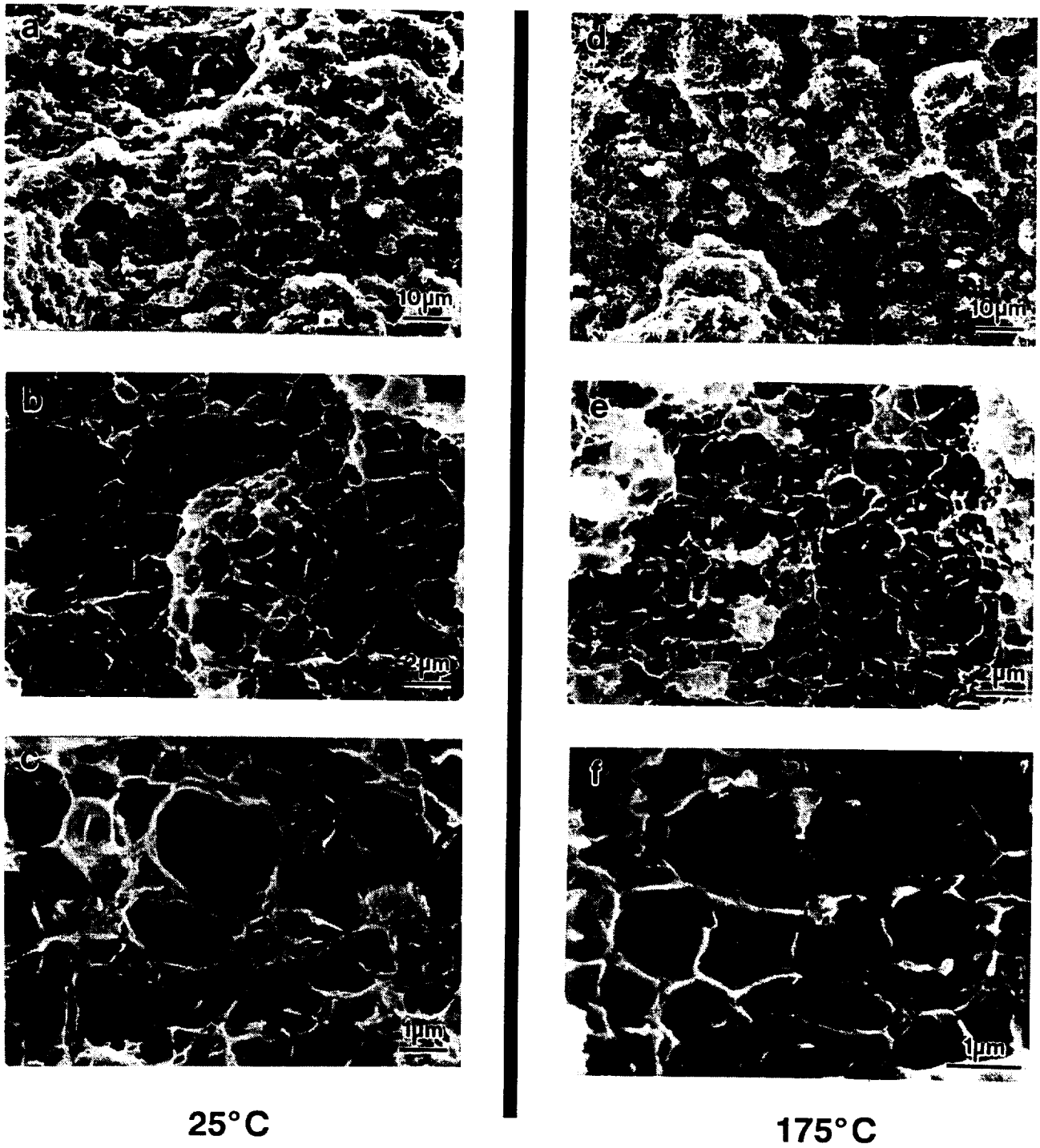

Figure 5 SEM fractographs of CM Al compact tension specimen fracture surfaces, at mid-thickness and for $\Delta a = 0.4 \pm 0.2$ mm, produced at: (a), (b) and (c) 25°C; and (d), (e) and (f) 175°C. Fractographs are arranged vertically in order of increasing magnification and the crack grew from right to left.

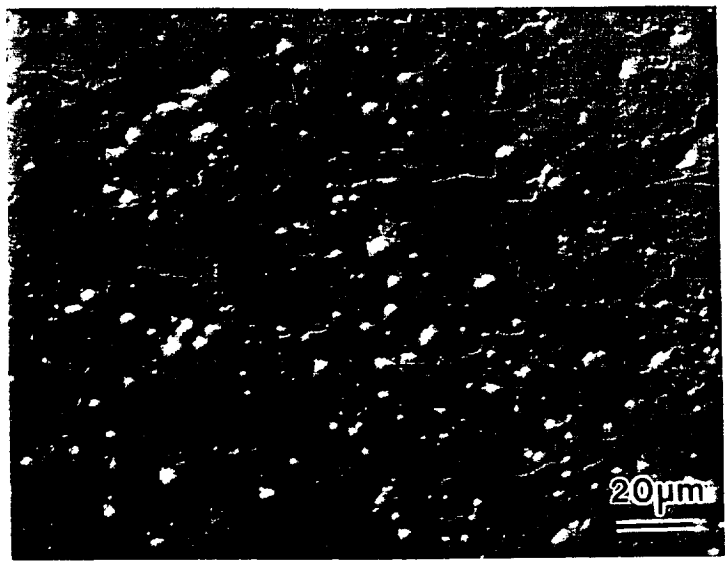

Figure 6 Nomarski contrast optical micrograph of spray formed N203 extrusion, showing 0.5 to 7 μm constituent particles and a resolved grain structure. The alloy was solution heat treated at 530°C for 3 hours and cold water quenched.

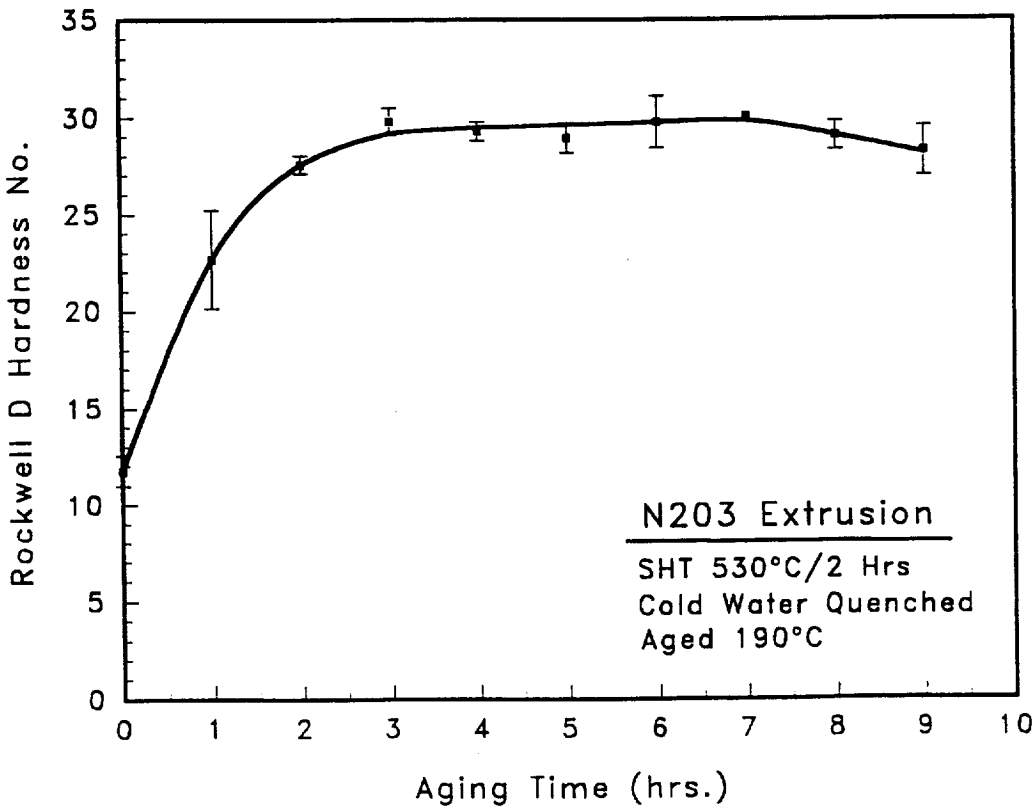

Figure 7 Hardness as a function of time for artificial aging of N203 extrusion at 190°C, showing a peak hardness time of 6 to 7 hours. The alloy was solution heat treated at 530°C for 3 hours and cold water quenched.

Project #2 **Cryogenic Temperature Effects On Deformation And Fracture Of Al-Li-Cu-In Alloys**

John A. Wagner and R.P. Gangloff

Objective

The objective of this PhD research is to characterize and optimize the crack initiation and growth resistance of Al-Li-Cu-Zr and Al-Li-Cu-Zr-In alloys for possible cryogenic propellant tank applications. The aim of the program is to understand microscopic fracture mechanisms as influenced by temperature, stress state and microstructure.

Approach

The approach to this objective was outlined in the proposal for the 1994 LA2ST Program[1]. In summary our approach focuses on several areas including: (1) produce experimental direct chill cast Al-Li-Cu-Zr alloys with and without indium additions, (2) characterize both experimental Al-Li-Cu-Zr alloys and commercially available 2090-T81 plate, (3) implement J-integral fracture mechanics methods to measure crack initiation and fracture resistance for primarily plane stress and plane strain conditions at ambient and cryogenic temperatures, (4) establish the effect of stress state, temperature and microstructure on fracture toughness, (5) analyze fracture surfaces and correlate fracture features with grain structure, and (6) develop and apply advanced mechanical test and metallographic techniques to investigate the deformation and fracture processes that are relevant to crack initiation and growth toughnesses.

Recent Research Focus

As documented in the two last progress reports[2,3], research conducted during the last four reporting periods has primarily focused on the mechanisms of fracture and the evolution of

fracture events in 2090-T81 plate at 25 and -185°C. Recent results from the past year focused on intermediate temperature tests and the application of Electron Backscattered Pattern (EBSP) techniques to fracture events. These findings are summarized.

Recent Results

Intermediate Temperature Tests

Tensile Experiments

Transverse (T) oriented smooth uniaxial tensile experiments were conducted in the temperature range from 25 to -185°C on specimens machined from fractured LT (longitudinal-transverse) compact tension (C(T)) specimens. Elastic modulus, yield strength and work hardening exponent were determined as a function of temperature and are tabulated in Table I. Work hardening behavior was determined according to ASTM Standard E646-91[4]. Due to the extensive amount of delamination fracture, ductility, as measured by the reduction in area, was not determined.

From Table I, it is observed that modulus and strength increase with decreasing temperature similar to what was observed for L-oriented specimens[5]. In addition the work hardening behavior, n, increases from an ambient temperature value of 0.052 to 0.081 at -185°C. The increase in work hardening is a consequence of more homogeneous deformation at cryogenic temperature[6], which contributes in part to an increase in fracture toughness at cryogenic temperatures.

Fracture Toughness

Fracture toughness behavior at intermediate temperatures was determined using elastic-plastic fracture toughness experiments which conformed to ASTM Standard E813-89[7] and employed the single specimen unloading compliance technique. Compact tension specimens 12.0 mm thick with 1.2 mm deep side grooves were machined from the midplane of the plate in the LT orientation. Specimens were tested in a closed-loop servohydraulic test machine interfaced

with a computer system which provides a programmable ramp single to the stroke controller, and reads load and clip gage displacement through analog to digital channels. Ramp rate, data acquisition rate for load-displacement and unloading slopes were individually programmed. Specimens were tested at a loading and unloading displacement rate of 4.0 μm/s. Data acquisition rate for the unloading compliance data was 15 points per second. The load drops were programmed to occur at every 12.7 μm of displacement. Approximately 400 data points were collected for each unloading slope.

J-values were calculated from the equation

$$J = J_{elastic} + J_{plastic} \quad [1]$$

where:

$$J_{elastic} = (K^2(1-\upsilon^2))/E \quad [2]$$

E is Young's modulus and υ is Poisson's ratio. $J_{plastic}$ is determined from the crack length, load displacement, slope of the unloading line and the corresponding area under the load-load line displacement record[7]. J_{Ic} values were determined from the intersection of the power law regression line of the data with the 0.2 mm offset from the blunting line according to ASTM Standard E813[7]. (The blunting line equals $2\sigma_{ys}\Delta a$.) This definition of J_{Ic} at an arbitrary Δa appeared to overestimate the J level corresponding to the crack initiation toughness. Therefore, an alternate definition of the J level at initiation was employed by using a 0.1 mm offset. A curve was fit through the data, and the intersection of the 0.1 mm offset and the data curve was defined as J_i. By using a 0.1 mm offset instead of the standard 0.2 mm offset, the effect of stable tearing on initiation toughness has been reduced and may give a more meaningful J initiation value. K_{JIci} values were calculated from measured J_i using the relationship[8]:

$$K_{JIci} = (J_i E/(1-\upsilon^2))^{1/2} \quad [3]$$

Tearing modulus, TR, was used to assess the materials resistance to stable crack growth after crack initiation and was determined from the relationship[9]:

$$T_R = (E/(\sigma_o)^2)(dJ/d\Delta a) \quad [4]$$

where σ_o is flow stress equal to the average of yield and ultimate stresses and $dJ/d\Delta a$ is the slope of the J- a curve in the region of stable crack growth[9]. Values of $dJ/d\Delta a$ were determined from a least squares linear regression analysis of J-Δa from Δa of 0.2 to 1.5 mm.

For all test temperatures, plane strain crack-initiation toughness, K_{JIci}, and stable crack-growth resistance, T_R, are reported in Table I and R-curves are presented in Figure 1a. Since B, thickness, and (W-a), width - crack length, were greater than $25J_{Ic}/\sigma_{ys}$, crack initiation was under J-control for each test temperature. For 2090-T81 in the LT orientation, K_{JIci} remains almost constant in the temperature range 25 to -155°C, Figure 1b. Crack- growth resistance, T_R, exhibits a slight increase in the temperature range 25 to -155°C, with a minimum value of T_R = 1.2 at -25°C to a maximum of T_R = 2.1 at -155°C. The largest increase in both K_{JIci} and T_R occurred in the temperature range -155 to-185°C. In this temperature range K_{JIci} increased from 26 MPa$\sqrt{m}$ at -155°C to 35 MPa$\sqrt{m}$ at -185°C. Similarly, T_R increased from 2.1 at -155°C to 2.8 at -185°C, Figure 1c.

Associated with the large increase in K_{JIci} and T_R at -185°C was the occurrence of numerous large delaminations on the order of 0.5 to 2.0 mm in depth with spacing less than 1.0 mm, Figure 2. This height and spacing of the large delaminations is on the order of the plastic zone size as estimated from the relationship r_p =

$(1/2\pi)(K_{Ic}/\sigma_{ys})^2$. The increase in delaminations at -185°C appears to be of sufficient size and number to relieve through-thickness stresses and significantly increase the initiation toughness, Figure 1b. This explanation assumes that the major delaminations occur prior to the initiation of the primary main crack and has been demonstrated for 2090-T81 at -196°C[10]. The apparent insensitivity of the initiation toughness 2090-T81 in the temperature range 25 to -155°C appears to be related to the absence of delaminations of a size which approaches the plastic zone size. This also suggests that if deformation becomes more homogenous going from a temperature of 25 to -155°C, similar to the observed deformation behavior between 25 and -185°C, then more homogeneous deformation appears to have little influence on the initiation toughness in this temperature range. The nature of the deformation at intermediate temperatures will be examined in future work.

One explanation for the increase in delamination depth and decrease in delamination spacing of 2090-T81 at -185°C follows the rational used by Porr and Gangloff[11] to explain the requirements for delaminations to occur and the effect of delamination fracture on the toughness of RS/PM 8009. As the applied K increases, the transverse stresses, σ_{22} , increase over a critical distance ahead of the crack tip. They argue that when σ_{22} is greater than the fracture strength of the oxide-decorated prior particle boundaries, σ_{fb}, at a stress intensity less than that of initiation toughness, delaminations occur prior to crack extension and results in a higher initiation toughness. Similarly for 2090-T81, it appears that σ_{22} only exceeds the fracture strength of the (sub)grain boundaries at stress intensity levels less than K_{JIci} at -185°C. This suggests that although it appears that there is a slight increase in σ_{fb} at -185°C as measured by short transverse tensile tests and reported in the last progress

report[3] this increase is not sufficiently high to compensate for the corresponding increase in σ_{ys} and σ_{22} at -185°C.

EBSP Application to Fracture of 2090-T81

As reported in the previous section, the fracture toughness of 2090-T81 increased at -185°C, as exhibited by a more steeply rising R-curve and an increased initiation toughness. The increase in toughness at -185°C was associated with an increase in the incidence of delamination along (sub)grain boundaries. A good understanding of the fracture/delamination process was aided by crystallographic characterization of regions around the delamination. Specifically microtexture analysis was conducted to characterize the region around the delamination fracture for 2090-T81 alloy tested at -185°C, using Electron Backscattered Pattern (EBSP) technique.

Samples for analysis were sectioned from tested C(T) specimens; mechanically polished and electropolished in a solution of 33 volume percent nitric acid in methanol. Grain orientations were determined on-line using an EBSP equipment attached to a JEOL model 840 Scanning Electron Microscope. The system was fundamentally similar to that of Dingley[12].

Figure 3 shows a polarized light micrograph of an L-S section of a fracture surface of a tested C(T) sample. It is evident that the microstructure was complex and varied irregularly throughout the section. EBSP patterns were obtained from a region, defined by a line 300 μm long (along Normal Direction - ND) across the tip of the delamination "x". The EBSP {111} pole figure in this area indicated that the region exhibits a Copper-type texture. The corresponding inverse pole figure showed that the grain orientations were distributed around S {123}<634> and Copper {112}<111> components. Despite the limited sampling size, the pole figures obtained from the EBSP technique were in good agreement with pole figures obtained by X-ray diffraction.

The usefulness of the technique is best illustrated by plotting the misorientation angle of neighboring (sub)grains along ND, as shown in Figure 4. Although the highest grain misorientation observed was 39°, the delamination occurred at grain boundary with a misorientation of 30° (x). Similar analyses were performed on regions around delaminations "y" and "z" (Figure 3) and other regions in companion samples. The data indicated that delaminations occurred along high angle boundaries (27° - 40°), but not necessarily at boundaries with the highest misorientation. This is not surprising since other factors such as stress state, precipitate distribution and morphology also influence the initiation of delaminations.

Recent Conclusions

1. Elastic modulus, yield strength and work hardening exponent of 2090-T81 increase over the temperature range 25 to -185°C.
2. The initiation toughness does not appear to be a function of temperature in the range 25 to -155°C. However, initiation toughness increases at -185°C.
3. The increase in toughness at -185°C is associated with numerous large delaminations, with size and spacing on the order of the plastic zone size.
4. Using the Electron Backscattered Pattern (EBSP) technique, it was demonstrated that delaminations occur along high angle boundaries, but not necessarily along boundaries with the highest misorientation.

Future Direction

Work will focus on the deformation behavior at intermediate temperatures between 25 and -185°C. Studies will continue on the mechanisms which govern the nucleation and propagation of transgranular and delamination fracture.

References

1. R.P. Gangloff, "NASA-UVA Light Aerospace Alloy and Structures Technology Program", University of Virginia, Proposal No. MSE-NASA/LaRC-6478-95, November, 1994.

2. R.P. Gangloff, "NASA-UVA Light Aerospace Alloy and Structures Technology Program", University of Virginia, Report No. UVA/528266/MSE93/112, March, 1993.

3. R.P. Gangloff, "NASA-UVA Light Aerospace Alloy and Structures Technology Program", University of Virginia, Report No. UVA/528266/MSE94/112, March, 1994.

4. "Standard Test Method for Tensile Strain-Hardening Exponents (n-Values) of Metallic Sheet Materials," Designation E646-91, Annual Book of ASTM Standards, ASTM, Philadelphia, PA, 1992, vol. 03.01, p. 667

5. J.A. Wagner and R.P. Gangloff: Scripta Metall., 1992, vol. 26, pp. 1779-1784.

6. J. Glazer, S.L. Verzasconi, R.R. Sawtell and J.W. Morris, Jr.: Metall. Trans. A, 1987, vol. 18A, pp. 1695-1701.

7. "Standard Test for JIc, A Measure of Fracture Toughness," Designation E813-89, Annual Book of ASTM Standards, ASTM, Philadelphia, PA, 1992, vol. 03.01, p. 732.

8. J.W. Hutchinson: J. Appl. Mech., Trans. , ASME, 1983, vol. 50, pp. 1042-51.

9. P.C. Paris, H. Tada, A. Zahoor and H. Ernst: in Elastic-Plastic Fracture, ASTM STP 668, Philadelphia, PA, 1979, pp. 5-36.

10. K.T. Venkateswara Rao and R.O. Ritchie: Acta Metall., vol. 38, No. 11, 1990, pp. 2309-2326.

11. W.C. Porr, Jr., and R.P. Gangloff: Metall. Trans. A , 1994, vol. 25A, pp. 365-379.

12. D.J. Dingley: Scanning Electron Microscopy, 1984, vol. 2, p. 569.

Table I. Transverse tensile* and LT toughness behavior of 12mm specimens as a function of temperature.

Temp (°C)	E (GPa)	σ_{ys} (MPa)	n	J_{Ic} (kJ/m^2)	J_{Ici} (kJ/m^2)	K_{JIc} (MPa$\sqrt{m}$)	K_{JIci} (MPa$\sqrt{m}$)	T_R
25°C	77.2	537	.052	10.7**	9**	30.5	28	1.5**
-25°C	81.4	548	.054	9.6	9	29.6	29	1.2
-75°C	83.4	570	.055	9.1	7	29.2	26	1.4
-125°C	84.1	588	.062	11.0	10	32.2	31	1.9
-155°C	85.5	595	.076	8.0	7	27.7	26	2.1
-185°C	87.6	607	.081	16.1$^+$	13$^+$	39.7	35	2.8$^+$

* Machined from fracture toughness specimen

** Average of four specimens

$^+$Average of two specimens

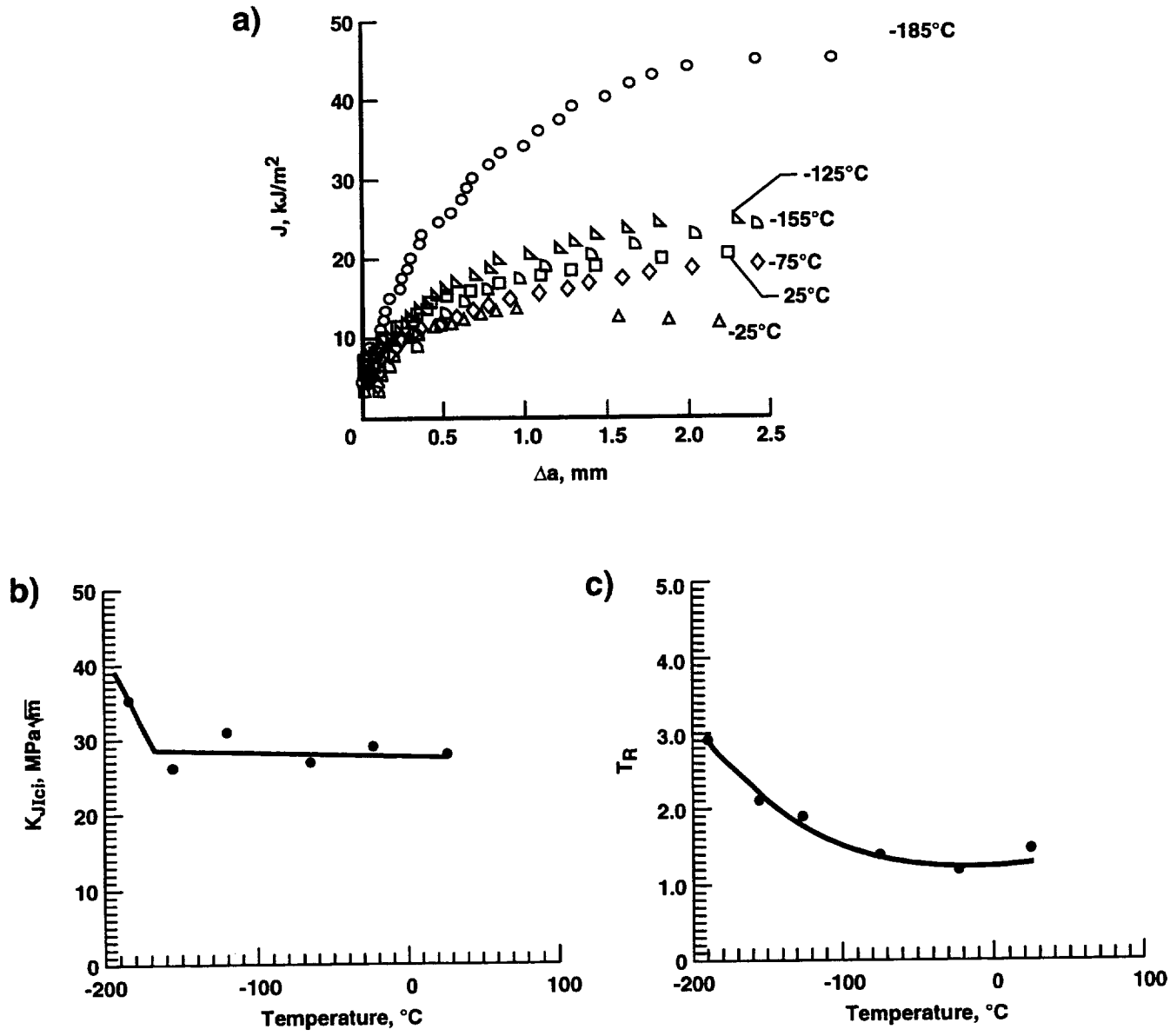

Figure 1. A. R-curves of 12mm thick specimens at -185°C to 25°C
B. Fracture toughness, K_{JIci}, of 12mm thick 2090-T81 as a function of temperature.
C. Tearing modulus of 12mm thick 2090-T81 as a function of temperature.

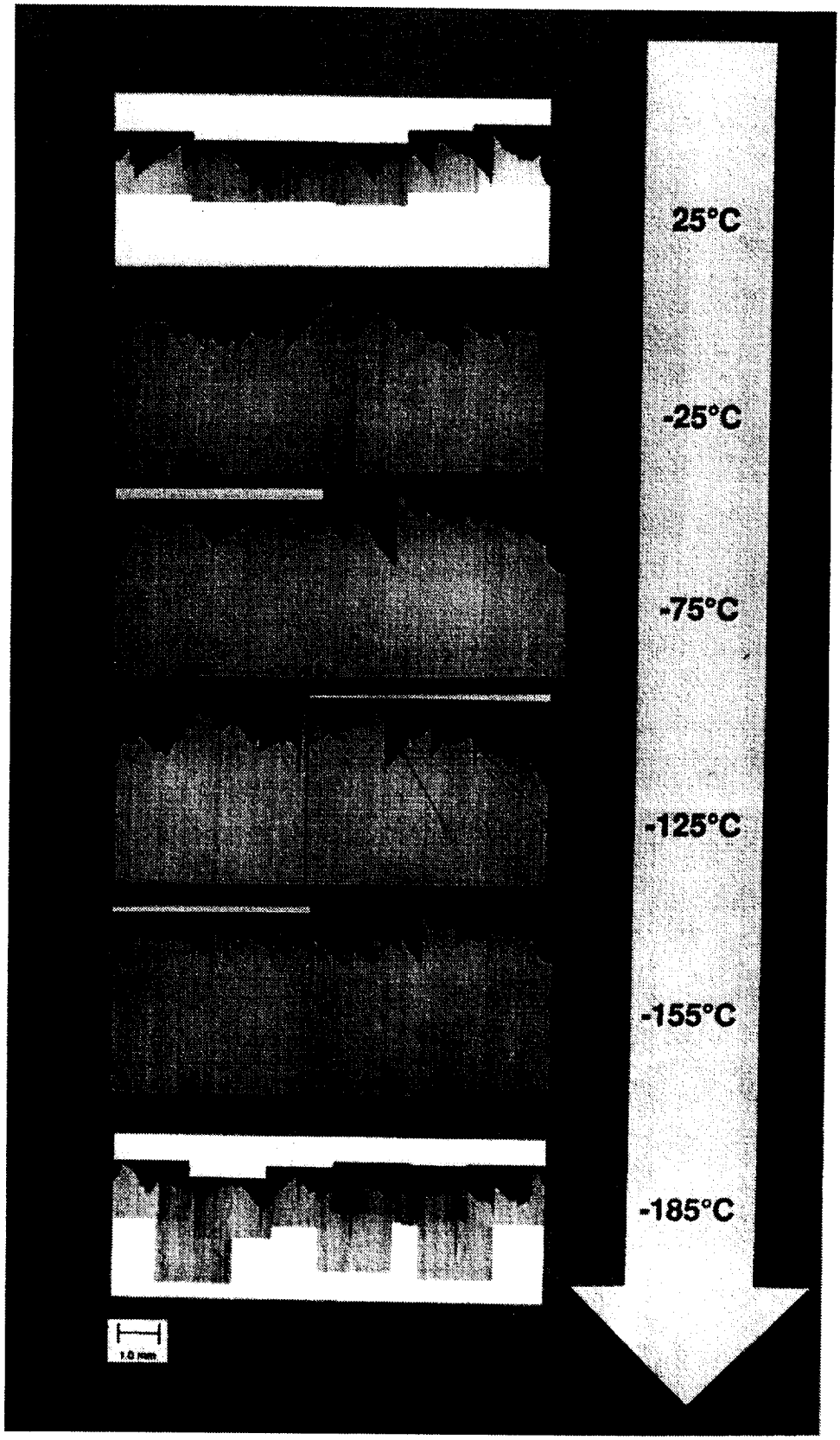

Figure 2. Fracture surface cross section of 2090-T81 as a function of temperature

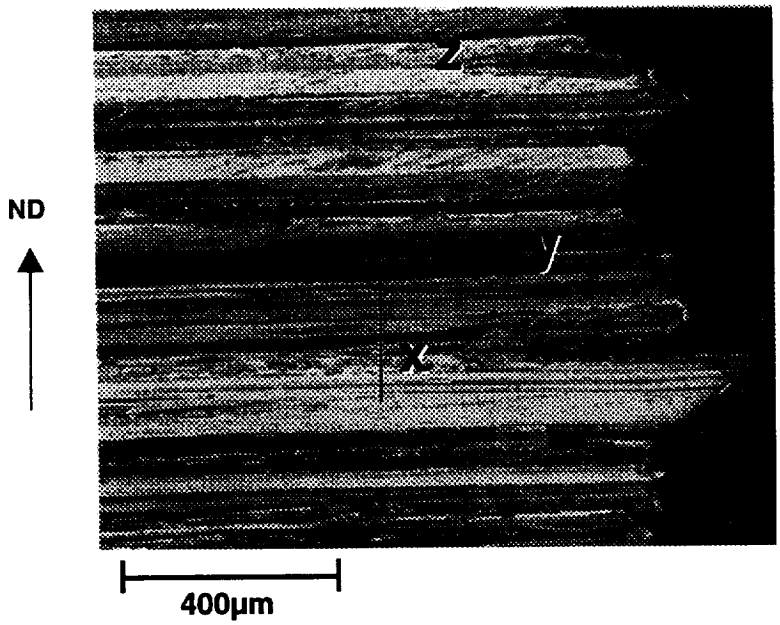

Figure 3. Optical micrograph in polarized light of an L-S section of sample tested at -185°C.

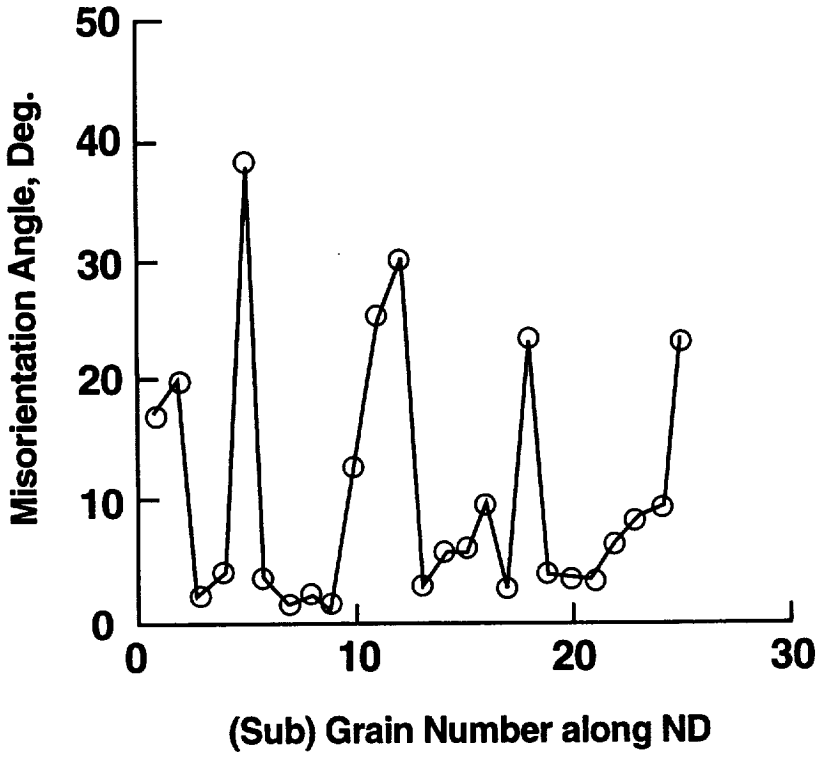

Figure 4. Misorientation angle as a function of the (sub)grain number, along ND.

micro & graph fig 3&4

Project #3 **The Effect Of Cryogenic Temperature On The Fracture Toughness Of Weldalite™ X2095**

Cynthia L. Lach and Richard P. Gangloff

Objective

The objective of this research is to characterize the effect of cryogenic to mildly elevated temperature on the tensile deformation and fracture toughness of an emerging composition of Weldalite™-type alloys. We will determine quantitative stress versus strain data, and initiation and growth fracture toughnesses, as well as the associated microscopic fracture mechanisms, and conduct micromechanical modeling to understand temperature-dependent fracture.

Background

Aluminum-lithium-copper alloys are being developed to replace conventional 2XXX and 7XXX aluminum alloys for aerospace structural applications. Al-Li-Cu alloys such as 2090 offer increased stiffness and decreased density due to lithium, and exhibit increased strength and potentially increased fracture toughness with decreasing temperature from room to cryogenic levels[1-4]. Increasing toughness at cryogenic temperature facilitates fracture mechanics damage tolerant designs because cold proof-testing is not required; a room temperature evaluation suffices. With the addition of Ag, Al-Li-Cu alloys exhibit exceptionally high yield strength, that further increases with decreasing temperature[5], without the necessity for post-solution treatment stretch deformation[6]. The fracture toughness of such alloy compositions must be understood as a function of temperature.

Technical Approach

The approach to this research was outlined in past renewal proposals[7,8].

Material

Two Weldalite™ compositions were selected for study to examine the limits of the Cu and Li levels for the alloy registered as AA2095[9]. Specifically, a high Cu-Li alloy (Al-4.64Cu-1.53Li- 0.34Ag-0.37Mg-0.17Zr; wt%) at the upper extreme of the AA2095 specification[9], and a low copper alloy (Al-4.04Cu-1.00Li-0.37Ag-0.36Mg-0.15Zr; wt%) at the low end of the AA2095 composition specification and in the middle of the AA2195 specification[9] were chosen for evaluation. For clarity in this report, the high Cu-Li alloy will be referred to as AA2095 and the low Cu-Li alloy will be referred to as AA2195 (old X2095).

The selected alloys should contain substantially different amounts of primary phase to enable examination of the effect of this feature on fracture toughness. Several artificial aging conditions, produced at NASA-LaRC, will be employed to vary yield strength, work hardening rate, and the volume fraction and distribution of the θ' and T_1 strengthening precipitates. Metallurgical and temperature effects on toughness will be assessed for similar flow properties.

Deformation and Fracture

The approach of the proposed research will follow that developed by Haynes in Project #1 and Wagner in Project #2. Measurements will produce uniaxial tensile stress-strain relationships and J-Integral based crack initiation and growth fracture toughnesses. This latter method will enable determination of plane strain fracture toughness data from relatively thin specimens (eg., 3.9 mm thick), as well as an estimate of the plane stress crack growth resistance. Microstructural effects on the complete crack initiation and growth resistance relationship will be studied.

Progress During the Reporting Period

The emphasis of recent research has been on addressing the following three important issues[10-12].

(I) ***Why are replicate fracture toughness values variable? Are such differences intrinsic to the alloys under study, or is ASTM Standard E813 inadequate for thin specimens of aluminum alloy?***

(II) ***What is the effect of temperature on the tensile deformation and toughness of optimally processed AA2095 and AA2195?***

(III) ***What is the mechanism for temperature-(in)dependent fracture in optimally processed AA2095 and AA2195?***

The AA2095 and AA2195 variants of Weldalite™ X2095 were characterized in terms of 25°C and -185°C tensile deformation behavior and fracture toughness. To investigate the effect of various strength levels on the fracture toughness of X2095, each alloy was aged at 143°C for 10, 20, 30 and 72 hours.

Issue I: Effects of Alloy Chemistry, Aging Condition and Test Temperature on Replicate Fracture Toughness Values.

Initially the effects of alloy chemistry, aging condition and test temperature on the tensile deformation behavior and fracture toughness of the X2095 alloy variants were investigated. The effect of chemistry on the fracture toughness behavior was apparent at any constant yield strength. For a given yield strength, the fracture toughness values were significantly lower for the high Cu-Li alloy variant at both test temperatures. This result was supported by the presence of a large volume fraction of undissolved particles in the high Cu-Li variant because its composition exceeds solid solubility at the solution treatment temperature that was employed, as discussed in previous progress

reports.[10-12] Thus, the low Cu-Li alloy variant (AA2195) is the preferred chemistry for fracture toughness optimization.

The effect of aging was more apparent for AA2195, where the fracture toughness was very sensitive to the age and therefore yield strength. Small changes in yield strength resulted in large changes in fracture toughness. This yield strength dependency could explain the increased scatter in the fracture toughness data for AA2195. Superior fracture toughness was observed in the underaged condition (10 hrs at 143°C) when compared to the peak-strength aged condition.

The effect of test temperature was negligible. For a given aging condition, both alloy variants maintained essentially constant fracture toughness as temperature decreased from ambient to -185°C, while experiencing a significant increase in yield strength. Toughness did not increase with decreasing temperature, as expected based on limited literature data for several Weldalite™ compositions.

Due to Langley Research Center involvement in the Super Lightweight Tank program (SLWT), additional AA2195-T3 (12.7 mm plate, referred to as plate "G") was obtained to further investigate pertinent fracture issues, specifically the yield strength dependency and variable results of the low Cu-Li alloy variant. The effect of aging (7, 10, 15, 24, and 30 hours at 143°C) on uniaxial tensile deformation and fracture toughness will be examined at ambient temperature. The additional time intervals of 7 and 15 hours were selected to characterize the increased toughness that was observed in the underaged condition. Ten 3.9 mm thick C(T) specimens have been heat treated and machined in the L-T orientation. Precracking of these specimens is underway, after which duplicate fracture tests will be conducted at ambient temperature.

The chemistry and metallography of plate G (AA2195) were defined to verify that the material was similar to the low Cu-Li alloy variant (AA2195, old X2095) studied previously. Inductively

coupled plasma (ICP) chemical analysis was conducted on samples, in the form of shavings, which were dry milled from various locations through the thickness (t/8, t/4, t/2, 3t/4 and 7t/8) of the 12.7 mm plates. AA2095, AA2195 (old X2095) and AA2195 (Plate G) were characterized. Plate G was produced in 1994 while the two X2095 alloy variants were produced in 1990 and 1991, respectively. The resulting values in Table I are the averages of triplicate analyses and exhibited little scatter. Table II shows the individual Cu analyses conducted on the X2095 alloy variants. The data appear well behaved and exhibit very little scatter. Table III shows the registered composition limits of Weldalite™ alloys[9].

The results of the chemical analyses suggest a significant level of Cu segregation, as indicated by the consistently low Cu content at the mid-plane (t/2) location. The least amount of Cu segregation with respect to the mid-plane was observed for AA2095, while the greatest was observed for AA2195 (old X2095). AA2095 has an average through-the-thickness chemistry of 4.72wt%Cu, which is outside of the registered composition specification (3.9 to 4.6wt%). For AA2195 (old X2095), the bulk chemistry is 4.05wt%Cu which falls within the specification (3.7 to 4.3wt%); however; the midplane chemistry is 3.58wt%Cu, which is outside of the composition specification. The SLWT material, AA2195(plate G), had a mid-plane chemistry of 3.55 and 3.65wt%Cu which are outside of the composition specification.

Metallography on AA2195-T3 plate G, revealed comparable through-thickness variation in grain structure as had been previously reported for AA2195 (old X2095). At the mid-plane, where the C(T) specimens were machined, the microstructure was predominantly unrecrystallized. The through-thickness chemistries and metallography revealed that AA2195 of 1991 vintage is similar to AA2195 plate G produced in 1994.

An aging study was conducted at 143°C for the two X2095 alloy variants to characterize more completely the age hardening

response of this alloy. Originally, the aging study was conducted up to 100 hours, as depicted by the open symbols in Figure 1, however, neither alloy overaged in that time frame. The extended aging study (24, 72, 100, 198, 334, 408, 502, and 768 hours) results are shown as filled symbols in Figure 1. AA2095 with high Cu-to-Li was stable with respect to hardness throughout the 768 hour time frame. No evidence of overaging was observed as a hardness of 92.0+/-0.4 HRB was maintained from 100 to 768 hours. AA2195 (old X2095) with low Cu-to-Li began to overage between 100 and 198 hours, which was followed by a hardness plateau through 502 hours, before significantly overaging. The overall hardness results of the extended aging study were approximately 2 hardness Rockwell B scale (HRB) lower than the original study; however, incremental hardness changes with corresponding time changes for 24, 72 and 100 hours, resulted in the same relative change in hardness for the two heat treat runs.

Issue II: The effect of Temperature on the Uniaxial Tensile Deformation of Optimally Processed AA2095 and AA2195.

Uniaxial tensile deformation and fracture toughness tests were conducted as a function of temperature (-185, -140, -125,-75, -25, 25 107, and 135°C) on AA2195 (old X2095) aged for 30 hours at 143°C. Selected tests were conducted on AA2095 aged for 20 hours at 143°C for comparison purposes. Increased yield strength and work hardening are observed for each alloy with decreasing temperature to cryogenic levels as shown in Table IV. An absence of work hardening was observed at 135°C for both alloys, and at 107oC for AA2195. AA2195 exhibited slightly higher tensile properties compared to AA2095 alloy for the two aging conditions and at each deformation temperature.

Data obtained from the fracture toughness experiments, addressing the effect of test temperature for a constant aging

condition, are undergoing analysis. The uniaxial tensile ductility of AA2195 (approximated by %RA) declined with decreasing test temperature, with the suggestion of a plateau below about-75°C. The intrinsic ductility of high Cu-to-Li AA2095 was a minimum at 25°C, and increased with both increasing and decreasing deformation temperature. The ductility increase between ambient and cryogenic temperatures was small. The ductility of the high Cu/Li alloy is lower than that of AA2195 at each test temperature, consistent with fracture toughness data. The tensile results in Table IV (and Table VI) are sufficient to predict the temperature dependence of the plane strain initiation fracture toughness, through a critical strain based micromechanical model, as discussed by Haynes in Project #1.

Variation was observed in these tensile data which were generated at two different times. It was shown previously that the fracture toughness of AA2195 is sensitive to small variations in yield strength. Therefore, potential sources contributing to these variations were examined more closely. The strength data for AA2195 at 25°C were approximately 4% higher when most recently measured compared to the original tensile experiments (see Table V). Hardness measurements of the AA2195 tensile bars tested at 25°C revealed an increase from 51 HRA to 53.5 HRA between the two test set-ups. Ductility (%RA) at 25°C did not decrease, as expected when correlated with these strength and hardness increases. The data for AA2195, in the second test set-up at-185°C, were 0.5% higher in yield strength than the original test set-up, which was consistent with the small increase in room temperature hardness (52 to 52.5 HRA). However, ductility (%RA) was substantially less for the second setup. The data for AA2095 at 25°C showed an increase in yield and ultimate strengths of 2.4% and 3.5%, respectively between test set-ups, which was consistent with the small increase in hardness (50 to 51 HRA).

For both tensile test sets, the same heat treatment oven, test apparatus, and personnel were employed. Minor time and

temperature differences could account for significant changes in hardness values. Thus, small variations in heat treatments and/or the occurrence of natural aging between test set-ups could have contributed to the differences observed in the hardness measurements. However, 1 to 3 tensile samples per condition may be too small of a sample size to make statistically sound measurements of the differences in tensile properties between test set-ups. With regards to the AA2195 -185°C yield strength data, for both test set-ups, most of the data were clustered with one outlier. Additional tests need to be conducted to define the actual range of the data, as well as the scatter. It is important to note that the highest source of variability was in the first test set-up for AA2195 where the yield strength at -185°C varied by ±6.9 MPa. Thus, the maximum variation within a test set-up was greater than between test set-ups.

No effect of temperature on the amount of variation in test data was observed. For the second test set-up, using duplicate tests, the yield and ultimate strengths either had no variation or were identical (±4.9 MPa). The ±4.9 MPa variation was a coincidence and did not correlate to the smallest load increment measurable. No systematic effect of temperature on the amount of variation in test data was detected during the first test set-up; where zero, ±4.0 MPa and ±4.9 MPa were observed. The issues of variation in tensile and fracture toughness tests will be addressed in the aging study of the SLWT plate G.

Tensile precision modulus tests were conducted on AA2195 (old X2095) aged for 30 hours at 143°C (see Table VI). Specimens were machined from the mid-plane of the plate in the longitudinal orientation. The tests were conducted in accordance with ASTM E111, the Standard Test Method for Young's Modulus, Tangent Modulus, and Chord Modulus at 25°C and -185°C. An average modulus was determined from three runs per specimen at each test condition. The modulus of AA2195 increased by approximately 6% from ambient to cryogenic temperatures (-185°C). The critical

alignment criteria was met for all of the tests, while the coefficient of variation was twice as good as expected for aluminum alloys.

Conclusions

- oo Chemical analyses of three variants of Al-Li-Cu-Ag Weldalite™ suggest a significant level of Cu segregation, as indicated by the consistently low Cu content at the mid-plane (t/2) location. The least amount of Cu segregation with respect to the mid-plane was observed for AA2095, while the greatest was observed for the AA2195 (old X2095).
- oo Metallography of AA2195-T3 plate G revealed similar through-the-thickness variation in grain structure, as previously reported for AA2195 (old X2095). At the mid-plane, where the C(T)specimens are machined, the microstructure was predominantly unrecrystallized.
- oo Through-thickness chemistry and metallographic analyses revealed that AA2195 produced in 1991 was very similar to AA2195 produced in 1994.
- oo The high Cu-Li alloy variant (AA2095) did not overage at 143°C in 768 hours, while the low Cu-Li variant (AA2195) began overaging after 100 to 200 hours.
- oo Increased elastic modulus, yield strength and work hardening are observed for each alloy with decreasing temperature to cryogenic levels, but intrinsic ductility (%RA) tends to decrease to a plateau, at least for AA2195. The ductility of AA2095 tends to increase with both decreasing and increasing temperatures from the ambient level. These data are sufficient to predict the temperature dependence of the plane strain initiation fracture toughness of AA2095 and AA2195.
- oo The modulus of AA2195 (aged for 30 hours at 143°C) increases by approximately 6% from ambient to cryogenic temperatures (-185°C).

Tasks for the Next Reporting Period

The fracture toughness experiments will measure the J-crack growth response, based on the automated unloading compliance method, to determine the effect of aging time at 143°C on the fracture toughness of AA2195 alloy (plate G) at ambient temperatures.

The uniaxial tensile deformation behavior of AA2195 alloy (plate G) will be measured as a function of aging condition (7, 10, 15, 24 and 30 hrs at 143°C) at ambient temperature. Tensile yield strength, work hardening and fracture strain (reduction in area) will be characterized as a function of temperature.

The critical strain-based micromechanical model developed by Ritchie and coworkers will be employed to predict the temperature dependence of KJIC based on measured tensile properties.

References

1. S. Suresh, A.K. Vasudevan, M. Tosten and P.R. Howell, "Microscopic and Macroscopic Aspects of Fracture in Lithium-containing Aluminum Alloys", Acta Metall., Vol.35, pp. 26- 46 (1987).

2. J. Glazer, S.L. Verzasconi, R.R. Sawtell and J.W. Morris, Jr., "Mechanical Behavior of Aluminum-Lithium Alloys at Cryogenic Temperatures", Metall. Trans. A., Vol. 18A, pp. 1695-1701 (1987).

3. K.T. Venkateswara Rao, Y. Weikang and R.O. Ritchie, "Cryogenic Toughness of Commercial Aluminum-Lithium Alloys: Role of Delamination Toughening", Metall. Trans. A., Vol. 20A, pp.485-487 (1989).

4. K.V. Jata and E.A. Starke, Jr., "Fracture Toughness of Al-Li-X Alloys at Ambient and Cryogenic Temperatures", Scripta Metall., Vol. 22, pp. 1553-1556 (1988).

5. W.T. Tack and L.W. Loechel, "Weldalite TM 049: Applicability of a New High Strength, Weldable Al-Li-Cu Alloy", in the Proceedings of the Fifth International Aluminum-Lithium Conference, T.H. Sanders, Jr. and E.A. Starke, Jr., eds., Vol. III, MCEP Ltd., Birmingham, UK, pp. 1457-1467 (1989).

6. Alex Cho and W. A. Cassada, "Effect of Cu and Cu:Li Ratio on T6 and T8 Temper Properties of Al-Cu-Li-Mg-Ag Alloys", Presented at Aero Mat 91, Long Beach, CA, May (1991).

7. R.P. Gangloff, "NASA-UVa Light Aerospace Alloy and Structures Technology Program", Proposal No. MS-NASA/LaRC-4841-91, University of Virginia, Charlottesville, VA (1992).

8. R.P. Gangloff, "NASA-UVa Light Aerospace Alloy and Structures Technology Program", UVa Report No. MSE-NASA/LaRC-5691-93, University of Virginia, Charlottesville, VA (1993).

9. A. Cho, R.E. Greene, M.H. Skillingberg, W.A. Cassada, H.M. Edwards, and P.S. Fielding, "Status of High Strength Al-Li Alloy Development at Reynolds Metals Company", presented at Aeromat '93, Anaheim, CA (1993).

10. R.P. Gangloff, "NASA-UVa Light Aerospace Alloy and Structures Technology Program", Report No. UVA/528266/MS93/111, University of Virginia, Charlottesville, VA, July (1994).

11. R.P. Gangloff, "NASA-UVa Light Aerospace Alloy and Structures Technology Program", Proposal No. MSE-NASA/LaRC-6074-94 University of Virginia, Charlottesville, VA (1993).

12. R.P. Gangloff, "NASA-UVa Light Aerospace Alloy and Structures Technology Program", Proposal No. MSE-NASA/LaRC-5669-93, University of Virginia, Charlottesville, Va (1992).

Table I. ICP Chemical Analysis of Weldalite™ 12.7 mm Plate
(Avg. of triplicate analyses)

X2095-T3 AA2095-T3	Cu	delta %	Li	Mg	Zr	Si	Fe	Ti	Mn	Zn	Ag
t/8	4.77	6.0	1.41	0.39	0.17	<mdl	0.08	0.04	<mdl	0.02	0.37
t/4	4.82	7.1	1.48	0.37	0.16	<mdl	0.08	0.04	<mdl	0.02	0.36
t/2	4.50	0	1.44	0.36	0.18	<mdl	0.07	0.05	<mdl	0.02	0.34
3t/4	4.78	6.2	1.44	0.40	0.16	<mdl	0.08	0.04	<mdl	0.02	0.36
7t/8	4.74	5.3	1.43	0.38	0.16	<mdl	0.08	0.04	<mdl	0.01	0.35
X2095-T3 AA2195-T3	**Cu**	**delta %**	**Li**	**Mg**	**Zr**	**Si**	**Fe**	**Ti**	**Mn**	**Zn**	**Ag**
t/8	4.18	16.8	0.87	0.36	0.15	<mdl	<mdl	0.02	<mdl	0.02	0.35
t/4	4.22	17.9	0.91	0.37	0.14	<mdl	<mdl	0.01	<mdl	0.02	0.38
t/2	3.58	0	0.92	0.33	0.16	<mdl	<mdl	0.02	<mdl	0.02	0.35
3t/4	4.13	15.4	0.93	0.36	0.14	<mdl	<mdl	0.01	<mdl	0.02	0.38
7t/8	4.12	15.1	0.91	0.37	0.14	<mdl	<mdl	0.01	<mdl	0.02	0.38
AA2195-T3 Plate G #1	**Cu**	**delta %**	**Li**	**Mg**	**Zr**	**Si**	**Fe**	**Ti**	**Mn**	**Zn**	**Ag**
t/8	4.05	11.0	0.94	0.42	0.096	*	*	*	*	*	0.41
t/4	4.04	10.7	0.94	0.42	0.10	*	*	*	*	*	0.42
t/2	3.65	0	0.93	0.40	0.10	*	*	*	*	*	0.41
3t/4	4.03	10.4	0.94	0.41	0.10	*	*	*	*	*	0.42
7t/8	4.01	9.9	0.94	0.42	0.10	*	*	*	*	*	0.44
AA2195-T3 Plate G #2	**Cu**	**delta %**	**Li**	**Mg**	**Zr**	**Si**	**Fe**	**Ti**	**Mn**	**Zn**	**Ag**
t/8	3.97	11.8	0.92	0.42	0.10	*	*	*	*	*	0.40
t/4	3.98	12.1	0.92	0.41	0.10	*	*	*	*	*	0.40
t/2	3.55	0	0.92	0.39	0.10	*	*	*	*	*	0.38
3t/4	4.01	13.0	0.94	0.43	0.09	*	*	*	*	*	0.38
7t/8	4.03	13.5	0.96	0.41	0.10	*	*	*	*	*	0.42

<mdl, less than the minimum detection limit
*, not tested

Table II. Individual ICP Chemical Analysis of Cu for X2095 Alloy Variants

Alloy	Location	Cu	Avg.	S Dev.
X2095-T3	t/8	4.793, 4.780, 4.749	4.774	0.023
AA2095-T3	t/4	4.760, 4.802, 4.904	4.822	0.074
	t/2	4.479, 4.520, 4.494	4.497	0.021
	3t/4	4.816, 4.735, 4.787	4.779	0.041
	7t/8	4.789, 4.778, 4.646	4.738	0.079
Alloy	**Location**	**Cu**	**Avg.**	**S Dev.**
X2095-T3	t/8	4.233, 4.159, 4.151	4.181	0.045
AA2195-T3	t/4	4.201, 4.213, 4.252	4.222	0.027
	t/2	3.601, 3.564, 3.584	3.583	0.019
	3t/4	4.114, 4.150, 4.110	4.125	0.022
	7t/8	4.104, 4.119, 4.127	4.117	0.011

Table III. Registered Composition limits of Weldalite^{TM}049 Alloys[9]

ELEMENTS	AA2095	AA2195
Cu	3.9-4.6	3.7-4.3
Li	.70-1.5	.80-1.2
Mg	.25-.80	.25-.80
Ag	.25-.60	.25-.60
Zr	.04-.18	.08-.16
Mn	.25 max	.25 max
Zn	.25 max	.25 max
Fe	.15 max	.15 max
Si	.12 max	.12 max
Ti	.10 max	.10 max
Al	Remainder	Remainder

Table IV. Tensile Properties of Peak-Aged Weldalite^{TM}X2095 Alloy Variants

X2095 Alloy Variant	Test Temp,°C	Yield Strength, MPa	Tensile Strength, MPa	% Elongation 25.4mm gage	%RA	Young's Modulus GPa	Strain hardening exponent, η
AA2195	135	537.8	537.8	13.6	44	76.5	0
AA2195	107	558.5	558.5	14.0	40	78.6	0
AA2195	25	599.8	627.4	11.4	32	75.8	0.0472
AA2195	25	606.7	627.4	10.6	31	75.8	0.0460
Average	**25**	**603.3**	**627.4**	**11.0**	**31.5**	**75.8**	**0.0466**
AA2195	-25	620.5	648.1	10.0	28	76.5	0.0494
AA2195	-25	620.5	648.1	10.0	26	77.9	0.0463
Average	**-25**	**620.5**	**648.1**	**10.0**	**27**	**77.2**	**0.0479**
AA2195	-75	641.2	668.8	9.4	21	80.7	0.0500
AA2195	-125	655.0	703.3	9.2	18	81.4	0.0528
AA2195	-125	661.9	696.4	11.2	22	82.0	0.0566
Average	**-125**	**658.5**	**699.9**	**10.2**	**20**	**81.7**	**0.0547**
AA2195	-140	661.9	710.2	10.4	22	80.7	0.0556
AA2195	-140	668.8	717.1	10.6	21	81.4	0.0591
Average	**-140**	**665.4**	**713.7**	**10.6**	**21.5**	**81.0**	**0.0574**
AA2195	-185	689.5	758.4	10.4	13	82.0	0.0671
AA2195	-185	696.4	758.4	10.6	17	81.4	0.0647
Average	**-185**	**693.0**	**758.4**	**10.6**	**15**	**81.7**	**0.0659**
AA2095	135	524.0	524.0	9.6	22	76.5	0
AA2095	107	551.6	558.5	8.8	15	77.2	0.0230
AA2095	25	586.1	620.5	7.2	9	77.9	0.0563
AA2095	-75	599.8	634.3	8.0	12	82.0	0.0539
AA2095	-140	620.5	668.8	9.4	11	82.7	0.0580

Peak-age of AA2195 (4.04Cu-1.00Li) = 30 hours at 143°C
Peak-age of AA2095 (4.64Cu-1.53Li) = 20 hours at 143°C

Table V. Comparison of Tensile Properties of Peak-Aged Weldalite™X2095 Alloy Variants

1st Test Set-up	Test Temp, °C	Yield Strength, MPa	Tensile Strength, MPa	% Elongation 25.4mm gage	%RA	HRA at 25°C	Young's Modulus GPa	Strain hardening exponent, η
AA2195	25	579.2	606.7	11.8	-	52	72.4	0.046
143°C (30 hrs)	25	579.2	599.8	10.0	23	51	72.4	0.045
	25	572.3	599.8	11.6	32	50	71.7	0.047
Average	**25**	**576.9**	**602.1**	**11.0**	**27.5**	**51**	**72.4**	**0.046**
AA2195	-185	689.5	744.6	10.2	-	52	83.4	0.067
143°C (30 hrs)	-185	696.4	751.5	10.0	23	52	83.4	0.065
	-185	682.6	744.6	10.4	22	51	82.7	0.068
Average	**-185**	**689.5**	**746.9**	**10.2**	**22.5**	**52**	**83.2**	**0.067**
AA2095	25	572.3	599.8	6.8	-	50	74.5	0.050
143°C (20 hrs)	-185	675.7	730.8	8.2	-	51	84.1	0.061
2nd Test Set-up								
AA2195	25	599.8	627.4	11.4	32	53	75.8	0.0472
143°C (30 hrs)	25	606.7	627.4	10.6	31	54	75.8	0.0460
Average	**25**	**603.3**	**627.4**	**11.0**	**31.5**	**53.5**	**75.8**	**0.0466**
AA2195	-185	689.5	758.4	10.4	13	53	82.0	0.0671
143°C (30 hrs)	-185	696.4	758.4	10.6	17	52	81.4	0.0647
Average	**-185**	**693.0**	**758.4**	**10.5**	**15**	**52.5**	**81.7**	**0.0659**
AA2095 143°C (20 hrs)	25	586.1	620.5	7.2	9	51	77.9	0.0563

- not measured

Table VI. Precision Modulus Tests of Peak-aged X2095(AA2195)

Spec. I.D.	Test temperature, °C	Young's Modulus (GPa)	Alignment % difference from avg.	Coefficient of Determination, r^2	Coefficient of Variation, %, V_1
4I	25	76.0	± 1.22	0.99999	0.043
4I	25	75.9	± 1.53	0.99999	0.043
4I	25	76.0	± 1.72	0.99999	0.035
4I	25	Average 76.0			
4H	25	75.6	± 2.24	0.99999	0.027
4H	25	75.7	± 2.66	0.99999	0.028
4H	25	75.3	± 2.45	0.99999	0.038
4H	25	Average 75.5			
4I+4H	**25**	**Overall Average 75.7**			
4I	-185	81.0	± 1.36	0.99987	0.262
4I	-185	80.1	± 1.49	0.99991	0.178
4I	-185	80.3	± 1.92	0.99995	0.092
4I	-185	Average 80.4			
4H	-185	80.3	± 1.51	0.99999	0.047
4H	-185	80.4	± 1.96	0.99998	0.065
4H	-185	80.2	± 1.81	0.99998	0.053
4H	-185	Average 80.3			
4I+4H	**-185**	**Overall Average 80.4**	(Peak-age for AA2195 is 30 hours at 143°C)		

ASTM E 111 Section 8.3

Note: Modulus determination was made at strains < 0.25%
The strain increments between the initial-load and the final-load measurement on opposite sides of the specimens should not differ from the average by more than **3%**.

ASTM E 111 Section 9.2 Note 12:

It is recommended that the coefficient of variation, V_1, be no larger than 2%; however with care, values less than **0.5%** have been found to be achievable in aluminum alloys.

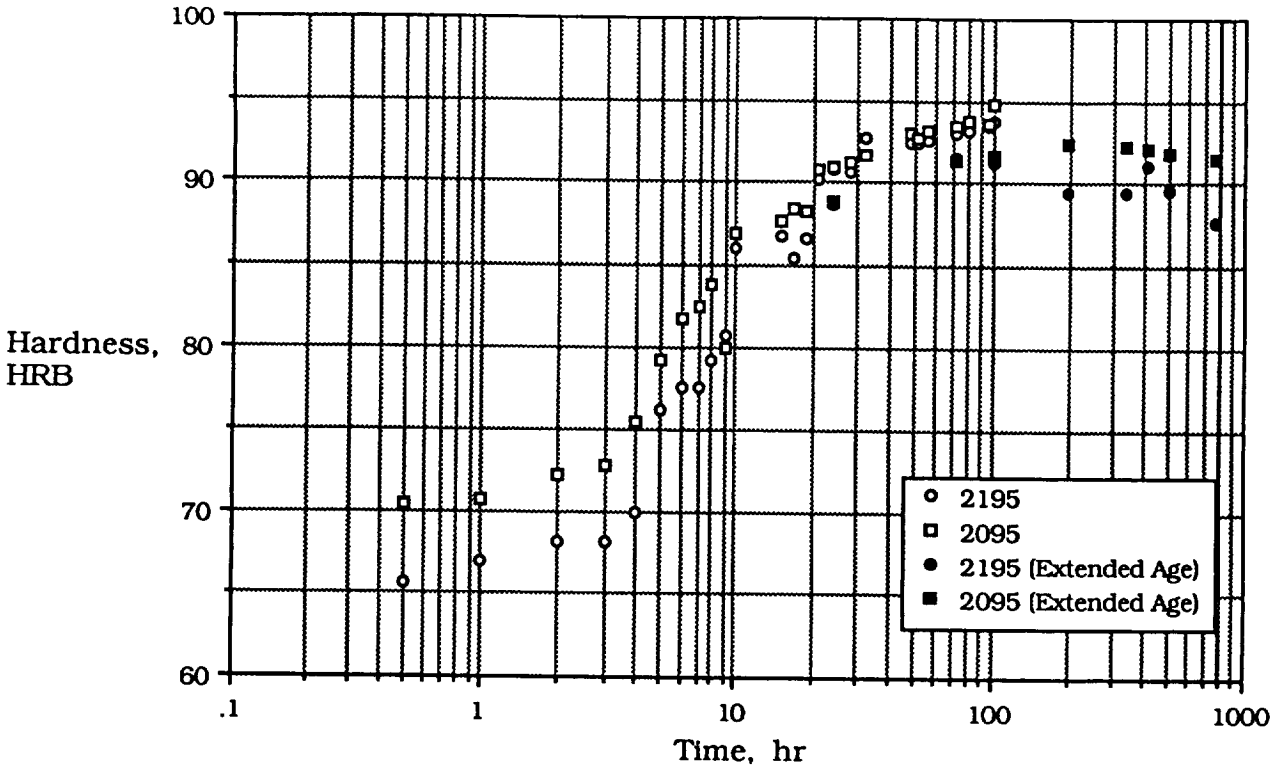

Figure 1. Age hardening response of X2095 alloy variants at 143°C.

Project #4 **Mechanisms Of Localized Corrosion In Alloys 2090 And 2095**

F. Douglas Wall and Glenn E. Stoner

Research Objectives

The overall objective of this research project is to elucidate a mechanism for environmentally assisted cracking (EAC) in advanced aluminum alloys based on the interactions of microstructural features and localized environments. The questions which have received the greatest attention to date include:

1. What are the conditions under which a crack will propagate in high strength aluminum-lithium-copper alloys?

2. What is the effect of material composition and temper on crack propagation rates and EAC fracture morphology?

3. Are there microstructural features which form pathways capable of sustaining dissolution based crack growth?

4. What is the occluded chemistry in an EAC crack?

Early research was focused on determining conditions in which a flaw would propagate sufficiently to cause failure in smooth-bar tensile samples under conditions of defined mechanical loading, bulk aqueous environment and applied electrochemical potentials. Next the electrochemistry of model microstructural features was assessed in order to propose candidate cracking pathways. Concurrent with this work was an initial investigation into occluded chemistries generated by large areas of material exposed to a small solution volume, intending to simulate the conditions of an isolated pit.

Over the last year the criteria established for propagation of cracks has been refined by the development of an experimental

setup which allows the simultaneous control of bulk environment, applied electrochemical potential and stress intensity. Using this apparatus, initial steps have been taken towards correlating crack propagation rates to applied stress intensity and material temper. Future research will be focused on careful examination of the roles of composition, temper, applied stress intensity and applied electrochemical potential in the environmental cracking of Al-Li-Cu alloys.

Background and Previous Results

Explanations for the environmentally assisted cracking (EAC) of aluminum-lithium-copper alloys fall broadly into two categories: (1) embrittlement mechanisms which usually cite hydrogen as the embrittling species[1-4] and (2) dissolution mechanisms which link heterogeneous corrosion of microstructural features to propagation of cracks[5-16]. The dissolution based models were used as the starting point for this research effort and will receive priority in this discussion. The research efforts of Smith and Scully uniquely address hydrogen interactions in Al-Li-Cu alloy 2090 and their review can be found elsewhere in this grant report.

A starting point for determining what causes cracking in any material/environment combination is to identify conditions in which cracking occurs and conditions in which cracking does not occur then attempt to isolate what critical feature or features differentiates the systems. In the Al-Li-Cu / Salt water system there is a propensity for rapid cracking to occur under conditions of alternate immersion whereas only pitting is observed for constant immersion[5-7]. Similarly, samples held under constant immersion then removed to laboratory air exhibit cracking while those removed to CO_2 free air do not appear to suffer from EAC[5-7]. These phenomena were first demonstrated by Holroyd and Craig for alloy 8090[5,6] and later by Moran for alloy 2090[7].

These early observations suggested that cracking of Al-Li-Cu

alloys in a chloride environment is dependent on removal of the bulk aqueous environment. In either alternate immersion testing or long term constant immersion testing followed by air exposure the wet portion of the test allows for pitting to occur on the material surface[7]. Upon removing the sample from the bulk environment, pits which have formed on the sample surface may retain electrolyte and subsequently develop a solution chemistry different from what was present during the wet cycle of the experiment. In an attempt to determine a probable isolated pit solution chemistry, Holroyd exposed turnings from an Al-Li-Cu alloy to small volumes of NaCl solution[5]. His data indicated that exposure of a large surface area of material to a small solution volume would result in the development of an alkaline pH (between pH 8 and 10) and a solution enriched in lithium ion content (concentrations ranging between 0.2 and 10 mMol). From the work of Holroyd and Craig a model was proposed to account for the behavior of 8090 in chloride environments: (1) under conditions of constant immersion the NaCl environment acts to depassivate the grain boundaries as well as grain interiors and initiation of a sharp crack is prevented, (2) removing a sample from the bulk solution allows the isolated environment to develop an alkaline chemistry due to the presence of atmospheric CO_2 causing precipitation of $LiALO_2$ and propagation of a crack due to the borderline active/passive behavior of the crack tip.

Moran[7] duplicated the experimental approach established by Craig and Holroyd demonstrating that the phenomenon of pre-exposure embrittlement was observed for alloy 2090. Moran proposed a more direct role for CO_2 in forming the passivating species (possibly Li_2CO_3) which resulted in EAC propagation. Additionally, he and others[7-10] suggested that the heterogeneous precipitation of the T_1 phase might provide a pathway along sub-grain boundaries for dissolution based EAC. Buchheit[10-12] furthered the argument for a T_1 based mechanism by investigating the

electrochemical behavior of a bulk ingot intended to simulate the T_1 phase. He determined that this phase is highly active compared to the matrix phase in a simulated crevice environment[11].

Continued work on 2090 by Buchheit and Wall[13-14] revealed a correlation between the electrochemical parameters of the T_1 and the matrix (α-Al) phases and the EAC behavior of the bulk material under conditions of specified environment, mechanical stress and applied electrochemical potential. In a simulated occluded environment such as 0.6M NaCl + 0.1M Li_2CO_3 the breakdown potential (E_{BR}) of α-Al is shifted to a more noble potential than that of the T_1 phase. The two E_{BR} values define a potential window in which the T_1 phase is highly active while the matrix remains passive. Smooth bar tensile samples loaded to 60%YS and polarized within this potential window showed rapid times-to-failure (less than 1 day). However, samples polarized cathodic to E_{BR-T1} did not fail nor show any signs of localized attack after five days of testing. From these results Buchheit concluded that rapid EAC failures in alloy 2090 can occur in a lithium carbonate crevice environment possibly due to the preferential dissolution of the T_1 phase.

Although the T1 phase has been observed to preferentially precipitate along sub-grain boundaries versus the matrix interior in Al-Li-Cu alloys[17-18], the coverage of sub-boundaries is not continuous. Additionally, elements added to enhance precipitation (i.e. Mg and Ag) as well as cold work prior to aging can result in a more homogeneous distribution of this phase[19-21]. These observations make it necessary to refine the model of EAC along an active T1 pathway in order to explain crack propagation in the regions separating the precipitates.

Early efforts of this research project examined the electrochemistry of a modeled copper depleted boundary in order to determine the feasibility of this feature as a pathway for anodic dissolution based EAC[15-16]. Scratching and straining electrode tests were used to determine critical electrochemical potentials

at which materials would undergo a transition from spontaneous repassivation to propagation of corrosion. Critical electrochemical potentials determined for Al-Cu binaries in aqueous $NaCl/Na_2CrO_4$ were observed to increase with increasing Cu content[16] similar to the effect reported by Gavele for pitting potentials of Al-Cu binaries in NaCl solution[22]. Critical potentials determined for tempered Al-Li-Cu alloys were seen to decrease with increasing aging time. Scratching electrode/ constant load testing performed on smooth tensile samples revealed a transition from no material failures to rapid failures occurring at the same critical potentials determined via scratching electrode experiments on unstressed coupons [15-16]. Based on these experiments it was concluded that under conditions of specific solution chemistry and applied electrochemical potential a Cu-depleted sub-boundary would be active compared to the grain interiors. Overall, electrochemical studies of modeled microstructural features indicated that a copper depleted zone and the T1 phase were likely candidates for defining an active pathway for anodic dissolution based EAC in Al-Li-Cu alloys.

The above conclusions were reached based on experimentation performed in either a 0.6M NaCl + 0.1M Li_2CO_3 or a 0.1M NaCl + 0.1M Na_2CrO_4 aqueous environment. While these environments have proven useful in studying EAC of Al-Li-Cu alloys, it is unclear if the they are suitable models for the occluded chemistries which develop during EAC of these alloys in a more standard marine environment. A number of experiments have been presented[15] which simulate an occluded chemistry by exposing large surface areas of material to small volumes of NaCl solution. These conditions are intended to model the condition of the solution within a pit during the dry cycle of an AI test in which there is no bulk solution in contact with the specimen. Experiments have indicated that an alkaline environment develops with Li^+ concentrations in the mMol range[15] in agreement with data presented by Holroyd[5]. It

appears that the $NaCl/Li_2CO_3$ environment is an acceptable first approximation to the solution which develops within an isolated pit; however, additional solution chemistry analysis is required to ascertain if quantitative information gained from experimentation in model environments is representative of in-service performance. To accomplish this it will be necessary to analyze solution chemistries which develop in growing EAC cracks under standard test conditions such as alternate immersion in sodium chloride solution.

The research presented in past reports details the electrochemistry of model microstructural features, EAC susceptibility of smooth bar samples, and the initial investigation of occluded chemistries. While these efforts provided information on the critical potentials, environments and tempers associated with EAC in Al-Li-Cu alloys, no information was gained concerning the ranking of EAC susceptibility as a function of temper, composition, or mechanical and electrochemical stresses. Hence the efforts of the last twelve months were directed at designing an experimental set-up capable of ranking EAC susceptibility through real-time monitoring of crack growth rates with concurrent control of stress intensity, applied electrochemical potential, and bulk environment. Initial results of the experiments performed using this technique will be presented in following sections.

Technical Approach

The results discussed in this report come from two types of EAC experiments and only the associated techniques will be reviewed here. Experimental methods used to obtain other data referenced in this document can be found in past reports[23-28].

Materials

The primary research materials for this project are aluminum alloys 2090 (Al-2.5 Cu-2.0 Li-0.1 Zr) and 2095 (Al-4 Cu-1 Li-0.25

Ag-0.25 Mg-0.1 Zr). For the experiments described in this report both alloys were used in UA (under-aged) and PKA (peak-aged) tempers. The material/ temper designations and descriptions are as follows:

(i) PKA 2090 : SHT + CWQ + stretch + age at 160°C to peak strength (as received).

(ii) 2090-B, UA : SHT + CWQ + 3 hrs @ 160°C.

(iii) 2095-A, UA : SHT + CWQ + stretch + 20 hrs @ 143°C (as received)

(iv) 2095-B, PKA : SHT + CWQ + stretch + 30 hrs @ 143°C (as received)

(v) 2095-D, UA : SHT + CWQ + 5 hrs @ 143°C

The UA 2090-B and 2095-D represents severely underage tempers whereas the UA 2095-A is only slightly underaged.

Constant Extension/ Scratching Electrode Experiments

These experiments were designed to characterize the behavior of smooth bar tensile specimens under conditions of constant displacement with concurrent control of bulk solution chemistry and applied electrochemical potential. Test specimens were round (d = 3.175 mm) bars with a gauge length of 17.78 mm. Samples were wet polished through 600 grit SiC (silicon carbide) grinding paper, ultrasonically cleaned in acetone then deionized water. Degreased specimens were mounted in a Plexiglas test cell with the grips and sample ends coated leaving only the gauge section exposed. The cell and sample were mounted in a screw-driven table top Instron load frame and a load corresponding to 60% of the YS was applied. The load train was then locked at the corresponding extension. Next the test solution was added to the cell and the sample was polarized to an initial potential between -0.600 and-0.700 V_{SCE}. After sample equilibration had occurred (indicated by a constant corrosion current), a glass stylus was used to create a physical flaw on the sample surface. This had the effect of exposing bare material to the environment/ potential conditions.

If the specimen repassivated the applied potential was stepped by 10 mV in the anodic direction and the scratching process was repeated. If repassivation did not take place, the sample remained in solution until failure occurred. The potential where corrosion resulted in sample fracture was recorded as the critical EAC potential ($E_{CRIT-EAC}$). This experiment also provided data in terms of time-to-failure (TTF) and fracture morphology of the specimens. The latter was determined using scanning electron microscopy.

Although materials could be distinguished based upon $E_{CRIT-EAC}$ values, in general it was difficult to rank materials in terms of EAC susceptibility based upon this technique. However, in previous reports notable differences in fracture morphology, times to failure and corrosion currents were observed between under-aged 2090 and peak aged 2090 and 2095. During the last reporting period experiments have been performed to reproduce the behavior of the UA 2090. Testing was also performed on UA 2095 to ascertain whether or not the behavior observed for 2090 carried over to another alloy.

Crack Propagation Rate Experiments

These experimental techniques were developed in order to provide a quantitative ranking of materials in terms of EAC propagation rates. The goals for the technique were to be able to measure crack lengths as a function of time for specimens in an aqueous environment with imposed and thus controlled electrochemical and mechanical stresses.

Specimens were wedge-opening loading (WOL) samples with a geometry similar to that of compact tension specimens. During development of the test technique various surface preparations were used in attempts to minimize corrosion of exposed surfaces. The treatment which has been the most successful is anodization of the sample prior to testing. The anodization was performed in 15w/o H_2SO_4 solution at ambient temperature. The specimen was

suspended from an alligator spring clip which also served as the electrical connection. Upon immersion in the sulfuric acid bath, the sample was anodically polarized via a platinized niobium counter electrode to sustain an imposed current of 0.8 amps, corresponding to an approximate current density of 0.019 A/cm^2. The polarization was carried out for forty minutes during which time the sample voltage ranged between 10 and 20 V. After the anodizing treatment the sample cured overnight at room temperature in deionized water. The conditions described for anodization should result in a film thickness of several microns [29,30].

Test specimens were exposed to environment by enclosing them in a Plexiglas cell fitted with a rubber gasket to prevent solution leakage. The cell contained ports for solution flow in and out, a port for placement of a calomel reference electrode, and symmetrically located counter electrodes.

A servo-hydraulic test frame was used in closed loop load control to apply the desired loading to the test specimen. Crack length information was calculated using direct current potential drop (DCPD). Software capable of calculating the crack length and controlling loads applied by the load frame was developed as a portion of this research effort.

Specimens were fatigue pre-cracked prior to performing crack growth-rate studies. Software controlled the fatigue cracking process using load shedding to maintain constant K_{min} and K_{max} values. Fatigue pre-cracking was performed in the aqueous environment used for EAC studies with the samples at their free corrosion potentials.

The EAC studies were carried out under conditions of either constant or ramped applied stress intensity; under software control in both cases. All of the crack propagation studies performed to date were carried out in an aqueous 0.1M NaCl + 0.1M Na_2CrO_4 environment at an applied potential of -0.547 V_{SCE}. Prior research [13,16,23-28] has indicated that under these conditions smooth bar tensile specimens suffer rapid EAC failures. It was

anticipated that the prescribed potential/ environment combination would result in preferential dissolution along an active microstructural pathway and contribute to environmental cracking.

Progress During this Reporting Period:

One of the most notable advances made in this reporting period was the establishment of experimental techniques and procedures capable of providing in situ growth and measurement of EAC cracks in Al-Li-Cu alloys. Using these crack propagation rate experiments in parallel with the scratching electrode/ constant extension experiments led to several significant observations concerning EAC in Al-Li-Cu alloys 2090 and 2095.

Constant Extension/ Scratching Electrode Experiments

The majority of the data collected using the constant extension/ scratching electrode technique has been discussed in previous reports[25-28]. In essence these experiments allowed a critical EAC potential to be defined such that mechanically stressed samples polarized cathodic to this potential would spontaneously repassivate when scratched with a glass stylus, whereas samples polarized anodic to this potential would undergo sustained corrosion and eventual material failure. It was found that the critical EAC potential was a function of temper, shifting in the cathodic direction with increased aging. This trend has been attributed to increased levels of copper depletion along microstructural boundaries with longer aging times.

While it was anticipated that time-to-failure (TTF) data from these experiments would allow ranking of materials in terms of susceptibility to EAC, it was found that the only significant differences in TTF were for UA 2090-B compared to PKA 2090 and PKA 2095. The UA 2090-B specimens all failed within 1.5 hours of initiating corrosion and the PKA materials failed within 5 to 24 hours after initiating corrosion. Recently these results have been duplicated using a second group of UA 2090-B specimens as

well as with a group of UA 2095-D specimens.

Additional differences for UA versus PKA material were observed in the recorded corrosion current (Figure 1) during the scratching electrode/ constant extension experiments and in the resulting fractography. In typical experiments (Figure 1) 500 times as much charge was passed in the PKA versus in the UA materials after scratching the electrode surfaces. It should be noted that extensive surface attack of the PKA material was observed in the form of pitting and intergranular attack which could account for the increased corrosion currents.

Comparisons of sample fractography were presented in an earlier report[28]. The regions of interest in the fractography are (1) surface attack/ pitting, (2) clearly defined EAC marked by corrosion products and evidence of intersubgranular or intergranular attack, and (3) the overload region. Both the UA and PKA samples appeared to have regions of surface attack and EAC marked by corrosion products although the extent of this EAC region was typically observed to be one to two orders of magnitude greater in the PKA materials. The third region, the overload region, is assumed to be material failure due to the reduction of cross sectional area to the point where the applied stress exceeds the strength of the remaining ligament. As such, this region might be expected to exhibit similar characteristics to that of a tensile sample fractured in an inert environment. In the case of the PKA 2090 and PKA 2095 the overload region did appear similar to the fracture surface of material broken in laboratory air. However, the fracture surface of the UA 2090-B was markedly different from that of a sample fractured in lab air. For the UA material, fracture in air resulted in a necked specimen with a highly contoured fracture surface suggesting ductile failure. UA specimens which failed via EAC in the scratching electrode experiment had fracture surfaces which appeared flat in comparison with the air fractures and did not have extensive ductile features. In light of these observations it is improper to refer

to the third region of the fracture surface in the UA materials as a pure overload region. Instead, the regions of fracture will be referred to as EAC region one (marked by detectable corrosion products and IG attack) and EAC region two (marked by a lack of corrosion products as well as a lack of similarity to air fractures). For the PKA samples the designation of an overload region will continue to be used at this time.

The presence of an overload region infers a sequence of events during EAC as follows: (1) Corrosion of the sample surface leads to the formation of a flaw or crack. (2) The crack grows by some EAC process reducing the effective cross section of the sample. (3) The remaining sample cross section reaches some value where the applied stress exceeds the native material properties and the specimen fractures. Samples failing by this mechanism under conditions of constant extension should have a well defined load-time history. During the first stage, surface corrosion, the load should remain constant within detection limits. While the crack grows in the second stage the load should decrease slightly according to the compliance relationships of the resulting sample geometry (this change may also be beyond the resolution of the load monitoring equipment). Finally, in the third stage, the sample cannot sustain the applied stress and catastrophic failure should occur with a rapid decrease in load - practically instantaneous on the time scale of the experiment.

Plots of load versus time and current verses time are given in Figure 1 for both UA and PKA 2090. Examination of the data for the PKA material reveals a load history with at least two of the regions described above - a period during which the load is approximately constant with time and a region in which the load drops rapidly to zero. Thus, in the case of the PKA material it appears a crack propagates until a critical flaw size is reached resulting in catastrophic failure. Although this indicates overload failure of a ligament, it does not rule out the possibility that the material properties of some portion of the

ligament have been affected by the EAC process. If such a change has occurred, it has not been resolvable with current experimental techniques.

Unlike the data for PKA material, the data shown for an UA 2090-B sample does not fit the predicted load-time history for catastrophic ligament failure. In this case the load remains constant for approximately 0.75 hours after corrosion has initiated. This section of the data may correlate to the first two stages mentioned above - surface corrosion and growth of the region 1 EAC crack. However, the portion of the data relating to the sample fracture is not indicative of catastrophic failure. The load data decreases from the initial value of 208 lbs (60% YS) to zero load in approximately 20 minutes. At first inspection it is not clear if this behavior reflects a difference in toughness and thus overload fracture behavior compared to the PKA material, or if the gradual decrease in load corresponds to an EAC process. Several points discount the first explanation. First, fracture of aluminum alloys is usually not considered time-dependent at room temperature. Second, if the crack were to propagate then arrest due to a decrease in driving force from unloading of the specimen, propagation should not resume until experimental conditions change in such a way that the mechanical driving force for crack extension exceeds the resistance of the material. Since the displacement is fixed, the driving force would not increase based on mechanical considerations; thus the gradual unloading process cannot be due to increased toughness of the material compared to PKA. Hence, sample geometry or material properties would have to be altered by some process in order for the driving force for crack extension to be altered. This statement implies that the UA 2090-B undergoes an EAC process which results in rapid crack propagation which is reflected in the load signal from constant extension experiments.

The combination of short times-to-failure, gradual specimen unloading and the observation of a second EAC region in UA 2090-B

and 2095-D specimens suggests an environmental cracking process in UA material which may not occur in PKA material. It appears that this cracking process is rapid in comparison to that observed for PKA material although the constant extension/ scratching electrode test does not provide any estimates of crack propagation rates - only total times to failure. The data presented in the next sub-section provides a more quantitative description of these cracking processes.

Crack Propagation Rate Experiments

Crack propagation rates have been determined for several tempers of alloys 2090 and 2095 in a 0.1M NaCl + 0.1M Na_2CrO_4 aqueous environment at an applied potential of -0.547 V_{SCE}. Under these conditions, electrochemical studies and constant extension/scratching electrode experiments have indicated that the T_1 phase or a Cu-depleted region along boundaries or sub-boundaries should be active in comparison to the grain interiors and can provide a pathway for dissolution based EAC[15,16].

Figure 2 shows v-K (crack velocity versus stress intensity) curves for UA 2090-B, PKA 2090, UA 2095-A (slightly under-aged) and PKA 2095-B. It should be noted that these are preliminary results and the data shown represents only one test. However, for the 2095-B and the 2090-UA the stress independent portion of the curve has been observed in duplicate experiments. In the case of 2095-A additional testing has been performed using samples of varying thickness but only one specimen has been tested using the current procedure. For the PKA 2090 no duplicate testing has been performed at the time of this writing.

The v-K data for 2095-A and 2095-B appear similar in terms of threshold stress intensities (K_{ISCC}) and stress intensity independent crack velocities (stage two cracking). There is more scatter in the growth rates for the A temper in the stage two region but the significance is questionable since this data

reflects only one test. Under the experimental conditions first indications are that near peak-aged and peak aged 2095 have K_{ISCC} values of approximately 12 MPa-$m^{1/2}$ and plateau cracking velocities near 10^{-5} mm/sec.

The v-K curve for PKA 2090 differs from the 2095 curves in terms of stress intensities where crack growth is observed. A K_{ISCC} value was not detected for 2090 in the initial test; however, it is evident that it would be well below that observed for the 2095. Stage two crack growth is observed at stress intensities as low as 7.2 MPa$\sqrt{m}$ which is approximately 5 MPa$\sqrt{m}$ less than the lowest stress intensity where crack growth was detected in the 2095. It is possible that the cracking observed at lower stress intensities in the 2090 alloy are due to differences in mechanical properties manifesting as varying degrees of constraint at the crack tip, though this issue has not been resolved.

The plateau cracking velocity for PKA 2090 is difficult to quantify from the data in Figure 2. Most of the data is concentrated at values near 10^{-5} mm/sec although there is considerable scatter - especially at high stress intensities. The unusually large values for da/dt correspond to changes in crack length which are discontinuous within the detection limits of the experimental technique. This phenomenon was also observed in cracking of PKA 2095-B during constant and rising K experiments and will be discussed in more detail later in this section of the report.

The data for UA 2090-B is shown at the bottom of Figure 2. Although there appears to be a well-defined K_{ISCC} for this material, duplicate testing has not provided similar values. In each test the apparent K_{ISCC} has corresponded to the stress intensity applied at the beginning of the experiment; therefore, the region of data which appears to be governed by stress dependent crack growth rates is more likely representative of an initiation stage for EAC: i.e. the crack is not instantly propagating at a rate of 10^{-2}

mm/sec but must "accelerate" to this rate from an initial rate of zero. In order to determine a K_{ISCC} value, rising K testing will have to be performed at a lower initial K or decreasing K testing will be performed using a fixed displacement experiment.

Despite the difficulty in determining a K_{ISCC} value for UA 2090, duplicate testing has generated a reproducible plateau cracking velocity of approximately 10^{-2} mm/sec. This value is several orders of magnitude greater than those observed for the other materials tested. This result compliments the constant extension/ scratching electrode testing reviewed earlier by providing quantification of the crack velocity. A change of three orders of magnitude in plateau cracking velocity between materials or tempers suggests a change in crack propagation mechanism. As mentioned earlier, the two schools of thought concerning EAC in Al-Li-Cu alloys are based on hydrogen embrittlement and anodic dissolution. While it is difficult to predict cracking velocities from diffusion of hydrogen, it is possible to use cracking velocities to approximate crack tip dissolution rates. Assuming the atomic spacing is 2.5 angstroms and a metal atom on average releases three electrons upon ionization into solution, the corrosion current density for cracking at 10^{-2} mm/sec can be calculated as follows:

$$i = \frac{\left(\frac{10^{-2}\,mm}{sec}\right) x \left(\frac{\dot{A}}{10^{-7}\,mm}\right) x \left(\frac{1\,atom}{2.5\dot{A}}\right) x \left(\frac{3e^-}{atom}\right) x \left(\frac{1.6x10^{-19}\,coul}{e^-}\right) x \left(\frac{1amp}{1coul/sec}\right)}{\left(2.5\dot{A} \times 2.5\dot{A}\right) x \left(\frac{1 \bullet 10^{-8}\,cm}{\dot{A}}\right)^2}$$

$$i = 20 \frac{amps}{cm^2}$$

From a similar calculation the dissolution rate for a cracking velocity of 10^{-5} mm/sec is found to be 0.02 amps/cm^2. These results indicate that a dissolution process could account for cracking at velocities in the 10^{-5} mm/sec range but dissolution capable of producing growth rates of 10^{-2} mm/sec would require unreasonable current densities to be sustained at the crack tip. Additionally, the high corrosion currents would generate large concentrations of metal ions in solution and consequently copious amounts of hydrolysis products. Corrosion products have not been observed on the fracture surfaces generated by cracking at 10^{-2} mm/sec although they have been observed on surfaces which were generated by crack growth at 10^{-5} mm/sec. Thus, post test observations suggest, in a very qualitative way, that the cracks which propagate at a lower rate may actually suffer from a greater degree of metal dissolution at the crack tip.

Since the plateau crack velocities recorded for 2095-A, 2095-B and PKA 2090 correspond to a dissolution rate of approximately 0.02 amps/cm2, these data cannot be used to support or discount a mechanism of anodic dissolution based crack propagation. However, the observation of corrosion products in combination with past electrochemical studies[15-16] imply AD controlled EAC for these material tempers. In contrast, the unusually high growth rates determined for UA 2090-B provide strong evidence against an AD based cracking mechanism under the given experimental conditions. Based on these arguments it appears likely that an embrittlement mechanism dominates cracking of the UA 2090-B specimens though it must be noted that only indirect evidence has been presented which supports embrittlement based cracking.

Thus far rapid crack growth rates (10^{-2} mm/sec) have only been discussed in reference to the UA 2090-B specimens; however, similar cracking velocities have been recorded for both peak aged 2090 and 2095-B as was mentioned earlier. In the peak-aged materials fast cracking has only been observed as a discontinuous

process - regions of slow crack growth interrupted by abrupt jumps in crack length. Figure 3 shows the behavior of a 2095-B (PKA) sample during a rising K experiment. The regions of fast crack growth can clearly be seen in the plot of crack length versus time. To explain this behavior in terms of a rising K test, three hypothesis can be examined. (1) The increasing stress intensity exceeds the material K_{IC} resulting in a crack jump, (2) crack growth occurs with an irregular crack front leaving behind ligaments which remain uncracked until local stresses exceed the material resistance to crack growth and the ligaments fail, (3) an embrittlement process occurs which lowers the material toughness in a region ahead of the crack tip to such an extent that the mechanical driving force for crack growth is sufficient to rapidly fracture the embrittled region.

The first hypothesis can be immediately discounted since crack jumps are observed at low stress intensities (23-25 MPa$\sqrt{m}$) and yet the material sustains larger stress intensities (i.e. 28 MPa$\sqrt{m}$) at later times in the experiment. If the test were being performed in CMOD control or under stroke control a crack jump would cause a corresponding decrease in load and thus stress intensity in which case a crack could arrest; however, these experiments have been carried out in load control and increases in crack length lead to a temporary increase in stress intensity until the software can correct for the crack extension. Thus a crack jump occurring due to exceeding material toughness should immediately propagate through the specimen and this is not observed.

It is more difficult to discount either of the second two hypotheses. Either the fracture of material ligaments or the cracking of an embrittled region would result in the type of data shown in Figure 3. Determining if the crack bursts are due to embrittlement and not ligament failure is an important point since the embritllement hypothesis would indicate a cracking process possibly under mixed control (anodic dissolution and

embrittlement). It may be possible to determine if the region ahead of the crack tip is becoming embrittled by the using the following experimental procedure:

(i) Grow a crack at a low stress intensity for an extended period of time.

(ii) Remove the sample from environment and stain the cracked region so that it can be easily identified in post test examination.

(iii) Perform a fracture toughness test on the sample in air and determine if cracking occurs at stress intensities below K_{IC}.

(iv) Examine the fracture surface immediately beyond the stained region to see if it differs significantly from the fracture surfaces generated by fracture toughness testing performed in an inert environment.

This procedure should provide quantitative and/or visual confirmation of an embrittleing process if one is occurring under the specified test conditions. This experiment is scheduled to be performed during the next reporting period.

Conclusions

The conclusions listed below are based on the research described in the previous section. For a compilation of conclusions for research prior to this reporting period refer to the reports from January and July of 1994[27-28].

(i) A novel method has been established which allows cracks to be grown and monitored in Al-Li-Cu alloys 2090 and 2095 under conditions of constant immersion, controlled electrochemical potential and controlled stress state. This technique should be valuable for evaluating EAC in other Al-Cu-X systems.

(ii) Constant extension/scratching electrode experiments have revealed significant differences in EAC behavior of under-aged versus peak-aged material for alloys 2090 and 2095. Times-to-failure,

fracture morphology and load-time history suggest a difference in crack propagation mechanism for the under-aged and peak-aged materials.

(iii) Crack growth rates were monitored as a function of applied stress intensity for several tempers of 2090 and 2095. The observed plateau cracking velocity for the UA 2090 was approximately 10^{-2} mm/sec and for the PKA 2090, 2095-A (slightly UA) and 2095-B (PKA) was approximately 10^{-5} mm/sec.

(iv) The rapid cracking in the UA 2090 provides a strong argument against anodic dissolution controlled EAC for this temper and suggests an embrittlement based mechanism.

(v) Insufficient data exists to discount either anodic dissolution or embrittlement as a primary mechanism for EAC in PKA 2090 and 2095.

(vi) Electrochemical data, crack growth rate information and observation of corrosion products on fracture surfaces support an anodic dissolution mechanism for EAC in PKA 2090 and 2095.

(vii) The observation of discontinuous cracking at rates as high as 10^{-2} mm/sec in PKA 2090 and 2095 indicate the possible role of an embrittlement based cracking process in the EAC of these materials. However, the possibility of ligament fracture causing discontinuous cracking has not been resolved.

Future Work

Rather than provide a detailed technical account of upcoming research objectives the priority goals for the next reporting period will be listed in summary form.

Crack growth rate experiments

The techniques which have been developed over the past year will be used to map out cracking behavior as a function of stress intensity, composition, temper and applied electrochemical potential.

(i) A complete aging study of 2095 will be pursued in an effort to isolate aging practices which result in a significant change in EAC behavior.

(ii) In addition to v-K curves, attempts will be made to determine v-E_{appl} relationships (crack growth rate as a function of imposed electrochemical potential).

(iii) Efforts will be made to resolve the discontinuous rapid cracking phenomenon in PKA 2090 and 2095 according to the procedure described in section 4.2.

(iv) Crack growth rate experiments will be performed on L-T samples and cracking pathways will be better characterized by comparing fractography from EAC of S-L and L-T specimens.

These experiments should round out the data concerning crack propagation for the alloys under study. The first experiment is aimed at determining plateau cracking velocities as a function of material temper. From this information it should be possible to determine if the transition from fast (10^{-2} mm/sec) cracking to slower (10^{-5} mm/sec) cracking occurs gradually from UA to PKA material or if the change is discontinuous and possibly due to the development of some critical microstructural feature.

Examining crack growth rates as a function of E_{appl} will determine if crack propagation varies significantly with overpotential. It will also indicate if the cracking process can be "turned off" at a particular potential. If crack growth rates appear to be discontinuous with changes in potential, then it may be possible to correlate the crack path to the electrochemistry of a microstructural feature.

The third experiment is an attempt to unambiguously reveal an embrittled region, if one exists, in the peak-aged material. The existence of an embrittled region would suggest the role of hydrogen in the cracking of these materials even at growth rates of 10^{-5} mm/sec.

The fourth experiment is designed to look at cracking in

another material orientation to provide fractographic evidence as to the pathway for EAC in these materials. In the S-L orientation it is difficult to distinguish ISG cracking from IG cracking - L-T specimens should provide some clarification of this point.

Occluded Chemistry Analysis

Capillary electrophoresis will be used in order to investigate possible occluded chemistries in Al-Li-Cu alloys.

(i) DCB specimens, after being subjected to alternate immersion conditions, will be frozen, fractured and sampled for chemistry analysis. Efforts will be made to obtain information on solution pH at the crack tip and species present in the crack path.

(ii) Chemistries generated from exposure of large material surface area to small solution volumes (to simulate an occluded, isolated corrosion site) will be analyzed. This represents a repetition of earlier work but will be performed with more rigorous solution analysis.

The occluded chemistry analysis is aimed at determining the critical species in solution leading to environmental cracking. Tests on the DCB specimens should provide an indication of the chemistry during an AI test. Thus far an alkaline $NaCl/Li_2CO_3$ environment has been used as the occluded chemistry model and results of capillary electrophoresis should provide validation or contradiction of this model.

Personnel

The faculty investigator for this project is Professor Glenn. E. Stoner and the graduate student is F. Douglas Wall.

References

1. R. Balasubramaniam, D.J. Duquette, K. Rajan, Acta Metallurgica et Materialia, 39, 11 (1991): pp. 2597-2605.

2. E.I. Meletis, Weiji Huang, "Environmentally Assisted Cracking in Al-Li Alloys", Al-Li Alloys V, E.A. Starke, Jr., T.H. Sanders, Jr., eds., 1989, pp. 1309-1318.

3. E.I. Meletis, W. Huang, Mat. Science and Engineering, A148, 1991, pp. 197-209.

4. E. I. Meletis, "Microstructural Effects on the Environmentally Assisted Fracture Mechanisms of Al-Li Alloys", Parkins Symposium on Fundamental Aspects of Stress Corrosion Cracking, Eds. S.M. Bruemmer et al., 1992.

5. N.J.H. Holroyd, A. Gray, G.M. Scamans, R. Hermann, Aluminum Lithium Alloys III, C. Baker, P.J. Gregson, S.J. Harris, C.J. Peel, eds., The Institute of Metals, London, 1986, p. 310.

6. J.G. Craig, R.C. Newman, M.R. Jarret, N.J. Holroyd, J. de Physique, 48, C3, 1987, p.825.

7. J.P. Moran, Ph.D. Dissertation, University of Virginia, 1990.

8. J.G. Rinker, Aluminum Lithium Alloys II, T.H. Sanders, Jr., and E.A. Starke, Jr., Eds. pp 597-622.

9. J.P. Moran, G.E. Stoner, Aluminum Lithium Alloys V, T.H. Sanders, Jr., E.A. Starke, Jr., eds., MCE Publications Ltd., Birmingham, UK, 1989, p. 1187.

10. R.G. Buchheit, Ph.D. Dissertation, University of Virginia, 1991.

11. R.G. Buchheit, G.E. Stoner, Aluminum Lithium Alloys V, T.H. Sanders, Jr., E.A. Starke, Jr., eds., MCE Publications Ltd., Birmingham, UK, 1989, p. 1347.

12. R.G. Buchheit, J.P. Moran, G.E. Stoner, Corrosion, vol. 46, 8, 1990, p.610.

13. R.G. Buchheit, F.D. Wall, G.E. Stoner, "The Effect of Applied Potential in Static Load SCC Testing of 2090 in Cl- and Cl-/CrO_4^{2-} Environments", Proceedings of the Electrochemical Society - Environmentally Enhanced Fracture Symposium, Fall Meeting, 1990.

14. R.G. Buchheit, F.D. Wall, G.E. Stoner, "Stress Corrosion Cracking of Al-Li-Cu-Zr Alloy 2090 in Aqueous Cl^- and Mixed $Cl^-/CO3^{2-}$ Environments", Corrosion/91, Paper No. 99, Houston, TX, NACE, 1991.

15. F.D. Wall, G.E. Stoner, "Electrochemical Characterization and Occluded Environment Analysis of Localized Corrosion in Advanced Aluminum Alloys", Corrosion/94, Baltimore, MD, NACE, 1994.

16. F.D. Wall, G.E. Stoner, "Critical Electrochemical Potentials Relating to the Rapid Environmentally Assisted Cracking of Advanced Aluminum Alloys", Proceedings of Aluminum-Lithium Alloys for Aerospace Applications Workshop, NASA George C. Marshall Space Flight Center, Huntsville, Alabama, May 1994, pp.122-131.

17. E.I. Meletis, Materials Science and Engineering, 93, 1987, pp. 235-245.

18. M.H. Tosten, A.K. Vasudevan, P.R. Howell, Aluminum Lithium Alloys III, Institute of Metals, London, 1986, pp.490-495.

19. F.W. Gayle, F.H. Heubaum, J.R. Pickens, Scripta Metallurgica et Materialia, vol 24, 1990, pp. 79-84.

20. K.S. Kumar, S.A. Brown, J.R. Pickens, Scripta Metallurgica et Materialia, vol 24, 1990, pp. 1245-1250.

21. T.J. Langan, J.R. Pickens, "Identification of Strengthening Phases in Al-Cu-Li Alloy Weldalite 049", Aluminum Lithium Alloys Volume V, T.H. Sanders, Jr., E.A. Starke, Jr., eds., MCE Publications Ltd., Birmingham, UK, pp. 691-700.

22. J.R. Gavele, S.M. de Micheli, I.L. Muller, S.B. de Wexler, I.L. Alanis, "Critical Potentials for Localized Corrosion of Aluminum Alloys," Localized Corrosion, Houston, TX, NACE, 1972, pp.569-575.

23. F.D. Wall, G.E. Stoner, "Mechanisms of Localized Corrosion in Al-Cu-Li-Mg-Ag Alloy X2095 and Compositional Variations", in "NASA-UVa Light Aerospace Alloy and Structures Technology Program", Report No. UVA/528266/MSE92/109, University of Virginia 1992.

24. F.D. Wall, G.E. Stoner, "Mechanisms of Localized Corrosion in Alloys 2090 and X2095", in "NASA-UVa Light Aerospace Alloy and Structures Technology Program", Report No. UVA/528266/MSE92/111, University of Virginia 1992.

25. F.D. Wall, G.E. Stoner, "Mechanisms of Localized Corrosion in Alloys 2090 and X2095", in "NASA-UVa Light Aerospace Alloy and Structures Technology Program", Report No. UVA/528266/MSE93/112, University of Virginia 1993.

26. F.D. Wall, G.E. Stoner, "Mechanisms of Localized Corrosion in Alloys 2090 and 2095", in "NASA-UVa Light Aerospace Alloy and Structures Technology Program", Report No. UVA/528266/MSE113, University of Virginia 1993.

27. F.D. Wall, G.E. Stoner, "Mechanisms of Localized Corrosion in Alloys 2090 and 2095", in "NASA-UVa Light Aerospace Alloy and Structures Technology Program", Report No. UVA/528266/MSE114, University of Virginia 1994.

28. F.D. Wall, G.E. Stoner, "Mechanisms of Localized Corrosion in Alloys 2090 and 2095", in "NASA-UVa Light Aerospace Alloy and Structures Technology Program", Report No. UVA/528266/MSE115, University of Virginia 1995.

29. S. Wernick, R. Pinner, P.G. Sheasby, The Surface Treatment and Finishing of Aluminum and its Alloys, ASM International, Metals Park, OH, 1987, pp. 292-293.

30. Metals Handbook, Desk Edition, ASM International, Metals Park, OH, 1994.

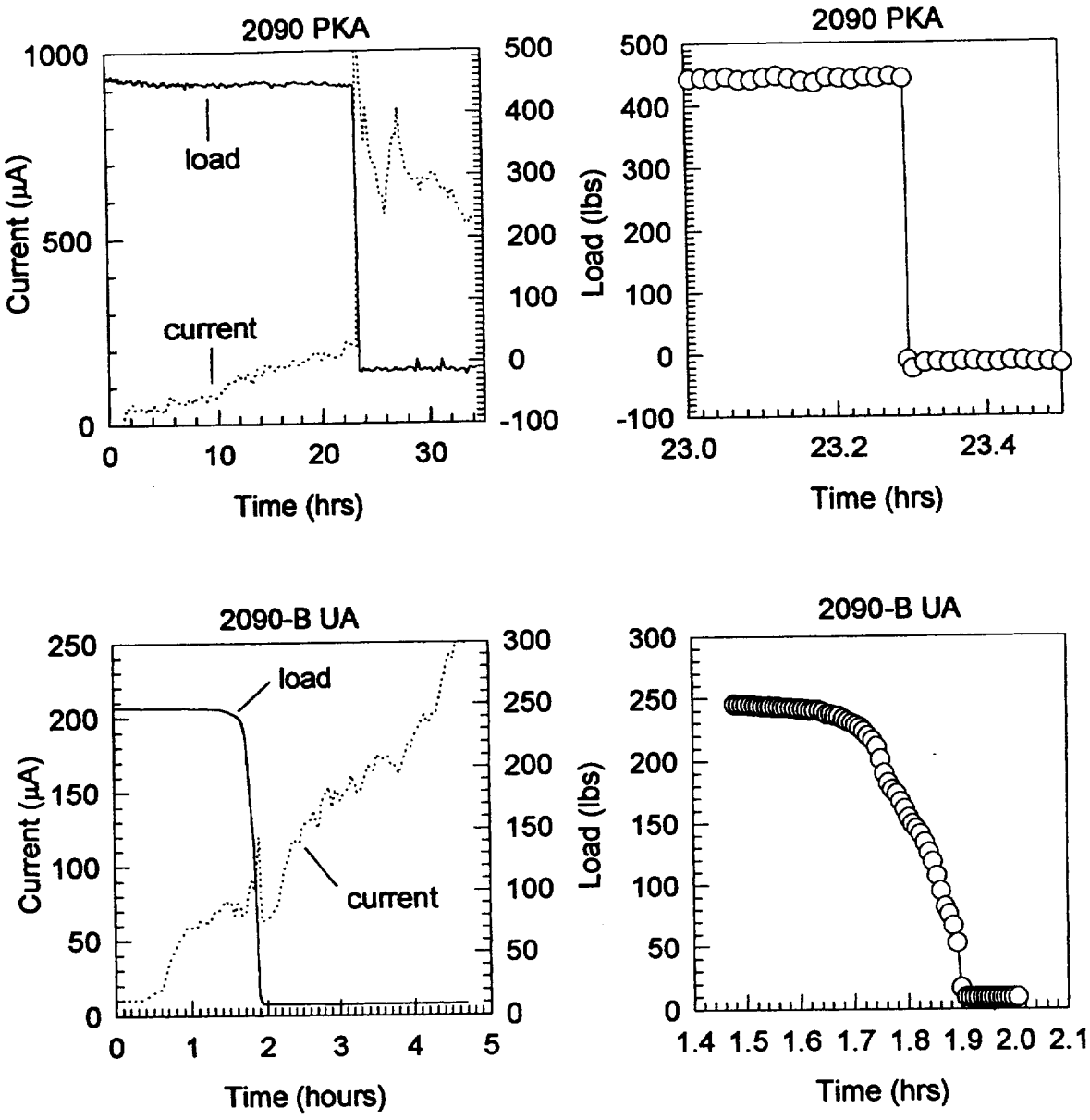

Figure 1. Load-time and current-time history for UA and PKA 2090 in 0.1M NaCl + 0.1M Na2CrO4 under conditions of potentiostatic polarization and constant extension corresponding to an initial load of 60% of yield strength.

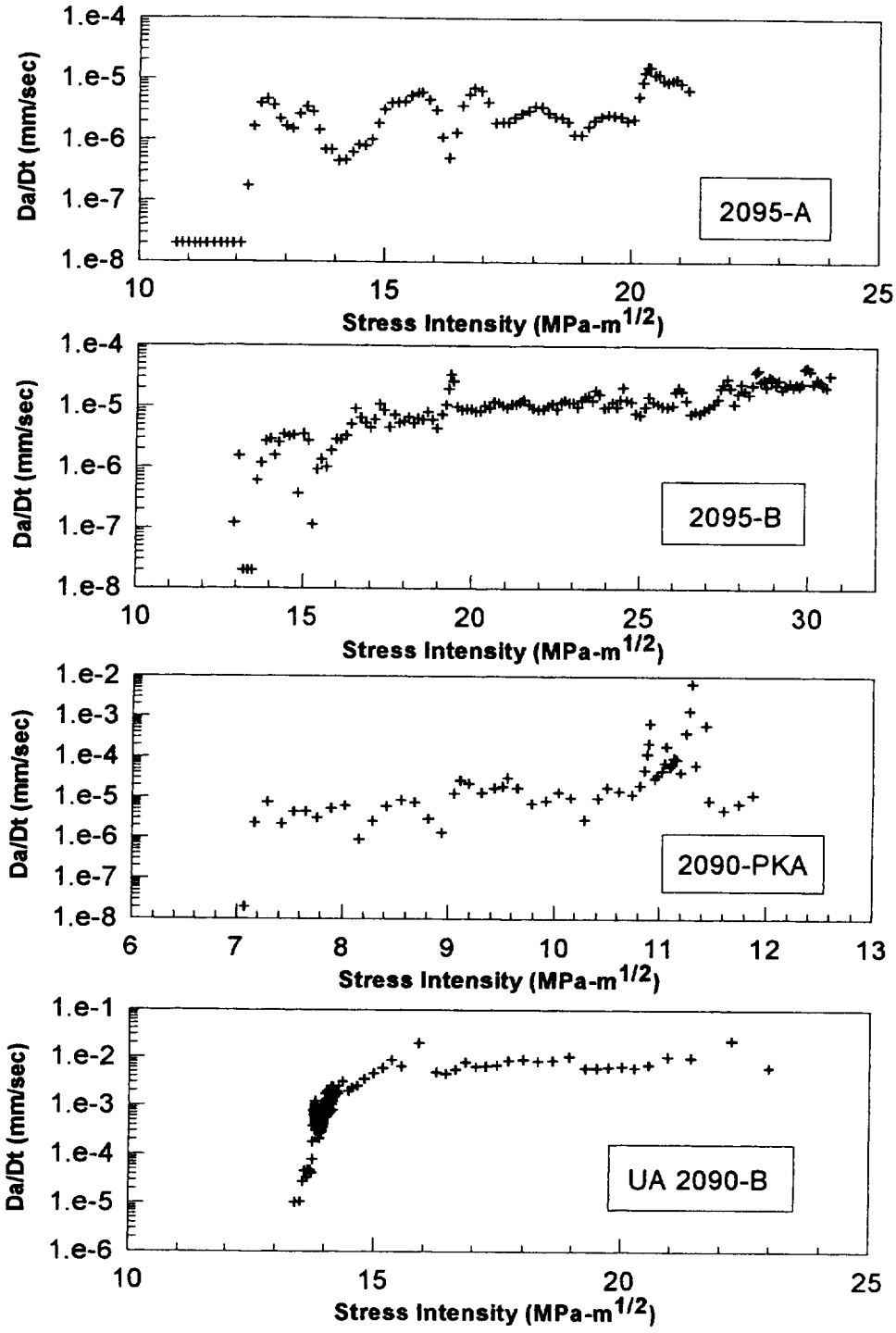

Figure 2. Crack growth rate as a function of applied stress intensity for Al-Li-Cu alloys under constant immersion in 0.1M NaCl + 0.1M Na_2CrO_4 at an applied potential of -0.547 V_{SCE}.

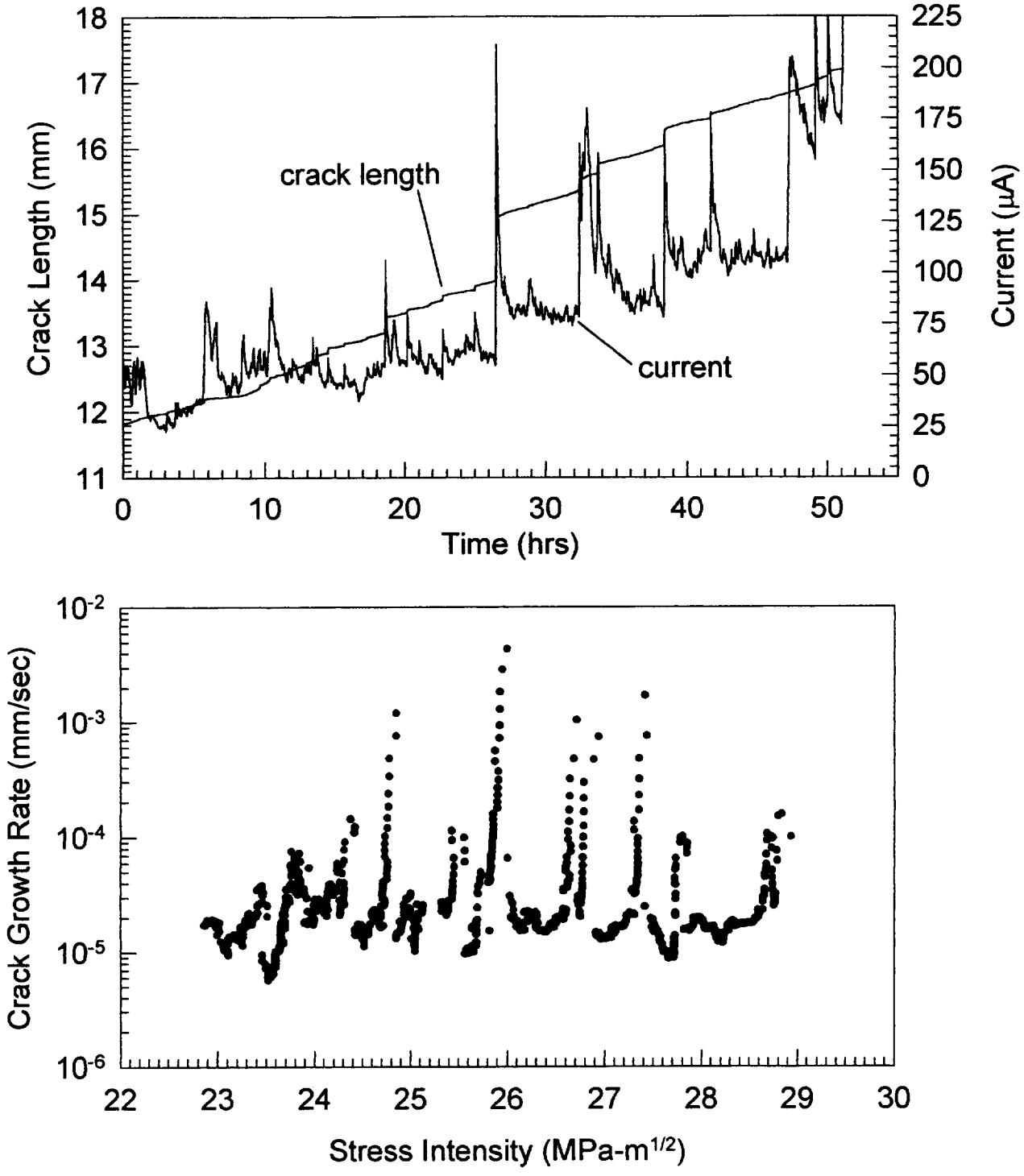

Figure 3. 2095-B PKA under conditions of constant immersion in 0.1M NaCl + 0.1M Na_2CrO_4, potentiostatic polarization at -0.547mV_{SCE} and increasing stress intensity at a rate of 0.11 Mpa-$m^{1/2}$/hr.

Project #5 **Hydrogen Interactions in Aluminum-Lithium Alloy 2090 and Selected Model Alloys**

John R. Scully and Stephen W. Smith

Research Objective

The goal of this project is to develop a fundamental understanding of the effects of internal lattice and trapped hydrogen on the mechanical properties of selected Al-Li-Cu-X alloys. The present program focuses on unrecrystallized alloy 2090, an Al-Li-Cu-Zr alloy within the specified compositional range of AA2090 which has been recrystallized to varying grain sizes, and complimentary model alloys. We propose to (a) distinguish HEAC from aqueous dissolution controlled EAC by using a novel precharging procedure, (b) correlate hydrogen induced EAC with mobile and trapped hydrogen concentrations, (c) identify significant trap sites and hydride phases (if any) through utilization of model alloys and phases. Following identification of relevant hydrogen trap sites, the emphasis during the last 2 quarters has centered on comparing hydrogen concentrations produced from the novel precharging procedure to hydrogen levels produced during conventional aqueous alternate immersion exposure and straining electrode testing. Additionally, the role of dynamic straining in promoting hydrogen uptake and repartitioning has been investigated during the last reporting period. This program will terminate in the spring of 1995.

Background and Problem Statement:

Neither the important metallurgical factors controlling the SCC resistance nor the effects of internal hydrogen on the fracture behavior of Al-Li-Cu-X alloys are fully understood. Yet, many studies point to an important role for crack tip hydrogen in the aqueous SCC behavior of this class of alloys. For Al-Li-Cu-X alloys intergranular, intersubgranular, and transgranular environmentally assisted cracking paths in aqueous solutions have

been attributed to boundary T_1 dissolution,[1] T_1 dissolution with hydrogen uptake,[2] $AlLiH_4$ formation and cracking,[3,4] and intrinsic hydrogen embrittlement involving mobile and or trapped hydrogen.[5] Both quantification of the crack tip hydrogen concentrations and unambiguous identification of detrimental trap sites which might be avoided in future alloy design are lacking in all of these studies.

Several problems are encountered when performing traditional hydrogen embrittlement tests on aluminum based alloys, thereby, making it difficult to unambiguously determine the influence of hydrogen on mechanical properties. Three major problems, which have impeded progress have been identified in the literature. These are: (i) intergranular and inter-subgranular fracture in Al-Li-Cu-X alloys when tested in the ST orientation in air or vacuum make it difficult to readily detect hydrogen induced fracture based on straight forward changes in fractography[6] (ii) the inherently low hydrogen diffusivity and solubility in Al alloys is further compounded by a native oxide which acts as a hydrogen permeation barrier; these factors complicate hydrogen, ingress, detection and quantification,[7] and (iii) hydrogen effects are masked by dissolution assisted processes associated with T_1 precipitates on subgrain boundaries or, concurrently, with Cu depletion at such boundaries when mechanical testing is performed in aqueous solutions.[8] This project has been developed to circumvent these experimental barriers and develop a better understanding of the role of hydrogen.

A hydrogen precharging procedure has been developed to decouple the effects of dissolution and hydrogen on tensile ductility and fracture toughness. In this manner hydrogen uptake, its interactions, and its effects on tensile ductility and fracture behavior are studied as non-competitive processes. Hydrogen uptake and trapping are then studied using thermal desorption spectroscopy on parallel specimens precharged with hydrogen in the same way. Mechanical properties may then be

correlated with trapping behavior in a less ambiguous fashion. The status of this project is reviewed below.

This program provides diagnostic procedures and a deterministic framework which will be useful for understanding the effects of internal hydrogen on ambient and cryogenic temperature mechanical properties for emerging Al-Li-Cu-X alloys. The diagnostic procedures and scientific framework are also extendable to the lifetime and reliability of 2XXX, 6XXX and 7XXX alloys in aging aircraft which might be subjected to hydrogen uptake over long exposure periods. Even in the case of aqueous exposure, absorbed hydrogen may be a contributory, if not dominant, factor in the SCC of alloy 2090.[2] The methodologies will also be extendable to aluminum based materials being developed for Advanced Metal Subsonic initiatives as well as High Speed Civil Transport Al-based materials. The present study will terminate with the completion of the internal hydrogen embrittlement study on alloy 2090 sheet and complimentary model alloys. The follow-on study will refocus on aqueous localized corrosion and SCC of an emerging Al-Li-Cu-Mg-Ag alloy but will utilize the hydrogen diagnostic procedures developed in this program.

Technical Approach

The research that has been performed on this project can be separated into four major phases: (a) total hydrogen concentration and trapping analysis of model Al-Li-Cu-Zr alloys and commercial AA2090 sheet precharged either by *(i)* electrochemically precharging nickel-coated specimens, *(ii)* straining electrode tests (SET) under full immersion with concurrent cathodic polarization, or *(iii)* alternate immersion (AI) exposure in accordance with ASTM G-44,[9] (b) examination of mechanical properties (tensile ductility and fracture toughness) under the influence of the internal pre-dissolved hydrogen concentrations achieved using the nickel-coated electrochemical precharging procedure, (c) correlation of hydrogen trapping analysis with

fracture toughness and fractography, and (d) examination of the role of dynamic plastic straining in promoting (i) hydrogen uptake and (ii) its selective partitioning to dislocations or repartitioning from dislocations to other trap sites. Phase (d) has been the point of major emphasis throughout the latest reporting period.

Recent results

Comparison of hydrogen concentrations obtained using different charging procedures

Previous NASA reports document the procedures used to achieve internal hydrogen concentrations under conditions which are decoupled from aqueous dissolution.[10-13] Additional charging procedures investigated for comparison include *(i)* straining electrode tests (SET) under concurrent full immersion and cathodic polarization (1M HCl at $-2V_{SCE}$ and $2x10^{-6}$ sec^{-1} strain rate), or *(ii)* alternate immersion (AI) exposure in accordance with ASTM G-44 for 84 days.[14] The hydrogen concentrations achieved by each method are shown in Figure 1.[14] The SET and AI test methods provide larger hydrogen concentrations than in the case of the nickel coated method. These results suggest that greater hydrogen concentrations within a local fracture process zone are possible under slow dynamically loaded aqueous stress corrosion cracking conditions than achieved by the nickel coating procedure. It can be concluded that trends in fracture initiation toughness observed with the increased absorbed hydrogen level produced by the nickel coating procedure would also apply to aqueous SCC. Since the hydrogen concentrations are likely to be greater in the latter condition. This point is further elaborated in a publication.[15]

Hydrogen trapping analysis - trap site identification

Thermal desorption spectroscopy has been emphasized as the primary method for identifying hydrogen trap sites in Al based alloys.[12,13] At least 6 internal trapping states have been

identified for AA2090.[14,16-18] As reviewed in Figure 2, these include the following peaks (each maxima in the desorption spectra corresponds to a trapping state) resolved with peak fitting software. The higher the temperature at which the desorption rate maxima occurs, the higher the binding energy associated with the trap site.

Peak number: probable metallurgical site

1. surface hydrogen and interstitial hydrogen
2. hydrogen attracted to elemental Li in solid solution
3. hydrogen associated with either the δ' interface or within the δ' phase
4. hydrogen associated with dislocations

5 and 6. hydrogen associated with high angle boundaries and T type particles (T_1, T_2, and/or T_B). The separate identification of each has not been possible.

Fracture Toughness Testing

Mechanical testing has been performed on Al-Li-Cu-Zr alloys in three different tempers (T3, UA - T3+5 hrs @ 160°C, and PA - T3+25 hrs @ 160°C), in the TL and LT orientations, as well as in four unique microstructures.[11] The alloys studied include one commercially available unrecrystallized sheet product (AA2090) supplied by Alcoa Technical Center, and three model recrystallized sheet products (Al-Li-Cu-Zr) of varying grain size with the same prestretch as the commercial product. J-integral resistance curve testing was performed on all four of the alloys in the UA and PA tempers described above using methods in accordance with ASTM standard E-1152.[19]

During the last reporting period, tests were completed on the commercial AA2090 alloy in the T3 condition for both the hydrogen precharged and uncharged conditions. The fracture initiation toughness was significantly lowered with hydrogen precharging for LT and TL oriented specimens (Table 1). The fracture initiation

toughness values for the precharged T3 specimens are lower than the values that were previously established for UA specimens tested under identical conditions. Tests performed within this reporting period, as well as work that has been previously documented, has shown that the introduction of pre-dissolved hydrogen does not produce any significant changes in the fracture initiation path in the underaged tempers (T3 and UA), however, the fracture initiation toughness is lowered.[14,15] These observations, along with separate experimental results showing that pre-dissolved hydrogen aids in the localization of slip in underaged AA2090, indicate that the lowering of the fracture initiation toughness is due to hydrogen affecting the deformation behavior of the underaged tempers. In order to lend support to this hypothesis it is necessary to show that there is a strong interaction between dislocations and hydrogen within a heavily deformed volume. We hypothesize that the association of hydrogen with dislocations promotes slip localization.

The role of dynamic straining on hydrogen uptake, trapping and repartitioning in the fracture process zone

Several observations point to a possible role of dislocation trapping and transport in Al based alloys during stress corrosion cracking or hydrogen embrittlement. In this study these include a) a strain rate dependency in CERT testing in dry air *(even though specimens were precharged with hydrogen)*, and b) high angle boundary cracking in J-Integral R-curve tests on fine grained recrystallized Al-Li-Cu-Zr, with evidence of dislocations markings on fracture surfaces. The question arises as to whether dislocations aided by a planar slip deformation mode can collect, transport, and deposit hydrogen at high angle boundaries. Three different experiments were devised to address this question.

Firstly, flat Ni-coated tensile specimens of the unrecrystallized alloy in each of the three tempers were cathodically charged, removed from solution and strained at a

constant crosshead displacement rate with a final strain rate of $2x10^{-6}$ sec^{-1}, to a total strain of 3% in laboratory air. Results from the desorption spectra of these strained specimens show an increased fraction of internal hydrogen associated with the trapping of hydrogen at dislocations (trap state 4 in Fig. 2 and 3). Additionally, there is a slight decrease in the total amount of hydrogen trapped at δ' particles, interstitially and at Li atoms. It appears that this repartitioning is due to dislocations picking up hydrogen as they sweep through the lattice. An additional effect may be due to a diffusional process where the generation of dislocations create additional trapping sites and in order to minimize the free energy of the system, hydrogen atoms trapped at lower energy sites diffuse to occupy the newly formed dislocation trapping sites. The pickup of additional hydrogen from laboratory air during straining was small in these tests.

Further evidence to support the dislocation assisted transport argument has been established in a second experiment involving concurrent straining and cathodic charging of tensile bars in a pH 1 HCl solution at $-2V_{SCE}$ to a total strain of 3%. Tensile specimens were analyzed in the TDS system immediately following the SET test (Fig. 4). In each of the tempers studied, the fraction of hydrogen trapped at dislocations (trap state 4) is significantly greater than seen in unstrained specimens. This effect is greatest in the PA temper, which has the highest degree of localized planar slip.[20] The increased hydrogen uptake by dislocations for PA specimens, results in a significant increase in the absorbed hydrogen concentration compared to UA specimens tested in the same manner (Fig. 1).

In a third type of experiment, thermal desorption spectroscopy experiments were conducted on AA2090 and recrystallized Al-Li-Cu-Zr alloy specimens which were cut from the plastic zone of compact tension specimens subjected to rising load J-integral testing after hydrogen precharging. In this way, the issue of hydrogen repartitioning into the intense plastically

deformed region of the fracture process zone and also the question over dynamic trap state creation such as by dislocation pile-ups at grain boundaries could be addressed. These tests were also conducted in laboratory air at slow load line displacement rates and were fatigue pre-cracked in lab air. Fatigue precracking was conducted for 8-12 hours and J-integral tests lasted for 12-24 hours, to allow the crack to propagate the entire width of the specimen. In order to provide a basis for comparison a second test specimen was sectioned from far outside the plastic zone of the same compact tension specimen. Both specimen were ground to the same mass to insure comparable specimen heating rates and mean diffusion distances. However, the estimated plastic zone dimensions were a small fraction of the total test specimen dimensions. If there were no hydrogen repartitioning or dynamic trap creation, then the TDS test pair should produce the same desorption spectra with the same number of trap states. This was not found to be the case. All specimens containing the plastic zone, even those that were not previously hydrogen charged by cathodic polarization, exhibited a 30-45 wt. ppb increase in hydrogen concentration. This suggests either that 30-45 ppb of hydrogen pick-up occurred in laboratory air or that hydrogen was redistributed to the plastic zone from the rest of the CT sample during dynamic straining. The latter scenario is not implausible even for the non-charged specimen since as-received 2090 material contains a residual hydrogen concentration of greater than 100 wt. ppb. However, it is more likely that some of hydrogen pickup occurred during monotonic loading in lab air. Notably, the 30-45 wt. ppb. increase is disproportionately found at trap state 4, identified as trapping by dislocations. This can be readily seen from TDS difference spectra (Figure 5), where the difference in desorption rate at each temperature is plotted for a specimen pair (one containing the plastic zone, one not) from the same compact tension specimen. This type of plot shows that the largest positive peak accounting for most of the 30-45 ppb gain is at the

position of peak 4. While this gain alone is not enough to trigger lower fracture toughness values in AA2090 tested in air without hydrogen precharging, it does underscore the possibility that fatigue in moist lab air may be hydrogen controlled since it provides direct evidence of hydrogen uptake under lab air exposure. Regarding the possibility of hydrogen pickup by dislocations and its redistribution to grain boundaries or some other high energy trap sites created by straining at the same position as trap states 5 and 6, the difference spectra almost always indicate a small positive difference in hydrogen at some high energy site near where states 5 and 6 are normally located. However, it can not be firmly stated that hydrogen picked up by dislocations has been redeposited at high angle boundaries. However, it is interesting that hydrogen pick-up at dislocations is again prevalent. Since dislocation pile-ups at high angle boundaries are conceptually likely and enhanced partitioning and/or uptake at dislocations has been demonstrated, the hypothesis could be made that this process contributes to intergranular fracture.

Summary of Important Conclusions

Mechanical Properties and Fracture Path

1. Elevated absorbed hydrogen levels result in HE of Al-Li-Cu-Zr alloys as demonstrated by fracture toughness testing of precharged specimens under the monotonic loading conditions utilized.
2. HE is operative in the T3, UA and PA tempers. The degree of embrittlement is significant when high angle grain boundaries are favorably oriented relative to the applied stress. When high angle boundaries are not favorably oriented HE appears to correlate with the effects of hydrogen on slip localization.
3. Absorbed hydrogen has been shown to be trapped at several sites in AA2090, including; solid solution lithium, δ', T_1,

dislocations, and high angle grain boundaries. Hydrogen trapping at high angle boundaries correlates with the preferred fracture path, but only when favorably oriented in the stress field, such as in fine grain recrystallized Al-Li-Cu-Zr in the UA and PA tempers.

4. Increased absorbed hydrogen has been shown to heavily influence the slip localization for underaged tempers of AA2090.

Hydrogen Analysis

1. Significant hydrogen concentrations in Al-Li-Cu-Zr alloys result from AI aqueous exposure. The resulting absorbed hydrogen concentrations are much greater than those needed to produce HE under the loading conditions utilized when other criteria are met.
2. Absorbed hydrogen has been shown to be trapped at several sites in AA2090, including; solid solution lithium, δ' particles, T_1 plates, dislocations, and high angle grain boundaries. The relative ranking of trap binding energies is Li_{ss} < δ' < dislocations < T_1 particles and high angle boundaries.
3. Dislocations can collect trapped hydrogen from lower energy trapping states during dynamic straining.
4. Repartitioning of hydrogen to higher energy sites, such as grain boundaries, within a plastic zone is possible but not confirmed.
5. Dynamic straining in 0.1 M HCl under cathodic polarization or in moist laboratory air results in hydrogen uptake that occurs preferentially at dislocations.

Tasks for the next reporting period

Steve Smith's Ph. D. work will terminate in the Spring of 1995. Limited experimental work will be conducted only to

complete unfinished tasks. The majority of the research effort during this period will be directed towards documentation of this investigation in the form of the Ph.D. thesis document and archival publications.

References

1. R.G.Buchheit, J.P.Moran and G.E.Stoner, Corrosion, Vol. 46, pp.610-617,1990.

2. E.I.Meletis, W.Huang, Mater.Sci. and Eng.,AI48,P.197,1991.

3. R.Balasubramaniam, D.J.Duquette, K.Rajan, Acta.Met., 39, pp. 2597-2605, 1991.

4. R.Balasubramaniam, D.J.Duquette, K.Rajan, Acta.Met., 39, pp. 2607-2613, 1991.

5. R.S.Piascik and R.P.Gangloff, Metall. Trans. A, in review.

6. R.J. Bucci, et.al., Cooperative Test Program for the Evaluation of Engineering Properties of Al-Li Alloy 2090-T8X Sheet, Plate and Extrusion Products, NSWC TR 89-106, 1989.

7. G.M. Scamans, R. Alani and P.R. Swann, Corr. Sci., 16, pp. 443-459, 1976.

8. J.W. Watson, M. Meshii, In Aluminum Alloys-Contemporary Research and Applications, eds. A.K. Vasudevan, R.D. Doherty, pp. 501-521, 1989.

9. ASTM. Standard Practice for Evaluating Stress Corrosion Cracking Resistance of Metals and Alloys by Alternate Immersion in 3.5 % Sodium Chloride Solution G 44-88, Vol. 03.02, pp. 162-165, 1991.

10. S.W.Smith, J.R.Scully, "NASA-UVa Light Aerospace Alloy and Structures Technology Program," U.Va. Report No. UVA/528266/MS92/111, January 30, 1992.

11. S.W.Smith, J.R.Scully, "NASA-UVa Light Aerospace Alloy and Structures Technology Program," U.Va. Report No. UVA/528266/MS93/111, July 1992.

12. S.W.Smith, J.R.Scully, "NASA-UVa Light Aerospace Alloy and Structures Technology Program," U.Va. Report No. UVA/528266/MS93/112, March 1993.

13. S.W.Smith, J.R.Scully, "NASA-UVa Light Aerospace Alloy and Structures Technology Program," U.Va. Report No. UVA/528266/MS94/113, July 1993.

14. S.W.Smith, J.R.Scully, "NASA-UVa Light Aerospace Alloy and Structures Technology Program," U.Va. Report No. UVA/528266/MSE94/116, July 1994.

15. R.J. Kilmer, G.E. Stoner, "NASA-UVa Light Aerospace Alloy and Structures Technology Program," U.Va. Report No. UVA/528266/MS93/112, March 1993.

16. S.W.Smith, J.R.Scully, "NASA-UVa Light Aerospace Alloy and Structures Technology Program," U.Va. Report No. UVA/528266/MS94/114, January 1994.

17. S.W.Smith, J.R.Scully, "NASA-UVa Light Aerospace Alloy and Structures Technology Program," U.Va. Report No. UVA/528266/MSE94/116, July 1994.

18. S.W. Smith, J.R. Scully, "Hydrogen Trapping and Its Correlation to the Hydrogen Embrittlement Susceptibility of Al-Li-Cu-Zr Alloys," 5th International TMS Conf. on Hydrogen Effects on Materials Behavior, eds. N. Moody and A.W. Thompson, Jackson, Wyoming 1994.

19. ASTM. Standard Test Method for Determining J-R Curves E 1152-87, Vol. 03.01, pp. 825-835, 1991.

20. K.V. Jata, and E.A. Starke, Jr., Met. Trans. A, 17A, pp. 1011-1026, 1986.

Table I. Fracture initiation toughness for unrecrystallized T3 AA2090 from J-integral testing.

Alloy	Charging Condition	J_i (kJ/m^2)	K_i (MPa$\sqrt{m}$)
AA2090 - T3 - LT	Uncharged	22.25	41.82
	Charged 28 days	11.40	29.93
AA2090 - T3 - TL	Uncharged	18.76	38.40
	Charged 28 days	13.04	32.01

All charged specimens were Ni-coated and precharged at -1 V_{SCE} in 0.25 M Na_2SO_4 buffered to pH 7.

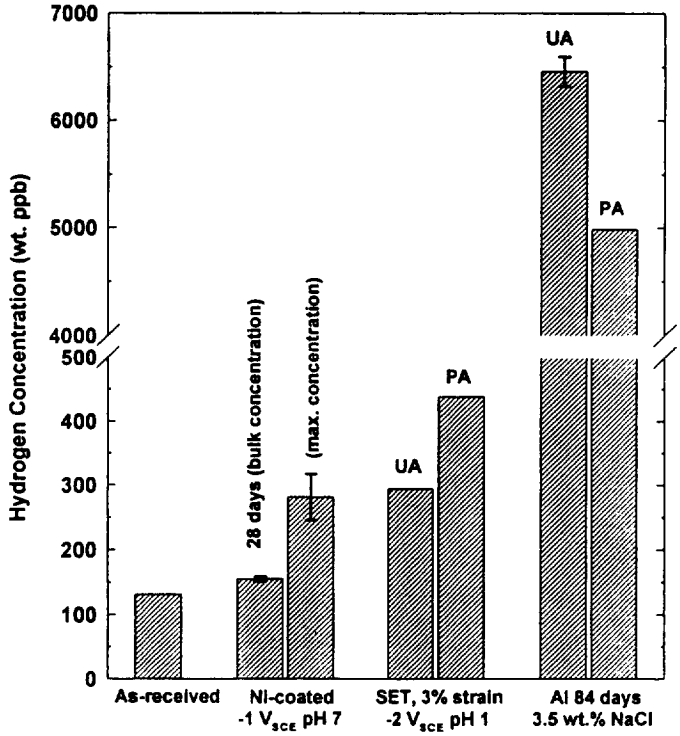

Figure 1. Comparison of total hydrogen concentrations (trapped + lattice) in AA2090 for Ni-coated, concurrent straining and cathodic charging, and alternate immersion charging procedures.

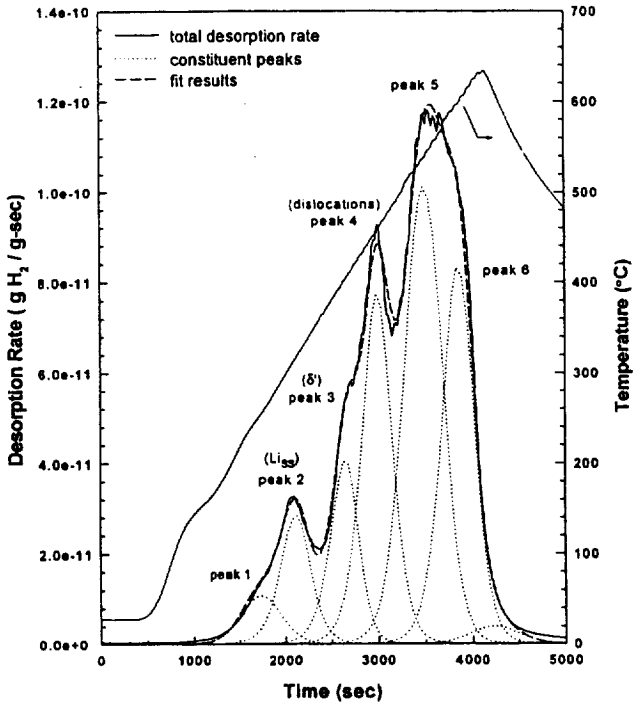

Figure 2. Desorption spectra for hydrogen charged UA AA2090 tested at 10°C/min, identifying trapping states. Specimen was Ni-coated and charged for 28 days at -1 V_{SCE} in pH 7 solution.

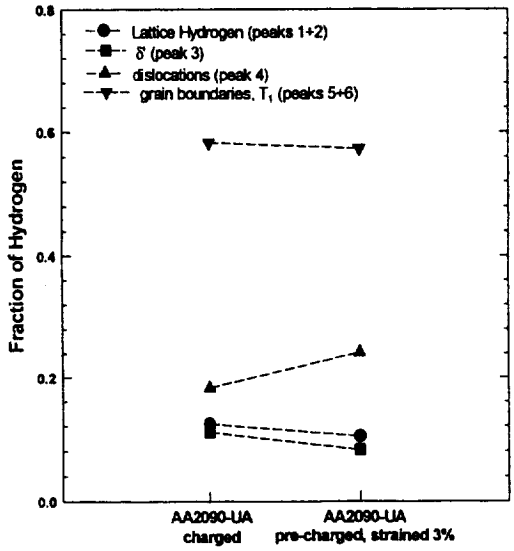

Figure 3. Hydrogen partitioning for AA2090, UA temper, precharged and strained 3% in air. Specimens were Ni-coated and charged at -1 V_{SCE} for 28 days in pH 7 solution.

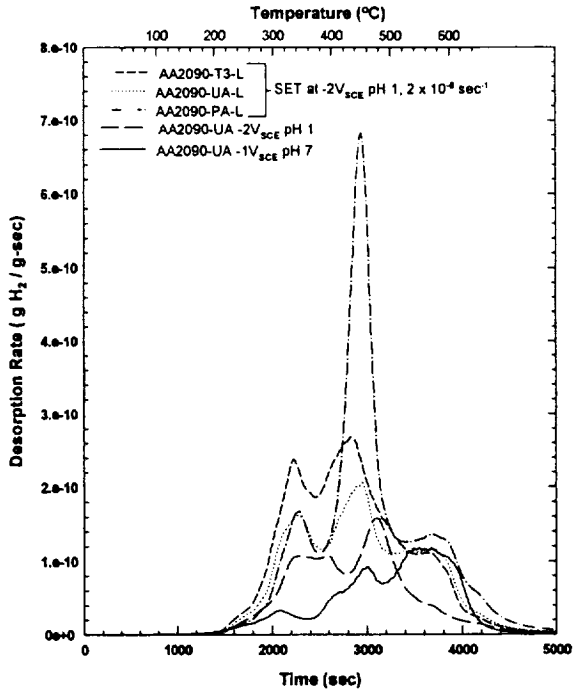

Figure 4. Desorption spectra for AA2090, tested at 10°C/min, for concurrent straining and charging in pH 1 HCl solution at -2 V_{SCE} to a total strain of 3%.

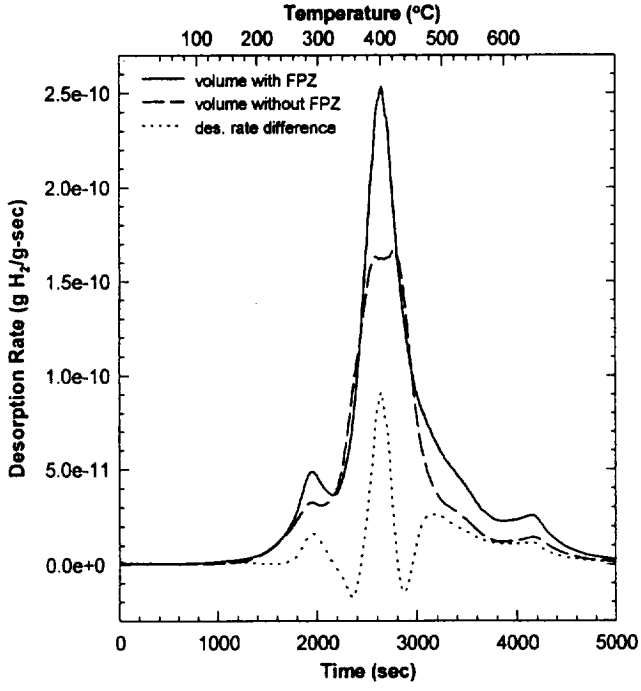

Figure 5. Desorption spectra for hydrogen precharged T3 AA2090-TL tested at 10°C/min, following fracture toughness testing.

Project 6 Mechanisms of Deformation and Fracture in High-Strength Titanium Alloys: Effects of Temperature and Hydrogen

Sean P. Hayes and Richard P. Gangloff

Background and Problem Statement

Metastable beta (ß) titanium alloys are being considered for the airframe of the proposed High Speed Civil Transport (HSCT), in part because of time-temperature independent mechanical properties. Such alloys must meet the requirements of high strength, high fracture toughness (K_{IC}), and high elastic modulus. The high ultimate strength goal is 1450 MPa, with K_{IC} equal to 65 MPa$\sqrt{m}$ and K_{APP} equal to 110 MPa$\sqrt{m}$. The maximum operating temperatures of the HSCT range from 125 to 200oC and life is on the order of 60,000 hours.

The fundamental mechanisms of deformation and fracture in high strength titanium alloys must be established to provide a basis for alloy and process development. While there has been substantial work in this regard for α/β alloys, studies of high strength metastable ß alloys with α precipitates are limited. A second challenge facing titanium alloy development is the uncertain effect of elevated temperature, hydrogen dissolved from prior service, and sustained or slow loading. While it is reasonable to expect mildly increasing fracture toughness with increasing temperature over the HSCT operating range, the potential effects of time-dependent deformation and strain aging must be examined. Additionally, dissolved hydrogen can embrittle α/β and metastable ß-titanium alloys by both transgranular cleavage and intergranular mechanisms. At issue is whether windows of mechanical, chemical and microstructural variables that promote embrittlement overlap with the conditions of HSCT operations. Hydrogen embrittlement of high strength alloys is relatively unexplored.

Objective

The broad objective of this research is to characterize and understand the relationships between microstructure, deformation mode and fracture resistance of high strength and tough titanium alloys for HSCT applications. The initial objective of this project is to characterize the effects of time, temperature and dissolved hydrogen on the fracture toughness of an advanced metastable ß-titanium alloy. The mechanisms for deformation and fracture will be defined physically and modelled micromechanically.

Technical Approach

Sean P. Hayes began PhD studies at UVa in the Fall of 1994, and has worked on this project for four months. The following areas are being examined.

Material

A metastable ß-titanium alloy was selected to meet the high strength goal cited in the HSCT program reports. This alloy is referred to as Low Cost Beta or TIMETAL LCB, and has the composition given in Table I.

Table I Chemical Composition of Low Cost Beta (weight pct)

Ti	Mo	Fe	Al	O
Balance	6.8	4.5	1.5	0.09

Iron and molybdenum are beta stabilizing alloy additions which lower the cost of alloy formulation to about the same level as pure titanium, hence the name Low Cost Beta [1]. In this alloy the martensite start temperature is less than 25°C to prevent

transformation during cooling. High strength is achieved in this thin sheet by solid solution hardening, coupled with microstructural refinement through thermal-mechanical processing. Rolling in the two phase ($\alpha+\beta$) field, solution treating above the ß-transus, cold rolling, solution treating in the α/β phase field, and then aging produces a fine $\beta+\alpha$ microstructure where the body-centered-cubic beta phase is continuous. Optimum strengthening is achieved when the α phase precipitates are fine and homogeneously distributed.

The LCB alloy was ordered from J. Fanning at TIMET and the following are the sheet dimensions; 1.397 cm x 15.24 cm x 30.48 cm (0.055" x 6" x 12"). TTT curves for LCB are being developed by H.J. Rack at Clemson University, and extensive microstructure-processing studies are underway at TIMET, so that the thermal-mechanical treatments that should be used for this alloy can be better understood. The alloy will be provided in a single peak aged condition selected by TIMET. The estimated yield strength and plane strain fracture toughness for this LCB sheet are 1500 MPa and 65 MPa$\sqrt{m}$, respectively. Plane stress fracture toughness should exceed 110 MPa$\sqrt{m}$.

Fracture Mechanics Characterization

Recent work at UVa has shown that fracture mechanics can be applied to characterize and understand the time-temperature dependent fracture behavior of advanced elevated temperature aluminum alloys [2-4]. These methods will be employed for testing titanium alloys. The experiment employs a rising load R-curve method, measured in terms of the applied J-integral (equal to $(K^2/E)_{elastic} + J_{plastic}$) versus crack extension, Δa. Using this technique, load, load-line displacement, crack length (from direct current electrical potential), and temperature will be measured as a function of time for a specimen contained in a convection furnace mounted on a computer-automated closed-loop servoelectric

test machine. This technique yields measurements of the plane strain initiation toughness (K_{ICi}) and the plane stress tearing resistance (T_R, K_C, or $K_{Applied}$ versus da/dt) with a single fracture mechanics specimen. We will employ 1.4 mm thick, fatigue precracked compact tension specimens, restrained with face-plates to prevent buckling. Specimen width will be 8.9 cm.

Hydrogen Embrittlement

A goal of this project is to understand the effect of lattice-dissolved and microstructure- trapped hydrogen on crack propagation in LCB at the high strength level. The LCB alloy will be precharged with hydrogen to produce several hydrogen concentrations between 50 and 1000 wppm. Literature on α/β alloys shows that hydrogen embrittlement is severe at concentrations ranging from 50 to 250 wppm [5,6], while higher amounts are generally required to embrittle β/α alloys [7,8]. Temperature, loading rate and yield strength effects on α/β alloys such as Ti-6Al-4V are well characterized and modeled [5,6], however, only a single value for each of these important variables has been examined for high strength metastable ß-titanium alloys [7,8].

LCB sheet has not been delivered to UVa; preliminary experiments are being conducted on Beta 21S plate (Ti-15Mo-3Al-3Nb, wt %). Three compact tension specimens were precharged with hydrogen to produce a total dissolved hydrogen concentration between 500 and 800 wppm. An electrochemical technique was used, with the CT specimens immersed and cathodically polarized in a solution of 10 ml sulfuric acid, 1000 ml water, and 0.8 g $Na_4P_2O_7$ at 90°C [9]. A cathodic current density of 0.15 mA/cm^2 was selected based on hydrogen charging results from a peak aged Beta-C alloy for which a calibration curve of total dissolved hydrogen concentration versus current density was established. A charging time of 168 hours was selected based on diffusion calculations (D_H = 0.00191* exp(-6640 cal/RT), cm^2/sec) to insure that the hydrogen

concentration is uniform throughout the CT specimen thickness. A Beta 21S blank was charged in the same way as the CT samples, and is currently being tested using a hot vacuum extraction method to determine the exact hydrogen level.

Compact tension specimens that are precharged with a single dissolved hydrogen concentration will be tested using the rising load R-curve method. The two parameters of interest for the precharged samples are loading rate and test temperature. The loading rate will vary such that tests will last from minutes up to one week, and the temperature range of interest is from room temperature to 200°C. Since the number of available Beta 21S CT specimens is limited, the R-curve fracture experiments will focus on 25 and 175°C. A single slow loading rate will be employed in an attempt to accentuate any deleterious effect of either elevated temperature or dissolved hydrogen [5].

Results During the Reporting Period

The rising load R-curve test method was used to determine the fracture toughness of Beta 21S plate at 150°C and with a load-line displacement rate of 0.22 μm/min. This loading rate is about 50 times slower than the level employed for a conventional fracture toughness experiment; the experiment required about 72 hours for specimen fracture. Direct current electrical potential data contained considerable noise so that crack length was not monitored and the R-curve was not established. Rather, the plot of load versus crack mouth opening displacement (CMOD) in Figure 1 was used to calculate the plane strain fracture toughness (K_{IC}) based on ASTM standard E-399 and a 95% slope-intercept method; K_{IC} equals 71.9 MPa$\sqrt{m}$ for Beta 21S at 150°C and the slow loading rate.

Figure 1 superimposes two load versus CMOD plots for Beta 21S plate at 25 and 150°C to show the effect of temperature on fracture toughness. These data for Beta 21S at 25°C were determined during previous research on this same lot of material [10]. From ASTM Standard E-399, K_{IC} equals 65.9 MPa$\sqrt{m}$ for Beta 21S at 25°C. These

results suggest that elevated temperature and slow loading rate do not degrade the plane strain fracture toughness of Beta 21S plate. It is unlikely that creep deformation and subcritical crack growth would reduce the initiation fracture toughness of a titanium alloy at the relatively low temperature of 150°C, consistent with the results in Figure 1. Dynamic strain aging (for example from dissolved oxygen), hydrogen embrittlement from the low level of as-received dissolved hydrogen, or environmental embrittlement from water vapor or oxygen in the moist laboratory environment could reduce KIC with increasing temperature and decreasing loading rate. The preliminary results in Figure 1 suggest that these mechanisms are not operative, at least for Beta 21S plate at 150°C. The increase in fracture toughness with increasing temperature for Beta 21S could be traced to declining yield strength (σ_{YS}), declining modulus of elasticity (E), increasing work hardening and increasing strain rate hardening [3]. These latter two factors act to increase the intrinsic fracture resistance (tensile ductility, ε_F) of an alloy [4]. Fracture toughness roughly equals the square root of the product of σ_{YS}, ε_F, and E [3].

The plane strain fracture toughnesses of high strength Beta 21S and Beta C vary significantly with yield strength and other undefined metallurgical factors [10,11]. Such variation must be considered when both ranking alloy performance, and evaluating temperature and dissolved hydrogen effects on fracture toughness. Table II shows the plane strain fracture toughness of plate Beta 21S, correlated with yield strength, for several replicate experiments conducted at 25°C [10,11], and the result of the single 150°C experiment. Each specimen was obtained from Beta 21S plate, and was aged to peak hardness by the same ß-phase solution treatment, air cool and α/β-phase field aging temperature and time. The microstructural source of the different yield strengths is not known. At 25°C, fracture toughness decreased with

Table II

Yield Strength-Plane Strain Fracture Toughness Results for Beta 21S Plate

Yield Strength (MPa)	K_{IC} @ 25°C (MPa$\sqrt{m}$)	K_{IC} @ 150°C (MPa$\sqrt{m}$)
1286	77.0	
1330	66.2	
1425	67.9	71.9
unknown	65.9	

increasing yield strength, explaining some of the variability in K_{IC} for seemingly replicate specimens. An empirical relation was developed to relate yield strength and plane strain fracture toughness for the 25°C case:

$$K_{IC} = 131.3 - 0.046 * \sigma_{YS}$$

where σ_{YS} is in MPa and K_{IC} is in MPa$\sqrt{m}$. Yield strength at 25°C is related to Rockwell C-scale (R_C) hardness by the following expression:

$$\sigma_{YS} = -97.93 + 33.67 * RC$$

where yield strength is in MPa [11]. The Beta 21S sample tested at 150°C had a hardness of R_C 45.2, which corresponds to a yield strength of 1424 MPa which is in the upper range of the strengths listed in Table II. The calculated K_{IC} for this strength level is 66.5 MPa$\sqrt{m}$ and the value measured for the identical yield strength is 67.9 MPa$\sqrt{m}$. The toughness measured at 150°C is somewhat higher

than these values, consistent with the expected mild effects of σ_{YS}, ε_F, and E on K_{IC}. These trends will be further developed when specimens of LCB are available.

Proposed Research

The following research is proposed for 1995:

- Establish rising load R-curves for Beta 21S at three temperatures (25, 75, and 150°C), for a single constant slow loading rate and precharged hydrogen concentration, and also for an uncharged sample at 150°C and a constant slow loading rate.
- Establish a calibration curve of total dissolved hydrogen content versus applied cathodic current density for thin sheet specimens of LCB at a fixed charging time (7 days at 90°C).
- Conduct replicate fracture toughness experiments with a single high strength LCB sheet microstructure with the as-received hydrogen content (20-50 wppm), using a single thickness CT specimen, a standard loading rate, and a 25°C test temperature to characterize K_{IC}, T_R, $K_{Applied}$, and a portion of the R-curve.
- Examine the effect of compact tension specimen thickness (1.0 to 13 mm) on the R- curve. Specimens of varying thickness will be machined from LCB plate obtained from TIMET.
- Characterize the interactive effects of temperature (-125 to 275°C) and loading rate (1 minute to 1 week duration tests) on the R-curve for LCB sheet, including both the as- received and a single precharged level (650 wppm) of dissolved hydrogen.
- Determine fracture modes with scanning electron microscopy.

References

1. P.J. Bania, J. of Metals, p. 16 (1994).

2. W.C. Porr, Jr. and R.P. Gangloff, Metall. and Matls. Trans. A, Vol. 25A, p. 365 (1994).

3. B.P. Somerday, Yang Leng and R.P. Gangloff, "Elevated Temperature Fracture Toughness of a Particulate Reinforced Aluminum Alloy Composite--Part I: Fracture Toughness Characterization", Fatigue and Fracture of Engineering Materials and Structures, in review (1994).

4. S.S. Kim, M.J. Haynes and R.P. Gangloff, "Localized Deformation Control of Elevated Temperature Fracture in Submicron Grain Aluminum with Dispersoids", Materials Science and Engineering A, in review (1994).

5. N.R. Moody and J.E. Costa, in Microstructure-Properties Relationships in Titanium Alloys and Titanium Aluminides, Y.W. Kim and R.R. Boyer, eds., TMS- AIME, Warrendale, PA, (1991).

6. J.P. Lucas, in Hydrogen Effects on Material Behavior, N.R. Moody and A.W. Thompson, eds., TMS-AIME, Warrendale, PA, p. 871 (1990).

7. G.A. Young and J.R. Scully, Corrosion, December, p. 919 (1994).

8. G.A. Young and J.R. Scully, Scripta Metall., Vol. 28, p. 507 (1993).

9. G.A. Young, "Hydrogen Effects in Metastable ß-Titanium Alloys", MS Thesis, University of Virginia, Charlottesville, VA (1993).

10. J.A. Grandle, B.P. Somerday and R.P. Gangloff, in Proc. of the Tri-Service Conference on Corrosion, T. Naguy, ed., USAF Wright-Patterson Air Force Base, OH, pp. 375- 392 (1994).

11. L.M. Young, G.A. Young, Jr., J.R. Scully, and R.P. Gangloff, Metall. and Matls. Trans. A, in press (1994).

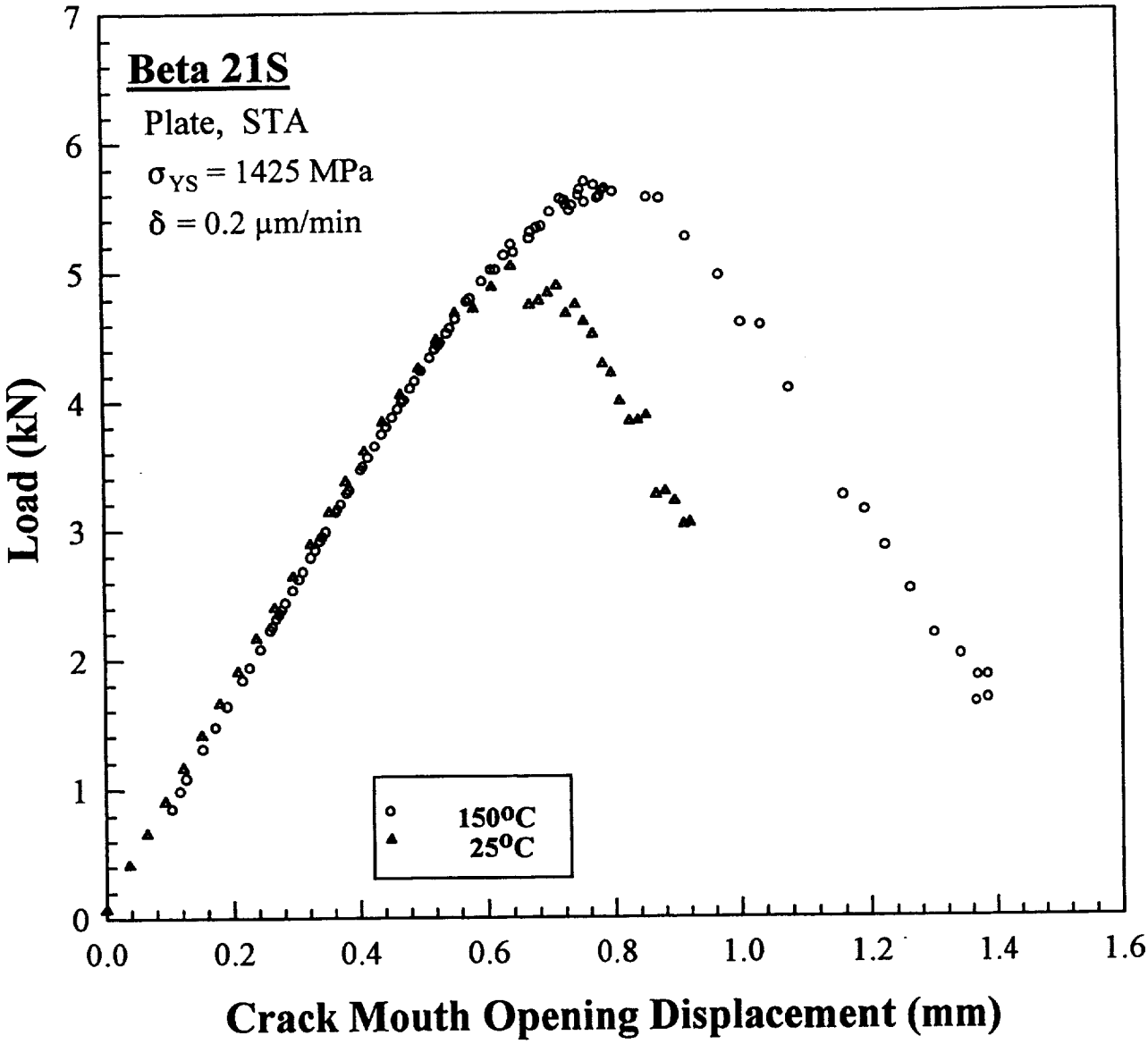

Figure 1 Load *vs* CMOD for peak-aged Beta-21S plate, in the as-received condition (without hydrogen charging), fractured at 25°C and 150°C.

Project #7 **Evaluation Of Wide-Panel Aluminum Alloy Extrusions**

Mark T. Lyttle and John A. Wert

Research Objectives

The overall objective of this project is to experimentally observe and model the effects of microstructure and texture on yield strength in wide panel aluminum alloy extrusions. The modeling results will enable the prediction of locations and tensile axis orientations corresponding to minimum yield strength where localized yielding could occur. A generalized form of these models can be applied to any combination of microstructure and texture found in other aluminum alloys.

Background and Approach

The large extrusion presses available in Russia offer the possibility of manufacturing wide panel extrusions with integral stiffeners. The manufacturing process used by the Russians involves extrusion of tubular forms with longitudinal L-shaped stiffeners protruding from the outer surface. The extruded tube is slit longitudinally and flattened in a series of rolling and stretching operations. The final product is a wide, flat panel with integral stiffeners on one side. The integrally stiffened panels may provide an economical alternative to conventional riveted or adhesively bonded aircraft and launch vehicle structures.

The manufacturing operations described above result in complex metal flow patterns in many portions of the panel, creating certain microstructure and crystallographic texture characteristics that are far different from those found in conventional rolled or extruded aluminum products. Because of the shape of the extrusions in the vicinity of the stiffeners, the metal flow pattern during extrusion and flattening operations varies greatly over short distances (on the order of several millimeters). Since mechanical properties depend on

microstructure and texture, the mechanical properties are virtually certain to vary with location in the panels, particularly in the vicinity of the stiffeners. In addition, substantial out-of-plane loading is likely to occur in the vicinity of the stiffeners. Knowledge of the variation of mechanical properties with location in the panels, and with loading direction at these locations, is needed for efficient and safe use of wide-panel aluminum alloy extrusions in aerospace vehicles.

As indicated at the briefing by Akad. Fridlyander and Professor Davydov, NASA Langley investigators and NASA contractors will perform mechanical tests in an effort of evaluate the variation of tensile properties as a function of location and stress axis orientation. However, the tensile specimen size is 10's of millimeters, while microstructure and texture variations are known to occur on a scale of millimeters in and near the stiffeners. As a result of the difference in size scale, conventional tensile specimens can only reveal the average yield strength in regions where the microstructure varies on a small scale. Use of the average yield strength for design purposes could lead to plastic flow regions where the yield strength is below the average value. In addition, only a few tensile specimen orientations are proposed for testing. The selected orientations are those that often correspond to extreme (high and low) tensile properties in conventional sheet materials, but will not necessarily correspond to the extreme properties at locations in and near the stiffeners. Microstructure and texture vary over such a small scale in and near the stiffeners that direct property evaluation would be difficult.

The proposed work will address this problem through a combination of experimental measurements and modeling of the influence of microstructure and texture on tensile properties. Four aspects of the material will be characterized experimentally at selected locations: texture, grain morphology, deformation substructure, and precipitate morphology. These characteristics will be incorporated into previously proposed models that predict

yield strength based on separate characteristics. An effort will be made to blend the previous models into an overall model to predict yield strength as a function of stress axis orientation for the selected alloy. The model will be tested and refined by comparison with tensile test results generated by NASA and NASA contractors, and by additional tests at UVa. The model will then be used to predict the extreme values of yield strength, and the associated stress axis orientations, as a function of location in and near the stiffeners. These results can then be used to define limiting load conditions for the panels such that localized yielding is avoided. It is possible that the results could also be used to recommend changes in processing conditions (for example: extrusion temperature, die geometry, or flattening procedure) that would raise the minimum yield strength or change its stress axis orientation, resulting in improved panel performance.

A major goal of this research is the prediction of yield strength as a function of microstructural characteristics. Models based on fundamental principles now exist for understanding the contribution of precipitate particles, solute in solid solution and dislocation substructure to yield strength [1-3]. However, due to the complexity of microstructural features found in real engineering materials, synthesis of these various strengthening mechanisms into a unified model that can accurately predict yield strength directionality has not been previously described.

The three primary microstructural aspects influencing yield strength that will be investigated are slip plane orientation, precipitate location and morphology, and grain morphology. Characterization of the microstructure will be focused on these three areas:

1. Use texture results to perform Taylor/Bishop-Hill yield anisotropy predictions for both in-plane and out-of-plane tensile axis orientations. Using texture results obtained from pole figure data, a set of grains representative of the orientations present in each area of the extrusion can be generated. Combining Taylor/Bishop-Hill analyses and this representative set of grains,

the active set of slip systems and corresponding Taylor factor in each grain can be determined. Averaging over all grains yields the average Taylor factor for the specified uniaxial stress orientation.

2. Microstructural assessment by TEM will reveal the precipitate type, size, habit plane, volume fraction, and morphology as a function of location. Since the dislocation substructure is inhomogeneous, the precipitate characteristics may vary as a function of location within the extrusions. The precipitate characteristics at each location will be inserted into the appropriate precipitate inclusion model to assess the contribution of precipitate strengthening to yield strength.

The plastic and elastic inclusion models for calculating precipitate strengthening assume plastically deformed precipitates (sheared precipitates) and elastically deformed precipitates (looped precipitates), respectively. By comparing the accuracy of the two methods for predicting the strengthening increment due to precipitates, one could gain some basic insight into the role of looping and shearing of precipitates by dislocations. By performing a statistical assessment of the fit between model results and experimental data, insight into the dislocation mechanism responsible for the precipitate strengthening in a given alloy could be gained. Since different regions in the wide-panel extrusions contain precipitates of various sizes, orientations, and morphologies, any change in the relative influence of looping and shearing will be readily observable. This information could be useful in establishing secondary precipitate characteristics that are desirable for enhanced panel properties.

3. Grain morphology will be determined by optical metallography. When grains are not equiaxed, some relaxation of the compatibility requirements of the Bishop-Hill model occurs. Modeling the effect of grain morphology and the concurrent relaxed constraint conditions, leads to a reduction in Taylor factor in certain orientations. Incorporation of grain morphology into yield surface predictions seems essential in cases where grain shape is not essentially equiaxed.

Because of texture variation on a microscopic scale and the desirability of conducting out-of-plane testing, compression testing on small samples is necessary to precisely isolate the variation of yield strength on a local scale. A compression apparatus has been developed which allows accurate and replicable determination of yield strengths using specimen of dimensions 5 x 2.5 x 2.5 mm.

Progress During the Reporting Period

A model has been constructed to predict the variations in yield strength due to grain orientation, grain morphology, and precipitate plane orientation for both the plastic and elastic inclusion assumptions. Using specimen texture obtained from pole figure data, an average Taylor factor can be determined for any uniaxial direction in the specimen. Combining specimen texture and precipitate plane orientation, the contribution to strengthening from precipitates with a specified habit plane orientation can be calculated.

Inspection of the variation in strengthening increment due to the plastic inclusion and elastic inclusion models reveal no significant differences. The variation in plastic and elastic strengthening increment for the flat region of the extruded stiffener is shown in Figure 1. For this example and all other textures measured in the extrusions, the correlation coefficient between predictions of the plastic and elastic inclusion models is greater than 0.90. Any differences between the predictions of the two models will be difficult to separate from the error in the experimental measurement of yield strengths. For this reason, the following results will be described using solely the plastic inclusion model, as the elastic inclusion model predicts virtually the same behavior.

The effect of grain morphology on yield anisotropy has previously been addressed only in concept, but development of a model and its application to measured grain shapes is currently in progress. Following the guidelines of several researchers [4,5], a predictive yield strength model incorporating grain morphology

has been developed. The present model predicts the deviation of Taylor factor from that predicted for equiaxed grains, for pancake- and lath-shaped grains with an infinite aspect ratio. An example of this variation is shown in Figure 2 for a rolling texture composed of different grain morphologies. Since the 2090 extrusions contain regions of pancake grains of varying diameter/height ratios, regions of fibrous grains, and regions of mixed (fibrous and pancake) grains [6], verification of the grain morphology portion of the overall model will be facilitated by measurement of yield strength at various locations in the extrusions.

Consideration of the effect of grain shape on yield strength anisotropy and magnitude reveals some interesting possibilities for further examination. Examining Figure 2, we see that, in the plane of the extrusion, pancake-shaped grains are expected to exhibit the same yield anisotropy as equiaxed grains, but at a lower strength. This results because as the compression axis is varied in the extrusion plane the morphological orientation of the grain with respect to the compression axis does not vary. Using in-plane testing, variations of yield anisotropy due to grain morphology can only be observed with lath-shaped grains, because of the variation in morphological orientation as the compression axis is shifted.

The more significant aspect of these modeling calculations is the apparent potential for the magnitude of the yield strength to shift significantly due to grain morphology considerations. When subjected to less constraint, grains have an effectively lower Taylor factor and subsequently lower yield strength. It appears that no significant experimental verification of this effect has been cited in the literature. Since the 2095 extrusions contain distinct regions of pancake- and lath-shaped grains, their effect on yield strength magnitude could be measured. From the model, it is predicted that in all orientations, the region with pancake-shaped grains should exhibit higher yield strengths than that in the region containing lath-shaped grains.

Compression testing of different regions of the 2090

extrusion in various in-plane directions in the as-received and the solutionized case has been conducted. Figure 3 shows the correlation between the yield strength prediction of the plastic inclusion model and the experimental results for the skin section of a 2090 extrusion. The correlation coefficient for the plastic inclusion model is 0.69. Comparison of experimental yield strengths measured from many regions of these extrusions will allow the refinement of morphological constants in the yield strength model.

Yield strength has been measured for the skin and cap regions in the 2090 extrusion which contain pancake- and lath-shaped grains, respectively. Variations in yield strength are observed in Figure 4 and can be compared roughly to the typical Taylor factor variations predicted in Figure 2. The cap region (lath-shaped grains) generally exhibits a lower yield strength than the skin region (pancake-shaped grains) for all orientations tested. This is consistent with the model predictions illustrated in Figure 2. Note in particular that equal transverse strength (90°) is predicted in the cap and skin locations, precisely matching experimental observations.

To critically evaluate the significance of these yield strength variations, precipitate and texture effects must be eliminated. Characterization of the microstructure will be conducted to ensure that precipitate morphologies and distributions are similar in both regions. If all aspects of the microstructure are similar except for grain morphology, most of the difference in yield strength magnitude will be attributable to the different grain morphologies.

Conclusions

A model has been developed that incorporates the effects of texture, precipitate characteristics, and grain morphology on yield anisotropy. The effect of precipitate characteristics was addressed by consideration of the precipitate as elastic and plastic inclusions in two separate models. Both of these models predict effectively the same behavior, so further research in this

area will mainly focus on refinement of the plastic inclusion model. Grain morphology is predicted to have a measurable effect on yield anisotropy and magnitude.

While the model does predict the trends observed for experimental yield strengths from pancake- and lath-shaped grains in regions of the 2090 near net shape extrusion, to achieve accurate determination of yield strength a more precise method is necessary to determine the reduction in constraint due to intermediate grain shapes. The experimental differences in yield anisotropy and magnitude in regions of pancake- and lath-shaped grains may be correlated to some of the predictions based on the modeled yield behavior.

Tasks for the Next Reporting Period

The capability to calculate average Taylor factor and the strengthening ratio of precipitates in the plastic and elastic inclusion models for a specified uniaxial stress orientation is complete. The yield strength model consisting of grain orientation and precipitate orientation data accurately predicts the general trends of yield strength variation for the alloys tested, but to generate a more complete and exact description of the yield anisotropy, the effect of basic grain morphology effects has been incorporated into the model. From model calculations, this modification is essential, especially for out-of-plane stress axis orientations. To quantify the magnitude of the influence of grain morphology on yield strength, determination of the experimental effect of grain shape on yield strength anisotropy and magnitude is an important project for the next year.

The first portion of this research, the construction of yield strength models, is complete. Accurate results have been predicted for two regions in the 2090 extrusion. To assess the general applicability and to fine tune the adjustable morphological parameters of these models, extensive yield strength testing and microstructural characterization will be conducted on newly arrived 2096 and 2195 extrusions, as well as the remaining microstructurally distinct regions in the 2090 extrusion.

Personnel

The faculty PI for this task is Professor J. A. Wert and the graduate student who will be conducting the proposed research is Mr. M. T. Lyttle. The student's anticipated completion date is September 1996.

References

1. P. Bate, W. T. Roberts and D. V. Wilson, Acta Metallurgica, **29** (1981) 1797.

2. P. Bate, W. T. Roberts and D. V. Wilson, Acta Metallurgica, **30** (1982) 725.

3. W. F. Hosford and R. H. Zeisloft, Metallurgical Transactions, **3** (1972) 113.

4. U. F. Kocks and H. Chandra, Acta Metallurgica, **30** (1982) 69.

5. Cl. Maurice, M. C. Theyssier and J. H. Driver, in *Advances in Hot Deformation Textures and Microstructures*, J. J. Jonas, T. R. Bieler, K. J. Bowman (eds), TMS, Warrendale, 1994, pp. 411-425.

6. W. D. Pollock and S. J. Hales, "Tensile Fracture of a 2090 Extrusion", to be published in The Fourth International Conference on Aluminum Alloys.

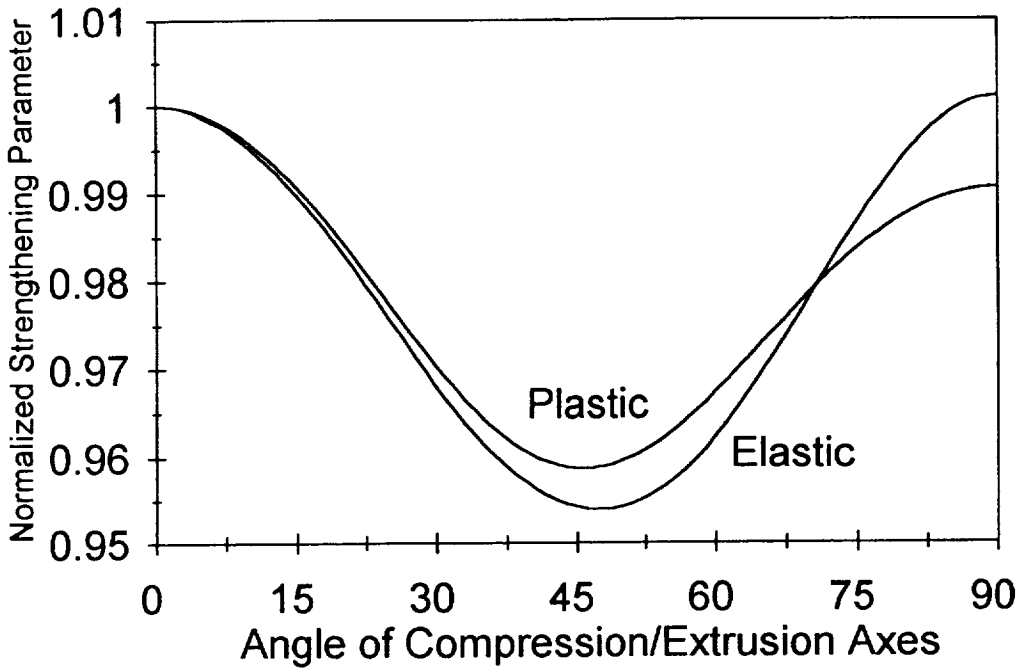

Figure 1. Calculated strengthening increment due to plastic and elastic inclusions in the cap region of a 2090 extrusion. Correlation coefficient between the two predictions is .98. Similar correlations are observed for all measured textures.

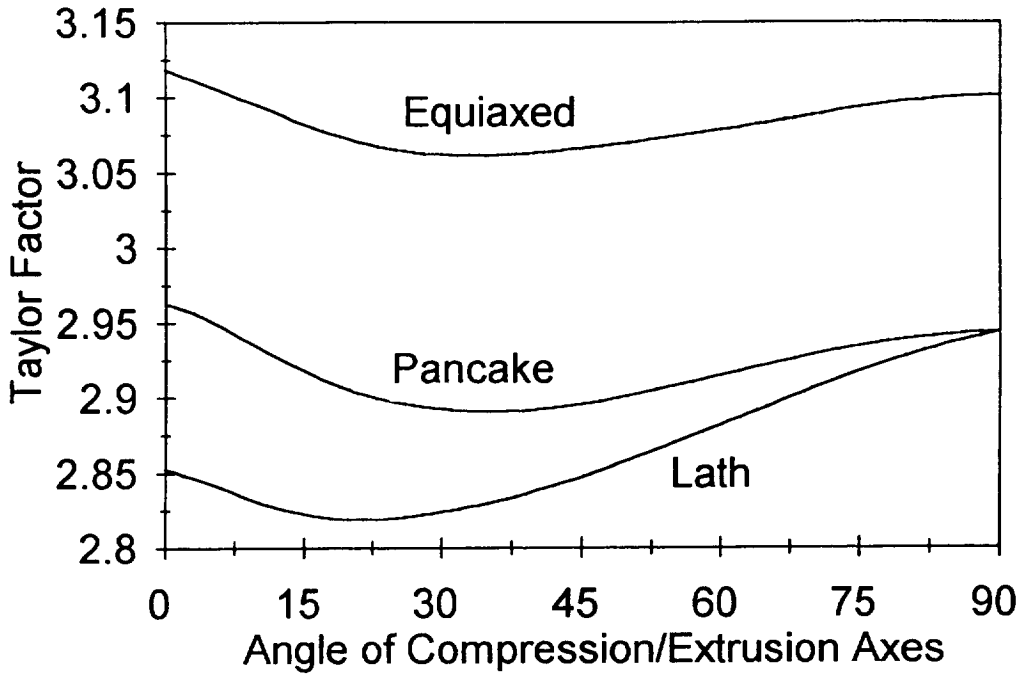

Figure 2. Calculated Taylor factor variation due to grain morphology in a specimen containing a weak rolling texture. Pancake-shaped and equiaxed grains exhibit the same yield anisotropy but different magnitudes of yield strength. Lath-shaped grains are predicted to cause a distinct yield anisotropy and strength from other morphologies given otherwise similar microstructures.

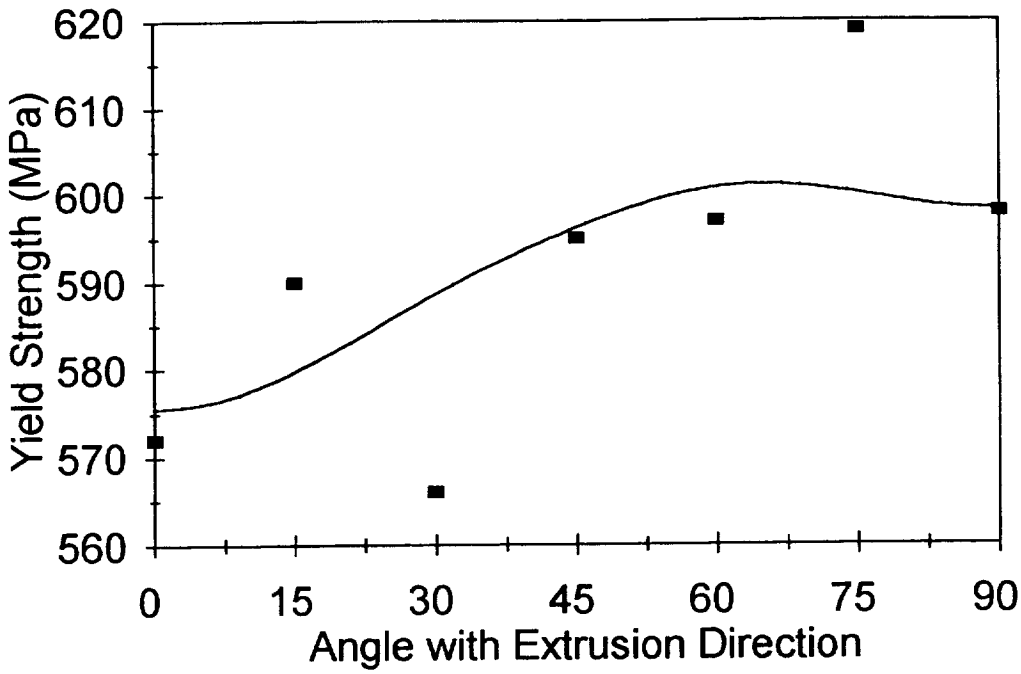

Figure 3. Comparison of experimental yield strengths and yield strengths predicted by the plastic inclusion model for the skin of the 2090 extrusion. The correlation coefficient is 0.69.

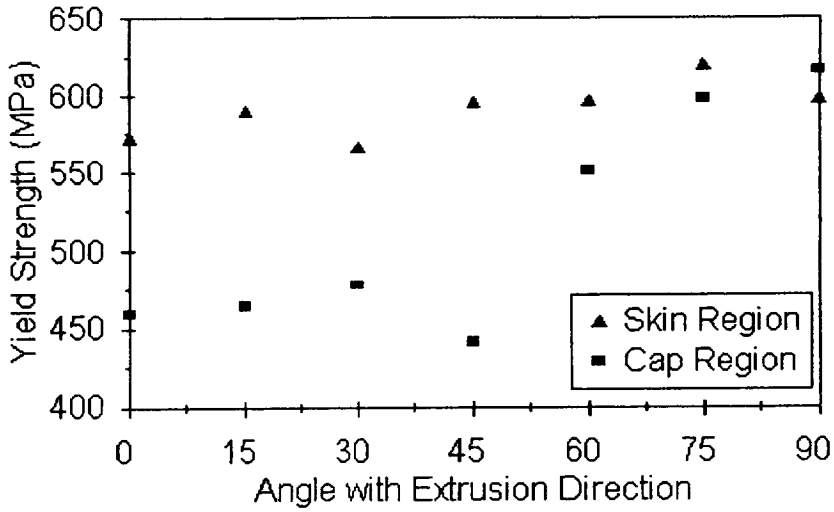

Figure 4. Comparison of yield strengths in the skin and cap regions of the 2090 near net extrusion. The skin and cap regions contain pancake-shaped and lath-shaped grains, respectively.

Project #8 **Al-Si-Ge Alloy Development**

H.J. Koenigsmann and E.A. Starke, Jr.

Research Objective

The objective of this project is to investigate the strengthening mechanisms and the void nucleation process in a recently developed Al-0.55Si-2.02Ge (wt.%) alloy. The relationship between precipitate size and critical strain for cavity nucleation during plastic deformation is of primary interest.

Background and Approach

Recently developed age-hardenable Al-Si-Ge alloys utilize a uniform distribution of very small SiGe precipitates that have an incoherent interface with the matrix and are looped by dislocations [1,2]. These features result in a high degree of hardening for a small volume fraction of precipitates [2]. SiGe precipitates have a diamond structure and can be expected to have a better thermal stability than precipitates of other age-hardenable aluminum alloys due to the low solubility of both Si and Ge in Al [3,4].

As compared to binary Al-Si and Al-Ge alloys, the precipitate density in ternary Al-Si-Ge alloys is one order of magnitude higher and the equiaxed SiGe precipitates are much more evenly distributed [3]. The explanation for this change is based on the fact that Si has a smaller and Ge has a larger atomic diameter than Al, and the atomic size misfit can be compensated by the formation of pairs of Si and Ge [5]. This effect is accentuated because of the similarities in the electronic structure between Si and Ge [3].

A ternary Al-0.55Si-2.02Ge (wt.%) alloy was provided by Alcoa. The composition of this alloy was chosen in such a way that the atomic size misfit is compensated after the formation of pairs of Si and Ge. An optimum homogenization temperature of

500°C was selected based on the thermal analysis using a Perkin Elmer Differential Scanning Calorimeter (DSC). The alloy was homogenized for 30 hrs, hot rolled, solution heat treated at 490°C, cold water quenched and aged in an air furnace for up to 16 days at 160°C.

Vickers microhardness measurements were performed at room temperature using a Kentron Microhardness Tester AK. Samples for Transmission Electron Microscopy (TEM) were prepared using standard techniques; all TEM examinations were conducted using a Philips EM 400T operated at 120kV. Measurements of both the average radius and the volume fraction of the SiGe precipitates as a function of aging time were performed by quantitative stereological methods [6] and corrected for truncation and overlap [7]; foil thicknesses were determined under two-beam conditions from oscillations in intensity of Convergent Beam Electron Diffraction (CBED) patterns [8].

Room temperature tensile tests [9] were performed using an 810 Material Test System (MTS). The samples were tested in longitudinal direction at a strain rate of $10^{-3}s^{-1}$ after aging for up to 16 days. The volume fraction of voids was determined as a function of strain and aging time through a pycnometer by measuring densities of the deformed gage section and the grip part [10]. The shear modulus of the SiGe precipitates was determined by ultrasonic velocity measurements in the ternary alloy and in pure Al.

The (111), (200), and (220) pole figures were determined from center sections of as-quenched samples using X-ray diffraction. The results were converted into an Orientation Distribution Function (ODF) in order to calculate the Taylor factor [11]. The lattice parameter of the matrix was determined as a function of aging time using a Scintag X-ray diffractometer. These results were correlated with measurements of both the electrical conductivity and the volume fraction of the SiGe precipitates as a function of aging time in order to

determine precisely when solute precipitates and whether there is still solute in solution in the T6 condition.

Progress During the Reporting Period

Table I shows the results of the room temperature tensile tests performed with the ternary alloy after aging at 160°C for different times; the average diameter of the SiGe precipitates as a function of aging time is shown in Figure 1a. With increasing aging time, i.e. increasing diameter of the SiGe precipitates, the tensile ductility decreases significantly, whereas the strength decreases only slightly. The total theoretical yield strength (σ_{th}th, also shown in Table I) can be estimated as follows [1]:

$$\sigma_{th} \approx \Delta\sigma_p + \sigma_{Al} + \Delta\sigma_b + \Delta\sigma_s \qquad (1)$$

where $\Delta\sigma_p$ is the contribution of the SiGe precipitates to the yield strength, σ_{Al} is the yield strength of pure Al, $\Delta\sigma_b$ is the

Table I. Tensile Properties of Al-0.55Si-2.02Ge (wt.%) after Aging at 160°C

Aging Time (d)	σ^*_{th} (MPa)	σ^*_y (MPa)	σ^*_{TS} (MPa)	ε^*_f(%)
1	107	105	164	17
2	90	103	162	16
4	80	100	158	13
8	75	100	155	9
16	67	94	153	9

* σ_{th} - theoretical yield strength, σ_y - experimental yield strength, σ_{TS} - experimental tensile strength, ε_f - experimental plastic strain after fracture

contribution from grain boundary strengthening, and $\Delta\sigma_s$ is the contribution from solid solution strengthening.

The contribution of the SiGe precipitates to the yield strength ($\Delta\sigma_p$) can be estimated using the modified Orowan equation if the precipitates are looped by dislocations [1]:

$$\Delta\sigma_p \approx M'\mu b\sqrt{f}/d \qquad (2)$$

where M' is the ratio between the Taylor factor calculated from X-ray diffraction data (2.86) and the Taylor factor calculated for face-centered cubic metals with a random distribution of grain orientations (3.06 [12]), μ is the shear modulus of the matrix (26GPa [1]), b is the Burgers vector (0.284nm [1]), f is the volume fraction, and d is the diameter of the precipitates. The volume fraction of the SiGe precipitates was determined from TEM micrographs (Figure 2a) using quantitative stereological methods [6], electrical conductivity measurements (Figure 2b) using Nordheim's rule [13], and lattice parameter measurements (Figure 2c) using Vegard's rule [14]. Figure 2d shows the average value determined from these three methods as a function of aging time. The contribution of the SiGe precipitates to the yield strength (equation (2)) was estimated for each aging time based on the size distribution of the SiGe precipitates from TEM micrographs (Figure 3) and the average precipitate volume fraction (Figure 2d).

The contribution of the SiGe precipitates to the yield strength decreases from 81MPa after 1 day of aging to 42MPa after 16 days of aging. The last three contributions in equation (1) which are independent of the SiGe precipitate size become therefore more important at longer aging times. The yield strength of pure Al is about 20MPa [15], grain boundary strengthening contributes about 5MPa [16] for a grain size of about 200 μm (determined using optical microscopy [17]), and the

contribution from solid solution strengthening was estimated to be about 1MPa [4,18,19] using Fleischer's approach [20].

After aging tensile samples of the ternary alloy at 160°C for different times (shown in Table I) and straining to different levels, the void volume fraction (V_f) was calculated as follows [21]:

$$V_f = (\rho_g - \rho_n)/\rho_g \quad (3)$$

where ρ_g and ρ_n are the densities of the grip part and of the deformed gage section, respectively. The results of these measurements performed before necking are shown in Figure 4a. They reflect the combined damage due to void nucleation and growth occurring during straining. Figure 4a shows that the volume fraction of voids determined in the ternary alloy decreases with increasing aging time, i.e. increasing diameter of the SiGe precipitates, at a given true strain value. Higher void volume fractions are observed at higher tensile ductilities corresponding to shorter aging times. The critical strain to nucleate cavities (ε_c) determined from the experimental data by linear regression increases from 0.008 for an average precipitate diameter of 5.0nm to 0.014 for an average precipitate diameter of 14.4nm.

Brown and Stobbs developed two models to describe cavity nucleation in materials containing a dispersion of hard second-phase particles [22,23]. The first model is based upon the criterion that the elastic energy released by removing stress from the particle has to be at least equal to the surface energy created [22]:

$$\Delta E_{el} + \Delta E_s \leq 0 \quad (4)$$

where ΔE_{el} is the internal elastic energy of the particle and ΔE_s

is the energy increase in forming new internal surfaces. Using this energy criterion, one can derive the following expression for the critical strain (ε_c) to nucleate cavities [22,23]:

$$\varepsilon_c \geq \gamma(1-\cos\theta)/2\mu_p b\sin^2\theta \qquad (5)$$

where γ is the precipitate-matrix interfacial free energy, θ is a geometrical correction factor, μ_p is the shear modulus of the precipitates, and b is the Burgers vector.

The precipitate-matrix interfacial free energy can be estimated from the slope of the graph shown in Figure 1b using the coarsening theory by Lifshitz, Slyozov [24], and Wagner [25]. This theory predicts that, when the rate of coarsening is controlled by the diffusion of the solute species through the matrix, the variation of the average radius (r) with time (t) is given by the following equation [26]:

$$r^3 - r_o^3 = 8\gamma D c_o V_m^2 (t-t_o)/9RT \qquad (6)$$

where r_o is the average precipitate radius when coarsening commences at the time t_o, γ is the specific precipitate-matrix interfacial free energy, D and c_o are the diffusivity and the equilibrium molar concentration, respectively, of the solute species in the matrix phase at the temperature T, V_m is the molar volume of the precipitate, and R has its usual meaning. The diffusivity data of Si in Al and Ge in Al used in the calculation are those published in [27]. A total equilibrium concentration of Si and Ge of 0.2wt.% was estimated from [19]. The molar volume was calculated based on the values published in [2] for Si and Ge diamond cubic structures. Note that the graph in Figure 1b is only drawn for longer aging times when the precipitate volume fraction stays approximately constant (Figure 2d).

The energy criterion by Brown and Stobbs predicts a critical strain of 0.008 independent of the precipitate size if one uses a value of $423 mJm^{-2}$ for the precipitate-matrix interfacial free energy (Figure 1b), a geometrical correction factor of 15° [22], a shear modulus of the precipitates of 49GPa (determined through ultrasonic velocity measurements in the ternary alloy and in pure Al assuming the Voigt linear law of mixtures [28] and using the density data published in [29]), and a Burgers vector of 0.284nm [1]. The experimental results (Figure 4a) agree approximately with this prediction, but the critical strain clearly depends on the precipitate size contrary to the prediction of this criterion.

The second cavity nucleation model by Brown and Stobbs is based upon a critical stress (σ_c) which is given by [23]:

$$\sigma_c \approx 4.2\alpha\mu b\sqrt{\rho} \qquad (7)$$

where α is a numerical parameter, μ is the shear modulus of the matrix, b is the Burgers vector, and ρ is the local dislocation density. Accounting for the local dislocation density as a function of strain [23]:

$$\rho \approx 5.1\varepsilon_c/db \qquad (8)$$

where ε_c is the critical strain and d is the precipitate diameter, the resulting stress criterion for cavity nucleation can be expressed as [22]:

$$\varepsilon_c \geq \sigma_c^2 d / 90\alpha^2\mu^2 b \qquad (9)$$

predicting a linear dependence of the critical strain on the precipitate diameter. Figure 4b shows that the experimental results agree qualitatively with this prediction. A good

quantitative agreement is observed if the critical strain is chosen as $\mu/40$ and if the numerical parameter α is chosen as 1/7 [22]. However, at this point the choice of these parameters is not further justified.

Conclusions

The volume fraction of the SiGe precipitates as a function of aging time was determined from TEM micrographs, electrical conductivity measurements, and lattice parameter measurements. The correlation between these three measurements shows that there is still solute in solution in the T6 condition and that precipitation in Al-0.55Si-2.02Ge (wt.%) continues to occur up to about 100hrs at 160°C. This observation led to a significant improvement of the theoretical yield strength prediction for this ternary alloy as a function of aging time.

The volume fraction of voids determined in tensile samples of Al-0.55Si-2.02Ge (wt.%) through a pycnometer decreases with increasing diameter of the SiGe precipitates at a given true strain value. The critical strain to nucleate cavities determined from the experimental data by linear regression increases linearly with precipitate size in agreement with the stress criterion by Brown and Stobbs [22,23].

Tasks for the Next Reporting Period

The future work will focus on the understanding of the void nucleation process in order to evaluate the current models and to develop a more quantitative model without introducing the empirical parameters present in the models by Brown and Stobbs [22,23]. This will include the calculation of the elastic strain distribution around the SiGe precipitates as a function of precipitate size and externally applied stress using the Finite Element Method (FEM) as well as the quantification of the precipitate-matrix interfacial structure using atomic resolution TEM. The quantification of the interfacial structure will allow

to calculate the stresses associated with ledges and steps using the model developed by van der Merwe and Shiflet [30]. In addition to this, the observation of voids around the SiGe precipitates will be attempted using TEM. This would allow to study the separate effects of void nucleation and growth: the void nucleation rate as a function of the SiGe precipitate diameter can be determined by plotting the areal void density as a function of strain for different aging times, i.e. different SiGe precipitate diameters, and a plot of the maximum void size as a function of strain for different aging times allows the determination of the void growth rate as a function of the SiGe precipitate diameter [21].

References

1. E. Hornbogen and E.A. Starke, Jr., Acta Metall. 41, (1993), 1.

2. E. Hornbogen, A.K. Mukhopadhyay and E.A. Starke, Jr., Z. Metallk. 83, (1992), 577.

3. E. Hornbogen, A.K. Mukhopadhyay and E.A. Starke, Jr., Proc. ICAA3, Vol. I (Trondheim, Norway: 1992), 201.

4. E. Hornbogen, A.K. Mukhopadhyay and E.A. Starke, Jr., Scripta Metall. 27, (1992), 733.

5. E. Hornbogen, A.K. Mukhopadhyay and E.A. Starke, Jr., J. Mat. Sci. 28, (1993), 3670.

6. E.E. Underwood and E.A. Starke, Jr., Proc. ASTM-NBS-NSF Symp. (Kansas City, MO: 1978), 633.

7. E.E. Underwood, Quantitative Stereology (Reading, MA: Addison-Wesley, 1970), 187.

8. P.M. Kelly, A. Jostons, R.G. Blake and J.G. Napier, Phys. Stat. Sol. 31A, (1975), 771.

9. P.C. Fazio et al., eds., Annual Book of ASTM Standards, Vol. 03.01 (Philadelphia, PA: ASTM, 1992), 130.

10. J.A. Walsh, M.S. thesis, University of Virginia, Charlottesville, VA, (1988), 39.

11. H.R. Wenk and U.F. Kocks, Metall. Trans. 18A, (1987), 1083.

12. P. Haasen, Physical Metallurgy (Cambridge, UK: Cambridge University Press, 1992), 292-293.

13. C.R. Barrett, W.D. Nix and A.S. Tetelman, The Principles of Engineering Materials (Englewood Cliffs, NJ: Prentice-Hall, 1973), 393.

14. O. Bruemmer et al., eds., Festkoerperanalyse mit Elektronen, Ionen und Roentgenstrahlen (Braunschweig, FRG: Vieweg, 1980), 52-53.

15. L.F. Mondolfo, Aluminum Alloys: Structure and Properties (London, UK: Butterworths, 1976), 72.

16. T.H. Courtney, Mechanical Behavior of Materials (New York, NY: McGraw-Hill, 1990), 170-171.

17. T. Lyman, ed., Metals Handbook, Vol. 8 (Metals Park, OH: ASM, 1973), 42-43.

18. E.A. Brandes and G.B. Brook, eds., Smithells Metals Reference Book (Oxford, UK: Butterworth-Heinemann, 1992), 15/2-15/3.

19. I.J. Polmear, Light Alloys: Metallurgy of the Light Metals (London, UK: Edward Arnold, 1989), 18.

20. T.H. Courtney, Mechanical Behavior of Materials (New York, NY: McGraw-Hill, 1990), 178-181.

21. J.A. Walsh, K.V. Jata and E.A. Starke, Jr., Acta Metall. 37, (1989), 2861.

22. S.H. Goods and L.M. Brown, Acta Metall. 27, (1979), 1.

23. L.M. Brown and W.M. Stobbs, Phil. Mag. 34, (1976), 351.

24. I.M. Lifshitz and V.V. Slyozov, J. Phys. Chem. Solids 19, (1961), 35.

25. C. Wagner, Z. Elektrochemie 65, (1961), 581.

26. J.D. Boyd and R.B. Nicholson, Acta Metall. 19, (1971), 1379.

27. M. Bishop and K.E. Fletcher, Int. Met. Rev. 17, (1972), 203.

28. M.E. Fine, Scripta Metall. 15, (1981), 523.

29. R.E. Bolz and G.L. Tuve, eds., CRC Handbook of Tables for Applied Engineering Science (Boca Raton, FL: CRC Press, 1987), 117 & 273.

30. J.H. van der Merwe and G.J. Shiflet, Acta Metall. 42, (1994), 1173.

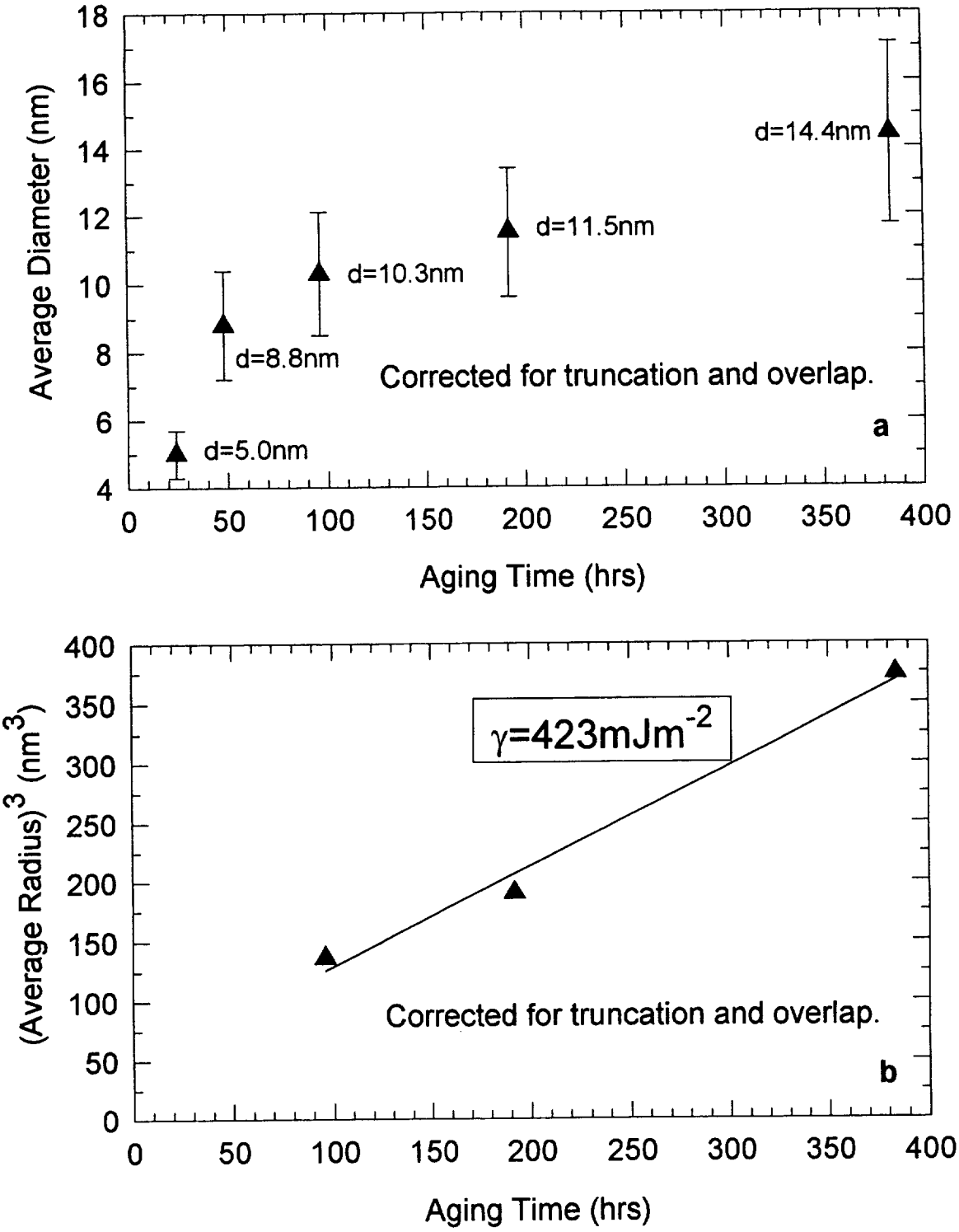

Figure 1. Change of the SiGe precipitate size in Al-0.55Si-2.02Ge (wt.%) during aging at 160°C. (a) Average precipitate diameters. (b) Relationship between cube of average precipitate radii and aging time, estimated precipitate-matrix interfacial free energy (γ).

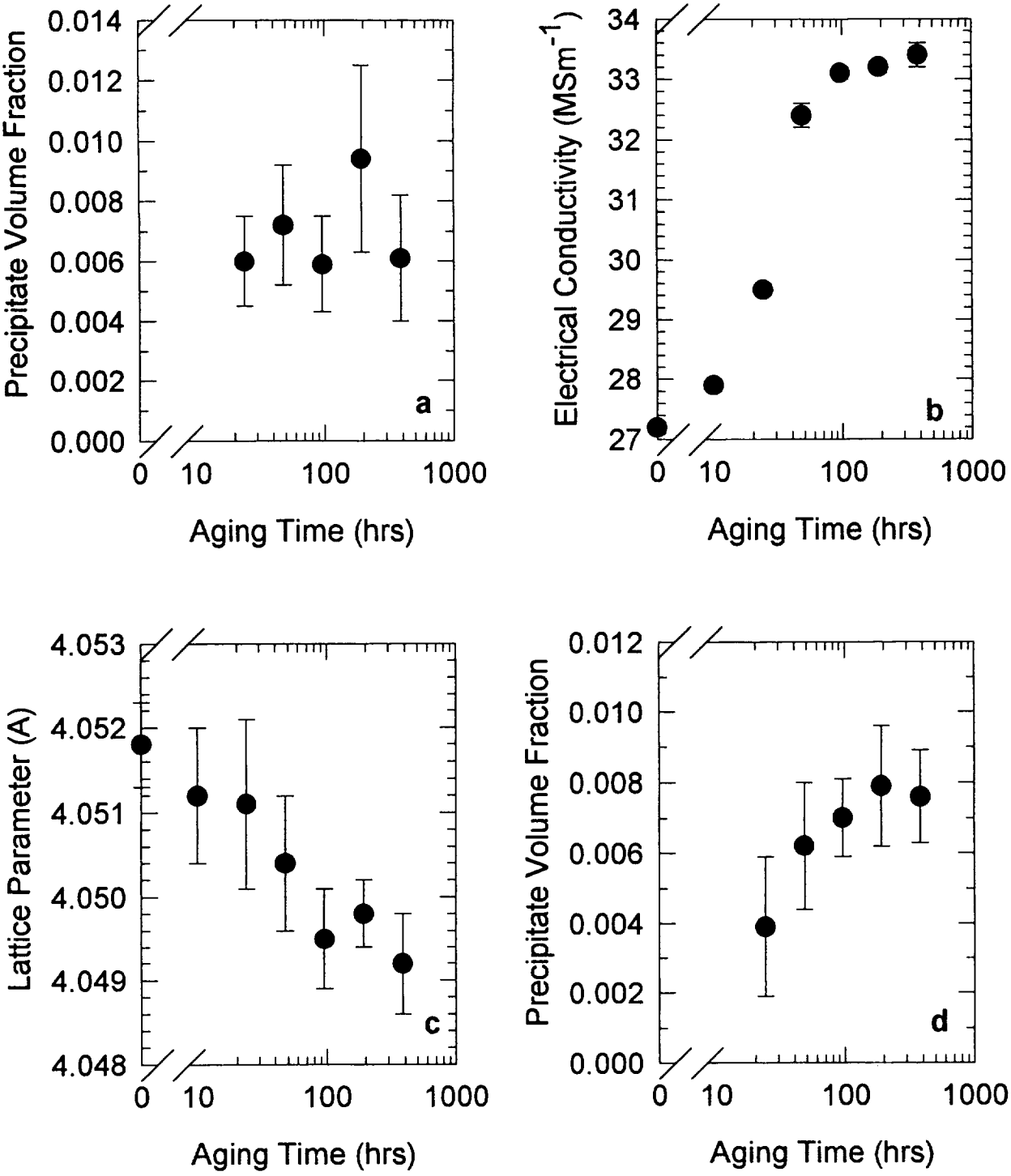

Figure 2. Determination of the SiGe precipitate volume fraction in Al-0.55Si-2.02Ge (wt.%) as a function of aging time at 160°C. (a) TEM micrographs. (b) Electrical conductivity measurements. (c) Lattice parameter measurements. (d) Average values of the three methods.

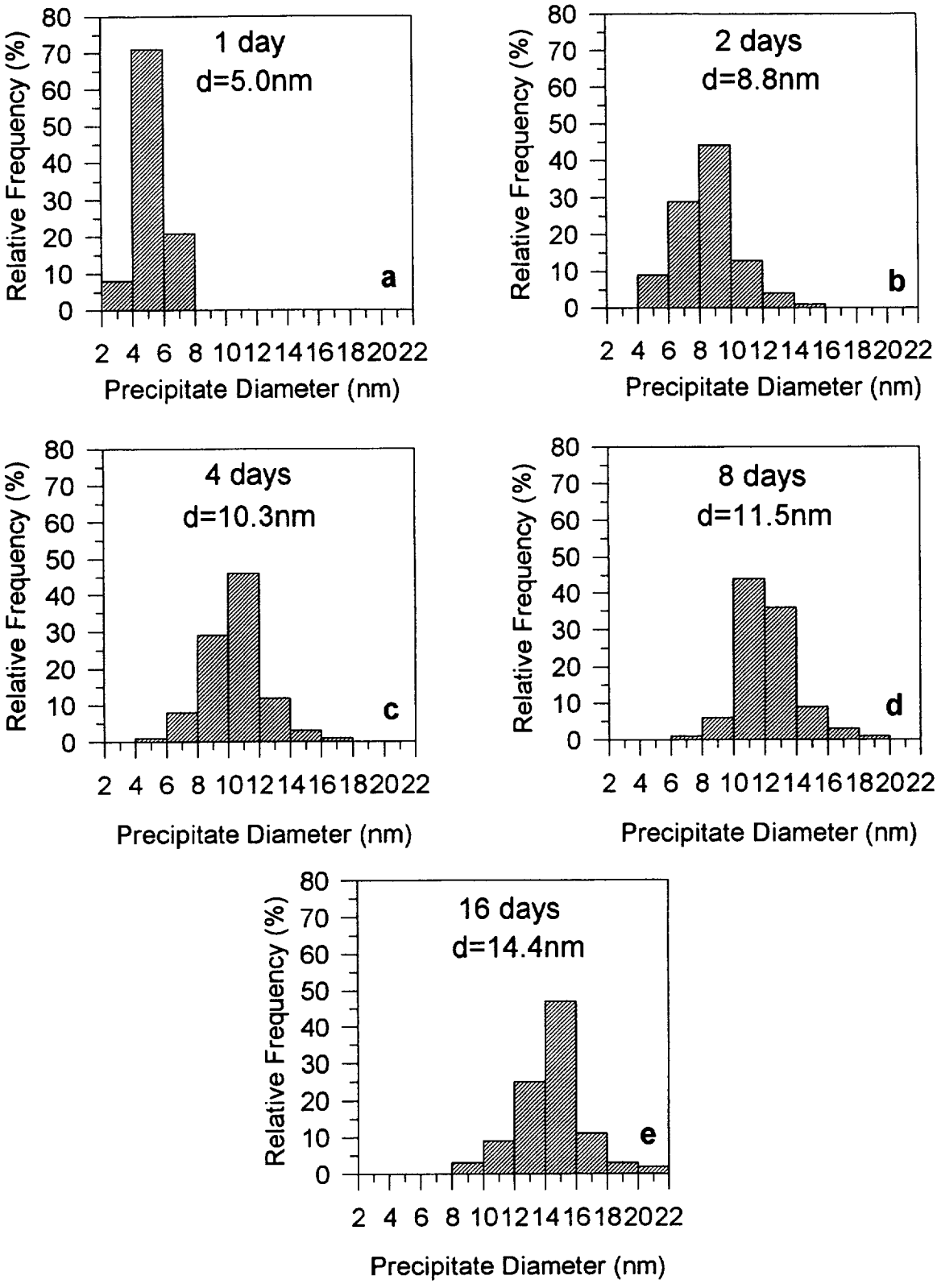

Figure 3. Precipitate size distribution in Al-0.55Si-2.02Ge (wt.%) during aging at 160°C.

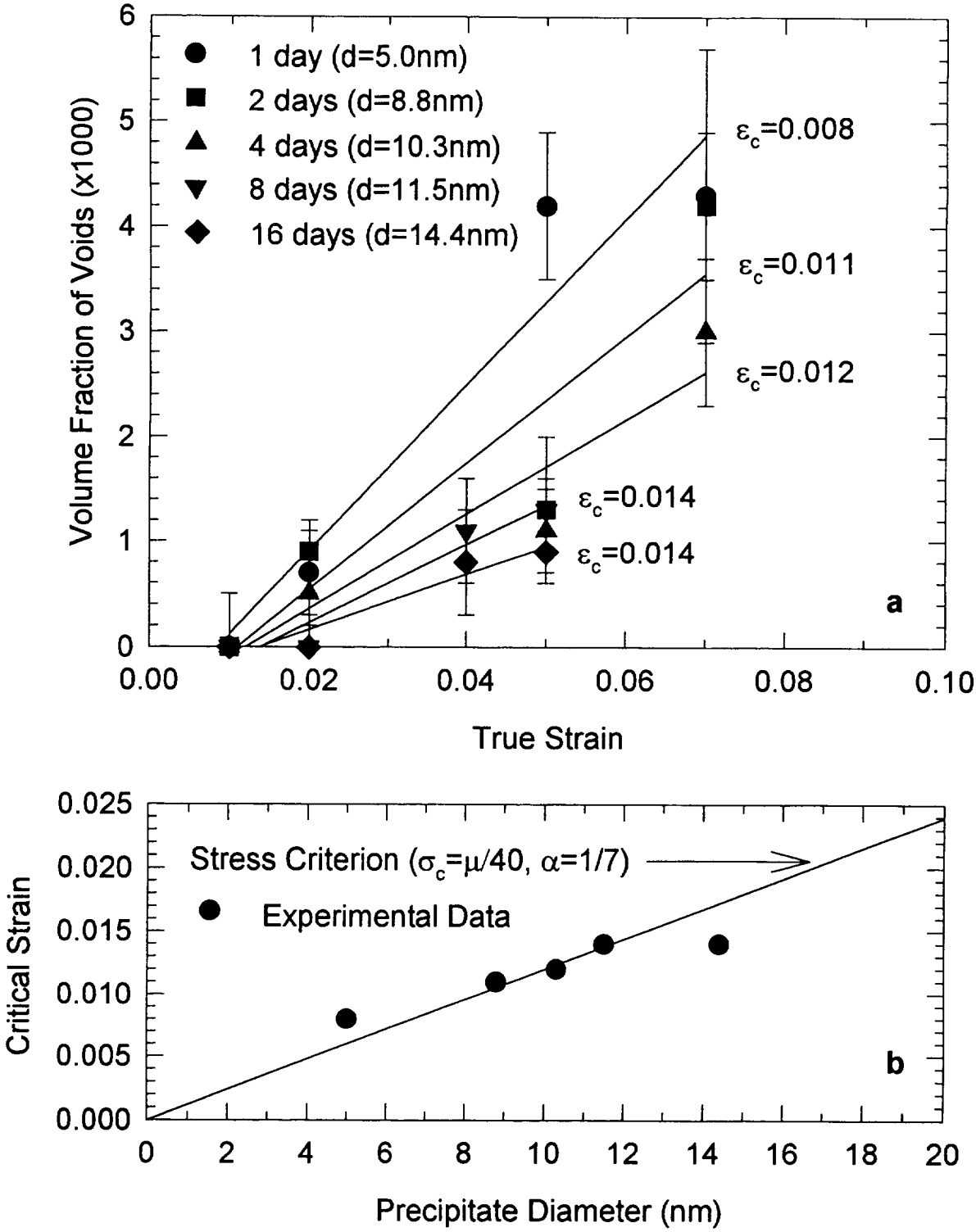

Figure 4. Volume fraction of voids as a function of strain determined in Al-0.55Si-2.02Ge (wt.%) after aging at 160°C for different times. (a) Critical strain for cavity nucleation (ε_c) determined by linear regression. (b) Comparison of stress criterion with experimental data.

Project #9 **Damage Evolution In Polymeric Composites**

Carl T. Herakovich and Robert D. Schroedter III

Research Objectives

The aim of this research is to assess the capability of damage models for predicting the cyclic, thermo-mechanical response of IM7/K3B graphite-polyimide composite laminates in the presence of damage. Specific objectives associated with this assessment are:

- assess the method of local states, as proposed by Ladeveze (1983, 1986, 1989, 1991), as a viable model for predicting the response of IM7/K3B
- conduct the necessary mechanical tests to determine the material parameters for the Ladeveze damage evolution model
- conduct mechanical tests on general laminates and compare the experimental results with the model predictions in order to critically assess the applicability, accuracy and robustness of the model
- investigate the micro-level mechanisms responsible for damage evolution in IM7/K3B
- assess other damage models (e.g. He, Wu, Evans & Hutchinson, 1994, and Aboudi & Herakovich, 1995) for application to the IM7/K3B material.

Background And Approach

The Ladeveze model has been utilized previously with a high degree of success to predict the nonlinear, inplane response and interlaminar stress failures for graphite-epoxy and woven ceramic-ceramic composite laminates. At present the model is being extended for application to metal matrix composites, time dependent phenomena and fatigue loading. Thus, its potential flexibility and adaptability bode well for a broad range of

fibrous composite systems and loading conditions. Advantages inherent in the Ladeveze approach include the relatively small number of parameters required by the model, the small number of laboratory tests required to determine these parameters, and the potential to predict damage evolution and the resulting nonlinear, inelastic response of laminated composites subjected to monotonic and cyclic thermo-mechanical load histories.

The required procedures includes monotonic and cyclic tension tests on the following laminates:

- $[45/-45]_s$ to obtain the shear response of the composite
- $[67.5/-67.5]_s$ to obtain the combined shear-transverse normal response
- $[0/90]_s$ to obtain the fiber direction strain limit
- $[45/0/-45/90]_s$ for model verification.

The material parameters and damage evolution laws are determined from the basic tests. The procedure continues with the model being used to predict the inelastic response of the quasi-isotropic laminate (or any other chosen lamina or laminate) and comparing the prediction with the actual experimental results.

A subsequent, complementary step is determination of the micromechanical damage mechanisms and correlation of these mechanisms with the mesoscale damage evolution law. Since the Ladeveze approach (mesoscale) assumes that the damage state is constant through the thickness of individual layers it does not provide specifics as to micromechanical damage mechanisms. Experimental methods such as edge replication, X-ray, C-scan, matrix digestion and microscopy are all candidate methods to determine the microlevel damage mechanisms.

Progress During The Reporting Period

Work during the current reporting period was concerned primarily with experimental determination of the fundamental cyclic tensile response of IM7/K3B graphite/polyimide laminates,

and use of these results to determine the material parameters that describe and govern the damage evolution in accordance with the Ladeveze model. Monotonic and cyclic tension tests were conducted on $[0/90]_s$, $[\pm45]_s$, $[\pm67.5]_s$ and $[45/0/-45/90]_s$ laminates. In addition, monotonic tests were conducted on [0] and [90] laminae for confirmation of engineering properties of IM7/K3B. Moreover, special tests were run wherein the imposed load was held constant at a high stress level for a test on a $[\pm45]_s$ laminate in order to assess its room temperature creep response.

The experimental results show that the axial stress-strain response of the $[\pm45]_s$ (Figs. 1-3) and $[\pm67.5]_s$ (Fig. 4) laminates exhibit nonlinearity and inelastic strains. As indicated in Fig. 1, the $[\pm45]_s$ laminate exhibits exceedingly large strains prior to failure, up to 18%! A cross-hair oriented along the fiber direction was marked onto each $[\pm45]_s$ specimen tested, and video and audio signals were recorded to capture fiber rotations and acoustic emissions during the test. Measurements of the change in fiber angle indicate rotations in excess of 20° resulting in approximately a $[\pm25]_s$ laminate at the highest stress levels. The audible acoustic emissions from the specimen during cyclic tensile tests exhibited a most unusual phenomenon. As indicated in Fig. 2, the acoustic emissions from the $[\pm45]_s$ specimen did not exhibit the usual Kaiser effect for materials. Materials following the Kaiser effect exhibit additional acoustic emissions when the previous maximum stress is exceeded and cease emissions when the specimen is unloaded. As the results in Fig. 2 indicate, the emissions did not initiate immediately upon exceeding the previous maximum stress and the emissions continued for a portion of the unloading curve. It was also determined that significant creep is present in the $[\pm45]_s$ specimen at high stress levels (Fig. 3). The large strains to failure, the unusual acoustic emissions and the room temperature creep all raise some interesting questions as to micro-level mechanisms responsible for the evolution of damage and

strain in this laminate.

The damage parameters for the Ladeveze model as determined from the experimental results (Figs. 5 & 6) exhibit well-defined curves which are consistent with results obtained by Ladeveze and his colleagues for other fibrous composites. These parameters will be used to predict the response of other laminates.

Conclusions

IM7/K3B graphite-polyimide composite exhibits unusual and interesting characteristics when studied in the context of damage evolution. The $[\pm 45]_s$ specimens proved to be the most dramatic in terms of overall behavior. Preliminary assessment of the results suggests that the damage mechanisms occurring in these specimens include fiber-matrix debonding, subsequent fiber pullout, and room temperature creep. Plots based on the experimental results and associated with the application of the Ladeveze model, such as those of the damage parameters as functions of the corresponding thermodynamic forces (Figs. 5 & 6), appear to be very well-behaved and generally in line with results obtained by other investigators for other materials. Thus, there exists positive reinforcement for the future success of this model in the prediction of the response of IM7/K3B laminates. The fact that acoustic emissions associated with the damage do not follow the well-known Kaiser effect is a most interesting result that needs further study, as does the occurrence of room temperature creep.

Tasks For The Next Reporting Period

The modelling efforts will be enhanced to incorporate fiber rotation into the analysis. Using this enhanced modelling capability, the parameters for the Ladeveze model will be determined anew and correlation between theoretical predictions and experimental results will be assessed. Attention will also be given to determination of the micro-level damage mechanisms that give rise to the inelastic deformations, acoustic emissions, fiber

rotations, room temperature creep, and large strains to failure. Experimental methods such as edge replication, X-ray, C-scan, matrix digestion and microscopy are all candidate methods to determine the microlevel damage mechanisms. A complete understanding of the fundamental micro-level damage mechanisms and their influence on response is necessary if a robust damage theory is to be available.

Time permitting, a micromechanics formulation for the nonlinear, inelastic response of fibrous composites with interfacial damage will be assessed for application to the IM7/K3B material system. This micromechanics model is based upon the generalized method of cells (Paley & Aboudi, 1992) and a new formulation that takes into account the changing volume of damaged material with increasing maximum stress during a cyclic load history (Aboudi & Herakovich, 1995). This approach has exhibited excellent results for predicting the nonlinear, inelastic response of metal matrix composites. Another microlevel model that is a candidate for assessment is that by He et. al. (1994). This model relates inelastic strains to constitutive properties, interfacial fiber/matrix sliding and debonding resistance

References

Aboudi, J. & Herakovich, C. T., (1995), "An Interfacial Damage Model for Fibrous Composites", (to be published in proceedings of the symposium on, SES Annual meeting, New Orleans.

He, M. Y., Wu, B.-X., Evans, A. G., & Hutchinson, J. W., (1994), "Inelastic strains due to matrix cracking in unidirectional fiber-reinforced composites", Mechanics of Materials, 18, pp. 213-229.

Ladeveze, P., (1983), "Sur une theorie de l'endommagement anisotrope", Rapport Interne no. 34, Laboratorie de Mecanique at Technologie, Cachan, France.

Ladeveze, P., (1986), "Sur l Mecanique de l'Endommagement des Composites, JN5, Pluralis, Paris, pp 667-683.

Ladeveze, P.(1989), "About a Damage Mechanics Approach", Proceedings Int. Conf. on Mechanic and Mechanisms of Damage in Composites and Multimaterials, MECAMAT, St. Etienne, France.

Ladeveze, P., Allix, O. & Daudeville, L.,(1991), "Mesomodeling of Damage for Laminate Composite: Application to Delamination', in Inelastic Deformation of Composite Materials, (G. J. Dvorak, ed), Spring-Verlag.

Paley, M. & Aboudi, J., (1992), "Micromechanical analysis of composites by the generalized cells model", Mechanics of Materials, 14, p. 127-139.

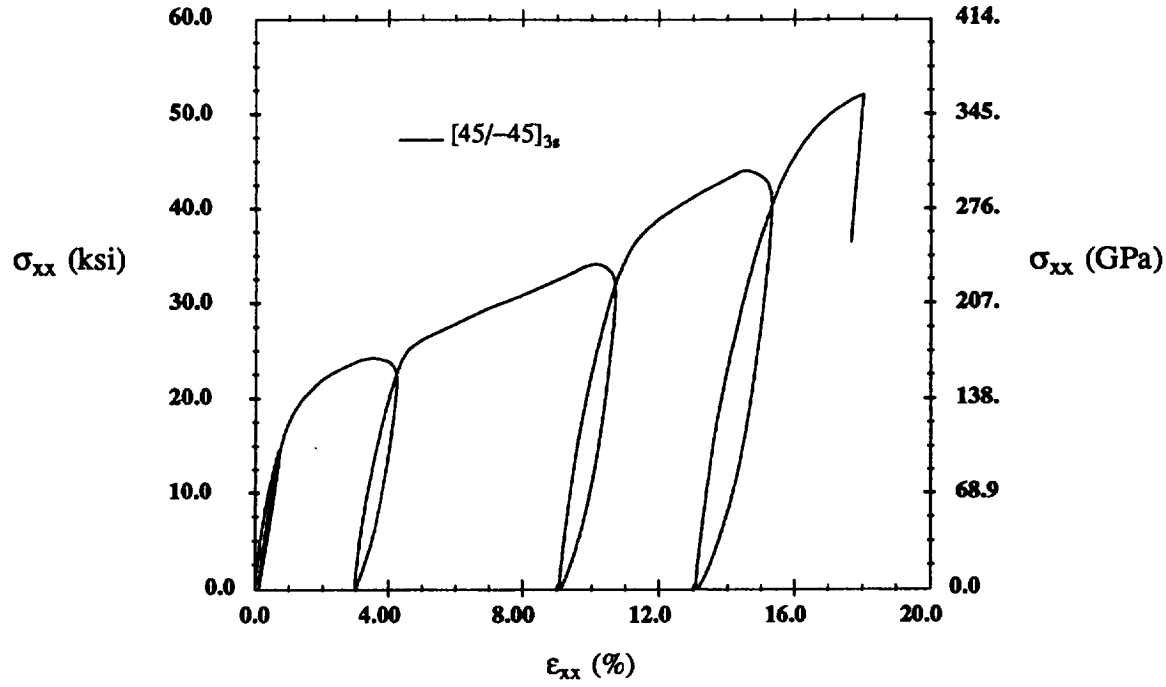

FIGURE 1. $[\pm 45]_s$ **IM7/K3B Stress-Strain Response**

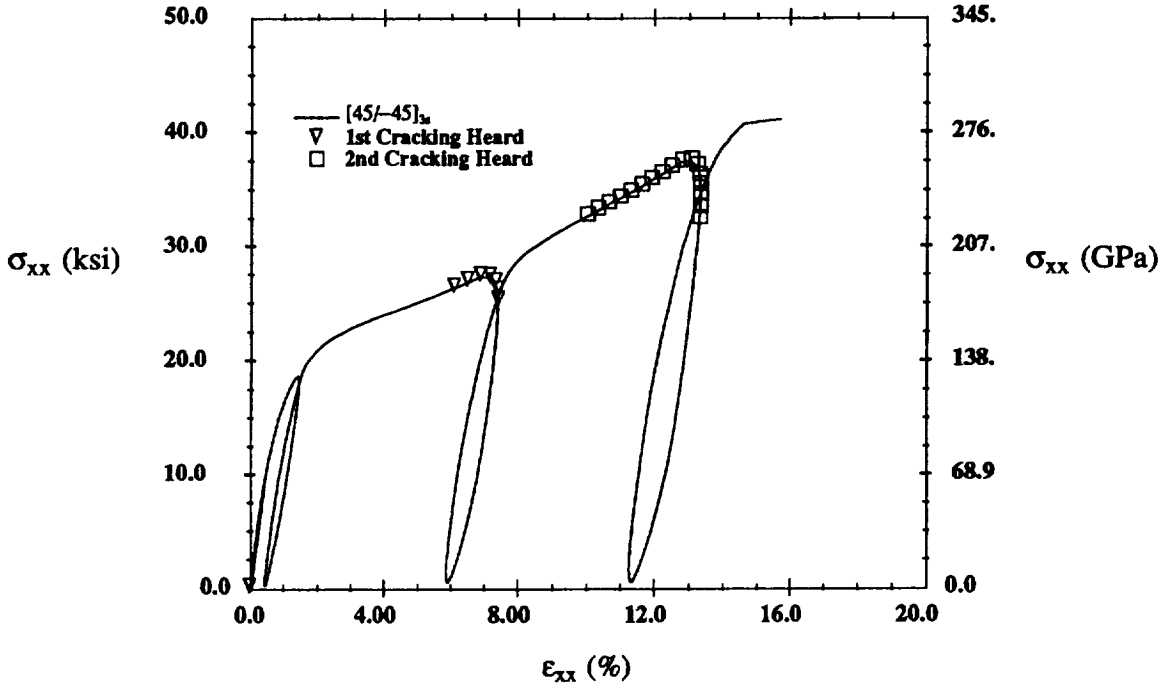

FIGURE 2. $[\pm 45]_s$ **IM7/K3B Acoustic Emissions Timing**

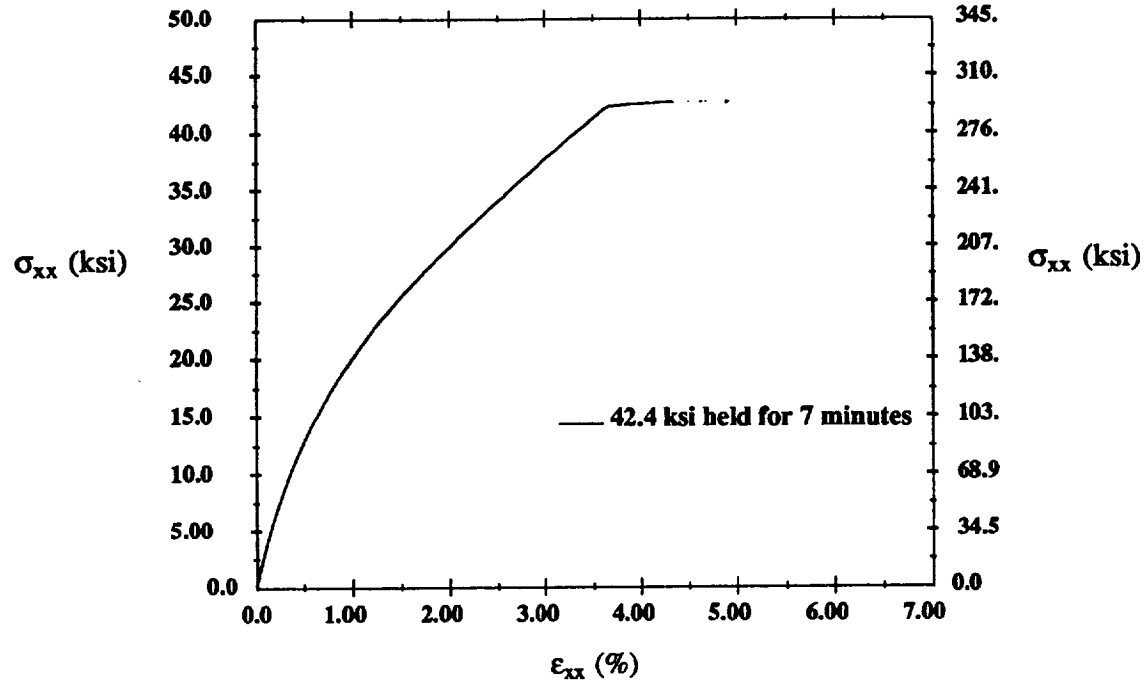

FIGURE 3. Room Temperature Creep in $[\pm 45]_s$ IM7/K3B

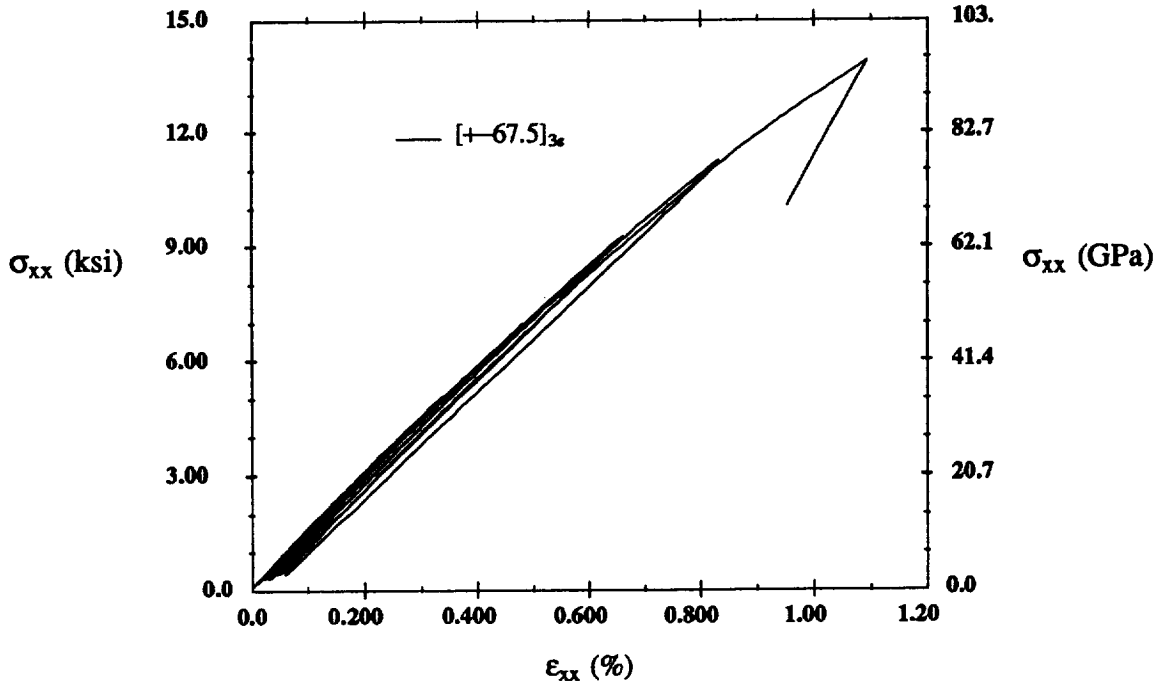

FIGURE 4. $[\pm 67.5]_s$ Stress-Strain Response

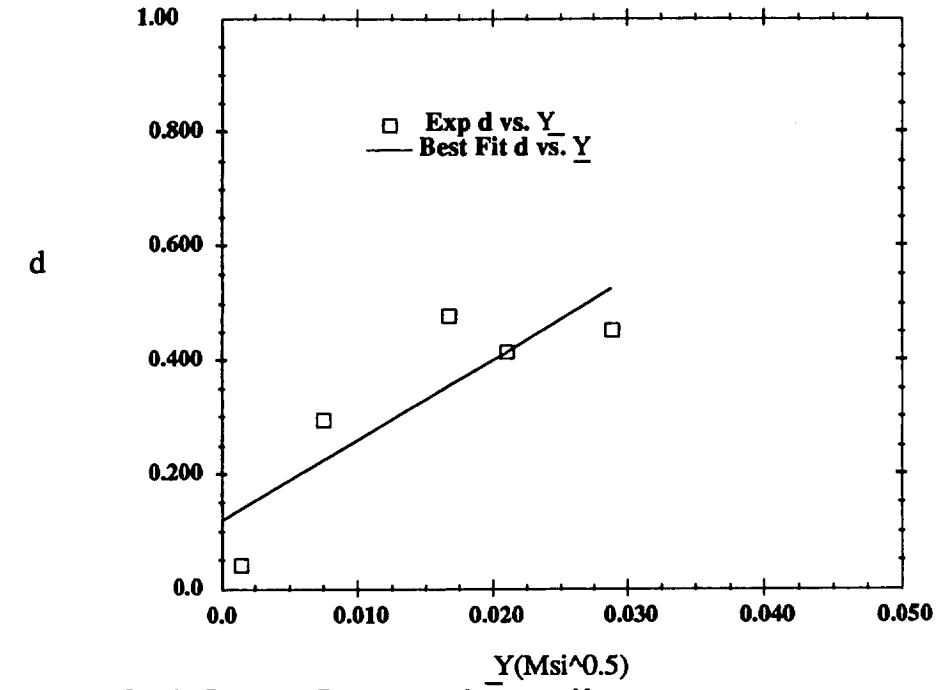

FIGURE 5. Transverse Strain Damage Parameter d versus Y

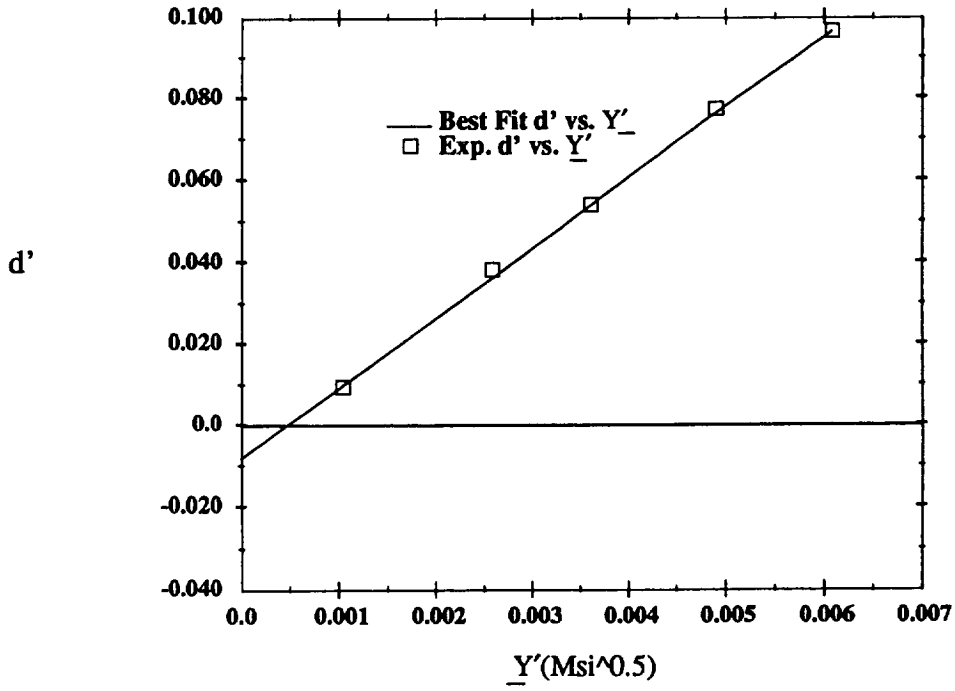

FIGURE 6. Shear Damage Parameter d' versus Y'

Project #10 **Environmental Effects in Fatigue Life Prediction: Modeling Crack Propagation in Light Aerospace Alloys**

Mark E. Mason, Edward Richey III, Zuhair Gasem and Richard P. Gangloff

Objectives

The objective of this project is to establish data and models for estimating and ultimately predicting environment enhanced fatigue crack propagation (FCP) kinetics for light aerospace structural alloys, particularly titanium and high strength aluminum alloys. This work is necessary to enhance computer-based fatigue life prediction codes such as NASA-FLAGRO.

During this past reporting period, two approaches to this goal were emphasized. One task (Mason and Gasem) focused on understanding the intrinsic and extrinsic elements of FCP in the AA7075/aqueous NaCl system. A second study (Richey) has developed empirical models to describe the complex stress intensity dependence of environmental FCP rate. Both linear superposition and interpolative curve-fitting methods were investigated, and cracking data were obtained for the Ti-6Al-4V (ELI)/aqueous NaCl system.

Project #10A **Time-dependent Chloride Environmental Fatigue Crack Propagation in AA7075**

Mark E. Mason and Richard P. Gangloff

Objective

The objectives of this research on environmental fatigue crack propagation in a 7000- series aluminum alloy in aqueous chloride are four-fold, including to: (1) test static load or displacement-based linear superposition predictions of da/dN vs ΔK and frequency, (2) determine if quasi-static load stress corrosion crack growth rates are affected sufficiently by crack

tip strain rate to enable improved linear superposition predictions of da/dN, (3) measure the frequency, load waveform and hold-time dependencies of environmental FCP da/dN, and (4) speculate on the metallurgical and electrochemical origin(s) of the variability in the time-dependence of environmental FCP in 7000 series aluminum alloys. The output of this work will be improved data and understanding on time-cycle-dependent EFCP kinetics for use in NASA-FLAGRO.

Current Status

This element of the research was completed in November of 1994, and Mr. Mason successfully defended his Master of Science thesis. The thesis will be published as a NASA-Contractor Report. The following conclusions were established by experiments and analysis conducted on a 5.1 cm thick plate of AA7075-T651, with compact tension specimens in the environmental cracking susceptible short-transverse (S-L) orientation, and exposed to acidified and chromate inhibited 1% NaCl solution at the free corrosion electrode potential.

Conclusions

1. Da/dt_{SCC} values are consistent with K-independent cracking above a K_{ISCC} of 5 to 10 MPa$\sqrt{m}$. However, da/dt_{SCC} ranges from 0.3 to 4.4 x 10^{-9} m/sec and is slower than literature results.

2. SCC is primarily intersubgranular for cracking under CMOD or constant stress intensity loading. High angle boundary cracking is not prominent.

3. Imposed constant crack mouth opening displacement rate does not accelerate environmentally enhanced da/dt above da/dt_{SCC}.

4. Da/dt is not enhanced by high frequency-low amplitude cyclic loading, designed to increase crack tip strain rate, in conjunction with a high sustained stress intensity.

5. Fatigue crack propagation rates for 7075-T651(S-L) in chromate inhibited, acidified NaCl solution are enhanced five to ten-fold over rates in moist air and are over an order magnitude faster compared to cracking in helium.

6. EFCP da/dN for 7075-T651 in NaCl shows a weak time-cycle frequency dependence above 0.001 Hz; here da/dN is proportional to $f^{-\beta}$, where ß is approximately 0.1.

7. Corrosion fatigue is predominantly intersubgranular for low frequencies and ΔK levels, with regions of transgranular fracture in the form of brittle striations, and steps between areas of intersubgranular fracture. Higher frequencies and ΔK levels showed primarily a transgranular fracture morphology.

8. EFCP da/dN is proportional to t_R^m for a wide range of rise times, where m is approximately 0.1 for both symmetric and asymmetric loading waveforms. For two constant stress intensity levels, there is only a very small effect of hold-time on environmental da/dN.

9. The NaCl environmental effect on time-cycle-dependent fatigue crack growth is identical for the S-L and L-T orientations of peak aged 7075, suggesting a minimal involvement of anisotropic high angle grain boundaries.

10. Compliance estimations of $K_{CLOSURE}$ indicate a negligible

effect of time-dependent crack closure on the frequency and rise time dependencies of da/dN for ΔK of 9 and 15 $MPa\sqrt{m}$. Intrinsic effects of stress ratio on da/dN in chloride were inseparable from the contributions of time-dependent closure.

11. Linear superposition predicts EFCP da/dN in the 7075-T651(S-L)/NaCl system for fatigue waveforms having K levels in excess of K_{ISCC} for more than 1000 seconds.

12. Alternate methods for establishing da/dt, based on enhanced crack tip strain rate ($d\varepsilon_{CT}/dt$), do not provide a means of enabling linear superposition modeling of EFCP da/dN in 7075-T651(S-L)/NaCl.

13. The environment assisted crack velocity for 7075-T651(S-L) in aqueous chloride is not enhanced for $d\varepsilon_{CT}/dt$ from 2 x 10^{-5} to 2 sec^{-1}, imposed by monotonic, ripple, and trapezoidal loading conditions.

14. Passive film rupture is not the rate limiting crack tip damage mechanism governing EAC of 7075-T651 in chloride, as indicated by the nil influence of $d\varepsilon_{CT}/dt$ on da/dt.

15. EFCP da/dN for 7075-T651(S-L) in chloride transitions from time-cycle-independent to time-cycle-dependent da/dN at a critical da/dN and frequency. Above f_{CRIT}, shorter cycle periods provide less time for diffusion and accumulation of embrittling hydrogen in the process zone, and da/dN becomes time-cycle dependent.

16. Da/dN_{CRIT} depends on the square root of f_{CRIT} through a proportionality constant γ_{CRIT}. This dependence supports

hydrogen embrittlement governed EFCP. The diffusivity of hydrogen in aluminum, the critical concentration of hydrogen in the process zone for embrittlement, and the concentration of hydrogen at the crack tip surface are incorporated into γ_{CRIT}. The complex dependencies of D_H, C_{CRIT}, and C_S on metallurgical, compositional, and environmental parameters cannot be determined from the results of this study.

17. Results from asymmetric triangle loading and trapezoidal loading of 7075-T651(S-L) in chloride indicate that loading time from K_{MIN} to K_{MAX} is a more general parameter than frequency for analyzing time-dependent EFCP da/dn.

18. A conservative approach using da/dN_{CRIT}, for frequencies above where da/dN_{SCC} becomes negligible, coupled with linear superposition below this frequency, is warranted for damage-tolerant life prediction for 7000 series aluminum alloys in aggressive chloride environments.

Project #10B **Computer Modeling Environmental Effects on Fatigue Crack Propagation in Light Aerospace Alloys**

Edward Richey III and Richard P. Gangloff

Objective

The objective of this research is to develop a method for estimating environmental effects on fatigue crack propagation (FCP) rates in metals for use in damage tolerant life prediction codes such as NASA FLAGRO. Specific goals of the research are to:

- Develop a set of computer modeling programs which estimate the effect of an aggressive environment on FCP behavior. Specifically:
  - Develop a computer program which implements the Wei and Landes linear superposition model.
  - Develop a curve-fitting based interpolative program, extending the approach used in NASA FLAGRO.
  - Develop a program which allows the user to fit multiple power law equations to fatigue crack growth rate vs stress intensity range data.
- Establish environmental FCP rate data for Ti-6Al-4V in aqueous NaCl to provide a basis for and tests of the empirical models. Specifically:
  - Determine the quasi-static load stress corrosion cracking susceptibility of Ti-6Al-4V (MA, ELI) in chloride through constant crack mouth opening displacement (CMOD) rate tests.
  - Determine the time-dependence of FCP in Ti-6Al-4V (MA, ELI) in moist air and a 3.5% NaCl solution.

Computer Modeling Methods

Linear Superposition Model

A computer program was developed* which implements the Wei and Landes linear superposition model. The program combines inert environment mechanical fatigue data ($da/dN_{fatigue}$), stress corrosion crack velocity data ($da/dt_{environment}$), and time dependent stress intensity (K(t)) to predict the effects of ΔK ($K_{max} - K_{min}$), stress ratio (R), frequency (f), hold time (τ), and loading wave-form on environmental FCP rate (da/dN). The program was tested for the same material-environment systems employed by Wei and Landes[1], Speidel[2], and Harmon et. al.[3] in an attempt to duplicate their results. The predictions generated by the current program agreed with the reported measured data, although not precisely with the superposition model predictions of Wei and Landes[1], Speidel[2], and Harmon et. al.[3] The current program yielded improved results due to a more accurate numerical algorithm used to calculate the stress corrosion component of corrosion fatigue, $(da/dN)_{stress\ corrosion}$. The linear superposition program, and the interpolative model that will be addressed next are discussed in detail in the NASA contract report "Computer Modeling the Fatigue Behavior of Metals in Corrosive Environments."[4]

Interpolative Model

A curve fitting based interpolative model was developed to describe the effects of an aggressive environment on FCP rates. The interpolative model allows the user to fit corrosion fatigue data to various crack growth rate equations such as the Forman Equation and the Paris Equation, all of which have the general form:

---

* This program was developed by Allen W. Wilson, a graduate student in the Department of Materials Science and Engineering at the University of Virginia.

$$\frac{da}{dN} = f(\Delta K) \qquad (1)$$

The parameters in the crack growth rate equations change with R, f, τ, load wave-form, and environment chemistry. Trends in fatigue behavior can be interpolated by relating the parameters in the crack growth rate equations to these variables. For example, if η is a parameter in the crack growth rate equation, then η can be expressed as a function of R, f, and τ. If the stress ratio is not constant, then the parameters can be expressed in terms of the frequency, hold time, and either K_{max} or K_{min}. The functions used to relate equation parameters to load characteristics are selected so that the functions are defined for allowable load characteristics. This model is based on a procedure discussed by Haritos and employed to model FCP in nickel based superalloys at elevated temperatures.[5-6]

The interpolative model has been tested for Ti-6Al-4V in 3.5% NaCl, 1.0% NaCl, and moist air environments, as well as for Ti-8Al-1Mo-1V in 3.5% NaCl. For Ti-6Al-4V in 3.5% NaCl and Ti-8Al-1Mo-1V, fatigue behavior was interpolated as a function of frequency. For Ti-6Al-4V/1.0% NaCl solution, fatigue behavior was interpolated as a function of stress ratio. Generally, this approach accurately interpolated da/dN vs ΔK when da/dN for a new value of f or R was interpolated inside the range of data used to determine the constants in the crack growth rate equations. Interpolative models do, however, show substantial deviation between interpolated and experimental results when the load characteristics at which data are interpolated are outside of the range of data used to establish the constants.[5] Empirical curve-fitting based models are particularly flawed when the damage mechanism for environmental fatigue changes either within or outside the establishing data base.

Multiple Power Law Model

Recently, the computer modeling aspect of this research

focused on developing a program which allows the user to fit multiple power law equations to da/dN vs ΔK data. The multiple power law equation uses Paris relation between da/dN and ΔK ($da/dN = C\Delta K^n$), except that the values of C and n change at one or more transition ΔK levels. By using multiple power law segments, environmental FCP data can be accurately represented in the regimes where environmental affects a complex crack growth rate response.

The user is given several alternatives for determining the equation parameters. The user can either:

1) Enter the desired slope offset necessary for a power law slope change (in percent).
2) Enter the desired number of power law segments over the range of ΔK considered.
3) Enter the number of segments and approximate ΔK values of the transition points.

If the user enters a fixed slope offset, the program begins by fitting the first two (ΔK, da/dN) points in the data set to a Paris Equation using least squares regression, and records the value of the slope, n_1. The program then fits a Paris Equation to data points 1 through 3, and records the value of n_2. The slope offset (in percent) is defined as:

$$\text{Slope offset} = \left(\frac{n_2 - n_1}{n_1} \right) \times 100 \qquad (2)$$

The program continues fitting additional data points to a Paris Equation until the slope offset is greater than the fixed input value. The last end point which yielded a slope offset lower than that desired becomes the first temporary transition point. Starting with this first temporary transition point, the process is repeated until either another temporary transition point, or the end of the data file, is reached. The final values for the transition points are determined by calculating the ΔK

values where two adjacent power law segments intersect.

If the user enters the desired number of power law segments, the program asks for an initial slope offset. Using this initial slope offset, the corresponding number of power law segments is calculated. The slope offset is then increased or decreased at successively smaller intervals until the desired number of segments is reached. If the desired number of segments can not be reached by a user-specified number of iterations, the process is stopped. The transition points are calculated by determining the ΔK level where two adjacent power law segments intersect.

The final option for determining the equation parameters involves the user entering the desired number of power law segments, and the approximate ΔK values of the transition points. The program uses these transition points to determine which data points to fit to each power law segment. The final values for the transition points are again determined by calculating the ΔK values where two adjacent power law segments intersect. This option often yields the best results.

Sample power law curves generated by the program are shown in Figure 1. The data in Figure 1 are for Ti-6Al-4V (MA, ELI) in moist air and a 1.0% NaCl environment at a fixed electrode potential of -500 mV_{SCE} for a stress ratio of 0.4 and a frequency of 5 Hz.[7] Table 1 compares the transition ΔK levels and power law slopes, determined by the computer program , with those reported by Kim and Gangloff. [7] The power law segments were determined by entering the number of transitions and the approximate ΔK locations of the transition points.

Future Work

Future work includes joining the three models just discussed (linear superposition model, interpolative model, and multiple power law model) into one stand-alone computer program. The final version of the program will be compiled using a professional

Table 1: Comparison of ΔK Transition Levels and Power Law Slopes

Comparison of ΔK Transition Levels

Environment	Transition	Kim Fit	Program Fit	% Difference
Moist Air	1	6*	6.45*	7.50
	2	7.4	7.42	0.27
	3	12	11.58	3.50
3.5% NaCl	1	4.4		
	2	7	6.35	9.29
	3	9	9.10	1.11
	4	9.5	9.55	0.53

*$MPa\sqrt{m}$

Comparison of Power Law Slopes

Environment	Segment No.	Kim Fit	Program Fit	% Difference
Moist Air	1		3.67	
	2	4.9	5.55	13.27
	3	5.6	5.62	0.36
	4	3.3	3.26	1.21
3.5% NaCl	1			
	2	4.8	4.83	0.63
	3	3.8	3.86	1.58
	4	12.6	13.19	4.68
	5	5.3	5.31	0.19

multi-platform 32 bit Fortran compiler from WATCOM Inc. This new compiler will increase the speed and performance of the program, as well as alleviate memory problems that were encountered when first compiling the programs. The original compiler utilized during this research used the first 640 kilobytes of memory, while the new compiler uses up to 32 megabytes of memory. This integrated program, along with the source code, will be provided to NASA-LaRC and NASA-JSC.

As a second task, future work on the computer program will incorporate the capability to calculate $(da/dt)_{environment}$ from $(da/dN)_{stress\ corrosion}$ data utilizing the linear superposition model. This will hopefully improve the predictive capability of the model by generating $(da/dt)_{environment}$ data that are more pertinent to the crack tip strain rates and damage conditions associated with cyclic loading. This involves solving for $(da/dt)_{environment}$ in the following equation:

$$\left(\frac{da}{dN}\right)_{stress\ corrosion} = \int_{\tau} \frac{da}{dt}[K(t)]\ dt \qquad (3)$$

This problem is simple when $(da/dt)_{environment}$ is modeled by a single Paris Equation and K(t) is modeled as a square wave with $K_{min} = 0$. The problem quickly becomes complex and nonlinear when more complicated wave forms or models for $(da/dt)_{environment}$ are utilized. The final program will hopefully allow the user to choose between sinusoidal, ramp, or square wave forms to represent K(t), and between the Paris Equation and a double power law to represent $(da/dt)_{environment}$. This work will be done by an undergraduate student beginning in the Summer of 1995.

Experimental Results for Environmental FCP

Mill annealed Ti-6Al-4V in the extra low interstitial (ELI) condition (α/β-annealed at 760°C for 8 hours and vacuum furnace cooled) was obtained from President Titanium. Compact tension (CT) specimens were machined in the L-T orientation with a width of 63.5 mm and a thickness of 6.4 mm. The chemical composition and selected mechanical properties of this alloy are shown in Table 2, as reported by the vendor.

Table 2: Nominal Chemical Composition and Mechanical Properties of Ti-6Al-4V

Chemical Composition (wt. %)

Al	V	C	N	Fe	O	H	Y	Ti
6.17	4.33	0.025	0.011	0.19	0.12	0.0055	0.0005	balance

Mechanical Properties

Yield Strength MPa (ksi)	Tensile Strength MPa (ksi)	Elongation Percent, %	Reduction Area, %
940 (163)	982 (142)	13	30.2

Constant Crack Mouth Opening Displacement (CMOD) Rate Tests

In order to the determine the stress corrosion cracking susceptibility of Ti-6Al-4V (MA, ELI), constant CMOD rate tests were run in moist air and a 3.5% NaCl solution at a fixed electrode potential of -500 mV_{SCE}. The tests were run in CMOD control via a clip gage mounted with knife edges at the front face of the CT specimens, and crack length was calculated using the direct current potential drop (DCPD) method.

J_{IC} Determination

A single experiment was conducted in moist air at a CMOD rate of 4.7 x 10^{-5} mm/sec, resulting in one of the load-displacement curves shown in Figure 2. From this test, J_{IC} was determined to be 49.7 kJ/m^2, while K_{JIC} was determined to be 78 MPa$\sqrt{m}$. Crack initiation was defined as the point where there was a sharp increase in the DCPD data. The method used to calculate J_{IC} complies with ASTM Standard E813-89.[8] The expected value of K_{IC} for mill-annealed Ti-6-4 is between 65 and 75 MPa m.[7]

K_{TH} Determination

Two experiments were conducted with Ti-6Al-4V in 3.5% NaCl solution at fixed CMOD rates of 3 X 10^{-5} mm/sec and 4.7 X 10^{-5} mm/sec. The load versus CMOD data for these two tests are shown in Figure 2. For 3.5% NaCl, the stress intensity for crack initiation, KTH, was calculated. For the CMOD rate of 3 x 10^{-5} mm/sec, K_{TH} equaled 55 MPa$\sqrt{m}$. For the CMOD rate of 4.7 x 10^{-5} mm/sec, K_{TH} equaled 48 MPa$\sqrt{m}$. For both tests crack initiation was defined as the point on the load-displacement curve where the data first deviated from a linear behavior. Crack initiation should have been defined based on DCPD data, as in the air case, however, NaCl deposits formed on the DCPD wires and interfered with the voltage signal. Visual measurements were used in each constant CMOD rate test to correct the crack lengths calculated from the DCPD signal. This was important because crack lengths were used when calculating the stress intensity values reported here.**

Several conclusions can be drawn from the two tests conducted

** As seen in Figure 2, the tests conducted at a CMOD rate of 4.7 x 10^{-5} mm/sec in air and NaCl, as well as the test where the load was increased to a K of 40 MPa$\sqrt{m}$ and then held statically, show good agreement during the linear portion of the load-displacement plot (i.e. elastic deformation). The test conducted at a CMOD rate of 3 x 10^{-5} mm/sec in NaCl differs because the specimen was precracked to an a/W of 0.7 compared to the standard condition of 0.5.

in the NaCl environment. Most importantly, the two K_{TH} values are much higher than the value for K_{ISCC} reported by Dawson and Pelloux[10] for mill-annealed Ti-6Al-4V. The major difference between the alloy studied during this research and that utilized by Dawson and Pelloux[10] is that the present alloy is in the extra low interstitial (ELI) condition. This increased value for K_{TH} means that stress corrosion cracking does not significantly contribute to time or R dependent corrosion fatigue for the range of stress intensities used during this study (5 to 45 MPa$\sqrt{m}$). Second, there is a mild dependence of K_{TH} on loading rate. Moskovitz and Pelloux[9] also reported a dependence of K_{TH} on loading rate for another $\alpha+\beta$ titanium alloy, Ti-6Al-6V-2Sn in 3.5% NaCl solution.

Environmental cracking occurred in Ti-6Al-4V (MA, ELI), albeit at high stress intensity levels, as seen by comparing the data in Figure 2. Two of the tests were run under identical loading conditions (CMOD rate = 4.7×10^{-5} mm/sec) with only the environment changing. For the test conducted in NaCl, there are sharp load drops of approximately 0.22 to 0.44 kN (50 to 100 lbs) at a constant CMOD. Each load drop corresponds to a "burst" of crack growth. The data for the air test do not exhibit these load drops, thus there are no "bursts" of crack growth. Since the only difference between the two tests was the environment, this would suggest that EAC occurred.

A final experiment was conducted where load was increased monotonically during 65 minutes to a level corresponding to a stress intensity of 40 MPa$\sqrt{m}$. The load was then held constant for 137 hours at this level. The specimen was polarized to -500 mV_{SCE} for the first 55 hours, and then switched to free corrosion for the remainder of the test. (The open circuit potential was measured as -240 mV_{SCE}.) The resulting load-displacement plot is shown in Figure 2. The crack did not grow during this time, since the load remained constant. A load drop of 0.11 kN (25 lbs) was

resolvable, and corresponds to 0.22 mm of crack growth. This strengthens the conclusion that K_{TH} is greater than literature values.

Corrosion Fatigue Tests

FCP experiments were conducted in a servo-hydraulic test machine in moist air and a 3.5% NaCl solution at a fixed electrode potential of -500 mV_{SCE}. A constant stress ratio of 0.1 was employed. Specimens were precracked in the environment in which they were to be tested at an R of 0.1, a frequency of 5 Hz, and a constant ΔK of 15 $MPa\sqrt{m}$. Wide range da/dN-ΔK data were generated using a computer automated ΔK gradient technique with $C=\pm 0.06 mm^{-1}$. Crack length and crack closure levels were measured using the unloading compliance technique with a clip gage mounted across the specimen notch for both environments. Crack length was calculated and stored in increments of 0.002 (a/W). Da/dN was calculated using the secant method. P_{cl}, the crack closure load, was calculated at the first deviation in slope of the load-displacement data, defined at an offset of 2% from linear behavior. The specimen dimensions, K gradient technique, and the method used to calculate da/dN comply with ASTM Standard E647-91.[11]

Ti-6Al-4V (MA, ELI) exhibits a complex relationship between da/dN and ΔK in both moist air and 1.0% NaCl solution, as seen in Figure 1.[7] This complex relationship is present when the effects of crack closure are considered, as seen in the plot of da/dN versus ΔK_{eff}. This multiple slope behavior was reported for α/β titanium alloys in moist air, distilled water, and aqueous chloride solutions.[10,12-13]

To date, single fatigue experiments were conducted with Ti-6Al-4V in moist air and NaCl. The experiment conducted in moist air was at a frequency of 5 Hz and R of 0.1; results were similar to those reported by Kim and Gangloff.[7] The test in NaCl was for a frequency of 40 Hz and an R of 0.1. Closure load was recorded and the closure stress intensity, K_{cl}, was calculated. Shown in

Figure 3 is a plot of K_{cl}/K_{max} vs ΔK.

For ΔK values between 10 and 40 MPa$\sqrt{m}$, K_{cl}/K_{max} centers around 0.3, consistent with plasticity-induced closure. A model by Newman[14] predicts that plasticity induced closure is important for R values less than 0.4. For example, the predicted value of K_{cl}/K_{max} is 0.3 for an R of 0.1 and 0.45 for an R of 0.4 for the titanium alloy used during this study. This model does not explain, however, the sudden rise in K_{cl}/K_{max} for ΔK values less than 10 MPa$\sqrt{m}$. Kim and Gangloff[7] found similar levels for K_{cl}/K_{max} for an R of 0.1 and a frequency of 5 Hz in moist air and a 1.0% NaCl solution, and also reported a rise in K_{cl}/K_{max} at low ΔK levels.

Future Work

Future experimental work will include generating corrosion fatigue data for Ti-6-4 in 3.5% NaCl at a frequency of 1 Hz, as well as da/dN versus frequency data at a constant ΔK. Closure levels will be measured so that a more detailed closure analysis can be performed. In particular the rise in K_{cl}/K_{max} at low ΔK levels will be examined. Additionally, limited fractography will be performed to characterize potential differences in the fatigue and fracture surfaces for moist air and NaCl. The Master of Science thesis will be written and defended by April, 1995.

References

1. R.P. Wei and J.D. Landes. "Correlation Between Sustained Load and Fatigue Crack Growth in High-Strength Steels," Materials Research and Standards, MTRSA, Vol. 9, No.7, 1969, pp. 25-27,44-46.

2. M.O. Speidel. "Stress Corrosion and Corrosion Fatigue Crack Growth in Aluminum Alloys, " Stress Corrosion Research, Hans Arup and R.N. Parkins, Eds., Sijthoff & Noordhoff International Publishers, the Netherlands, 1979, pp. 117-176.

3. D.M. Harmon, C.R. Saff, and J.G. Burns. "Development of An Elevated Temperature Crack Growth Routine," AIAA Paper 88-2387, American Institute of Aeronautics and Astronautics, 1988.

4. E. Richey, III, A.W. Wilson, J.M. Pope, and R.P. Gangloff. "Computer Modeling the Fatigue Behavior of Metals in Corrosive Environments," NASA Contractor Report 194982, NASA Langley Research Center, Hampton, VA, 1994.

5. G. Haritos, T. Nicholas, and G.O. Painter. "Evaluation of Crack Growth Models for Elevated Temperature Fatigue," Fracture Mechanics: Eighteenth Symposium, D.T. Reed and R.P. Read, Eds., American Society for Testing and Materials, Philadelphia, PA, 1988, pp. 206-220.

6. R.H. Van Stone, O.C. Gooden, and D.D. Krueger. "Advanced Cumulative Damage Modeling," Materials Laboratory, Air Force Aeronautical Laboratories, Wright Patterson Air Force Base, OH, 1988.

7. S.S. Kim and R.P. Gangloff. "NASA-UVa Light Aerospace Alloy and Structures Technology Program," UVa Report No. UVA/528266/MSE94/114, March, 1994, pp. 181-202.

8. "E813-89 Standard Test Method for JIC, A Measure of Fracture Toughness," 1992 Annual Book of ASTM Standards, ASTM, Philadelphia, PA, 1991, pp. 713-727.

9. J.A. Moskovitz and R.M. Pelloux. "Dependence of KISCC On Loading Rate and Crack Orientation in Ti-6Al-6V-2Sn," Corrosion, Vol. 35, 1979, pp. 509-514.

10. D.B. Dawson and R.M. Pelloux. "Corrosion Fatigue Crack Growth of Titanium Alloys in Aqueous Environments," Metallurgical Transactions, Vol. 5, 1974, pp. 723-731.

11. "E647-91 Standard Test Method For Measurement of Fatigue Crack Growth Rates," 1991 Annual Book of ASTM Standards, ASTM, Philadelphia, PA, 1991, pp. 654- 681.

12. P.E. Irving and C.J. Beevers. "The Effect of Air and Vacuum Environments on Fatigue Crack Growth Rates in Ti-6Al-4V," Metallurgical Transactions, Vol. 5, 1974, pp. 391-398.

13. D.A. Meyn. "An Analysis of Frequency and Amplitude Effects on Corrosion Fatigue Crack Propagation in Ti-8Al-1Mo-1V," Metallurgical Transactions, Vol. 2, 1971, pp. 853-865.

14. J.C. Newman, Jr. International Journal of Fracture, Vol. 24, 1984, pp. R131-R135.

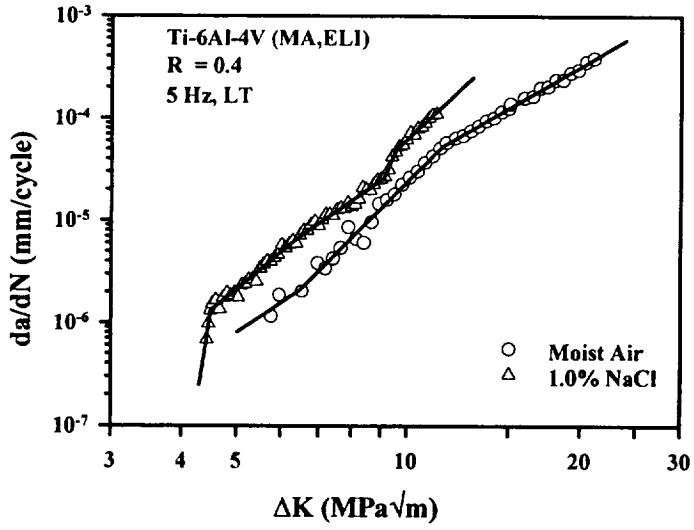

(a)

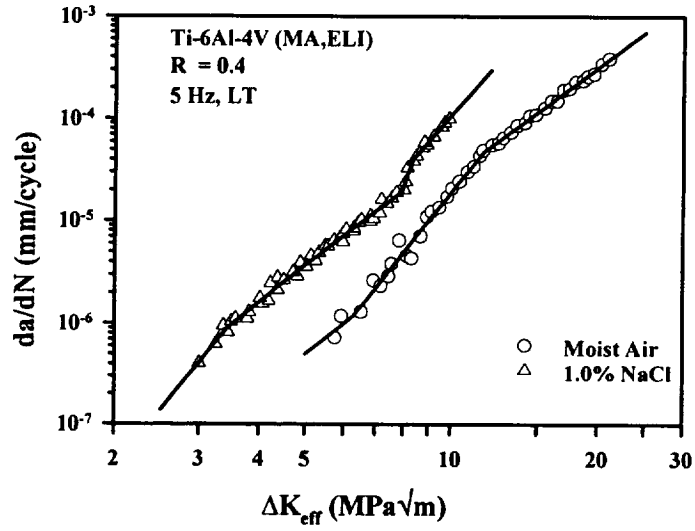

(b)

Figure 1: Sample power law fits for Ti-6Al-4V (MA,ELI) in moist air and a 1.0% NaCl solution for R = 0.1, and f = 5 Hz when plotting a) da/dN versus ΔK and b) da/dN versus ΔK_{eff}. Both the number of transitions and the approximate locations of the transition points were entered into the program.

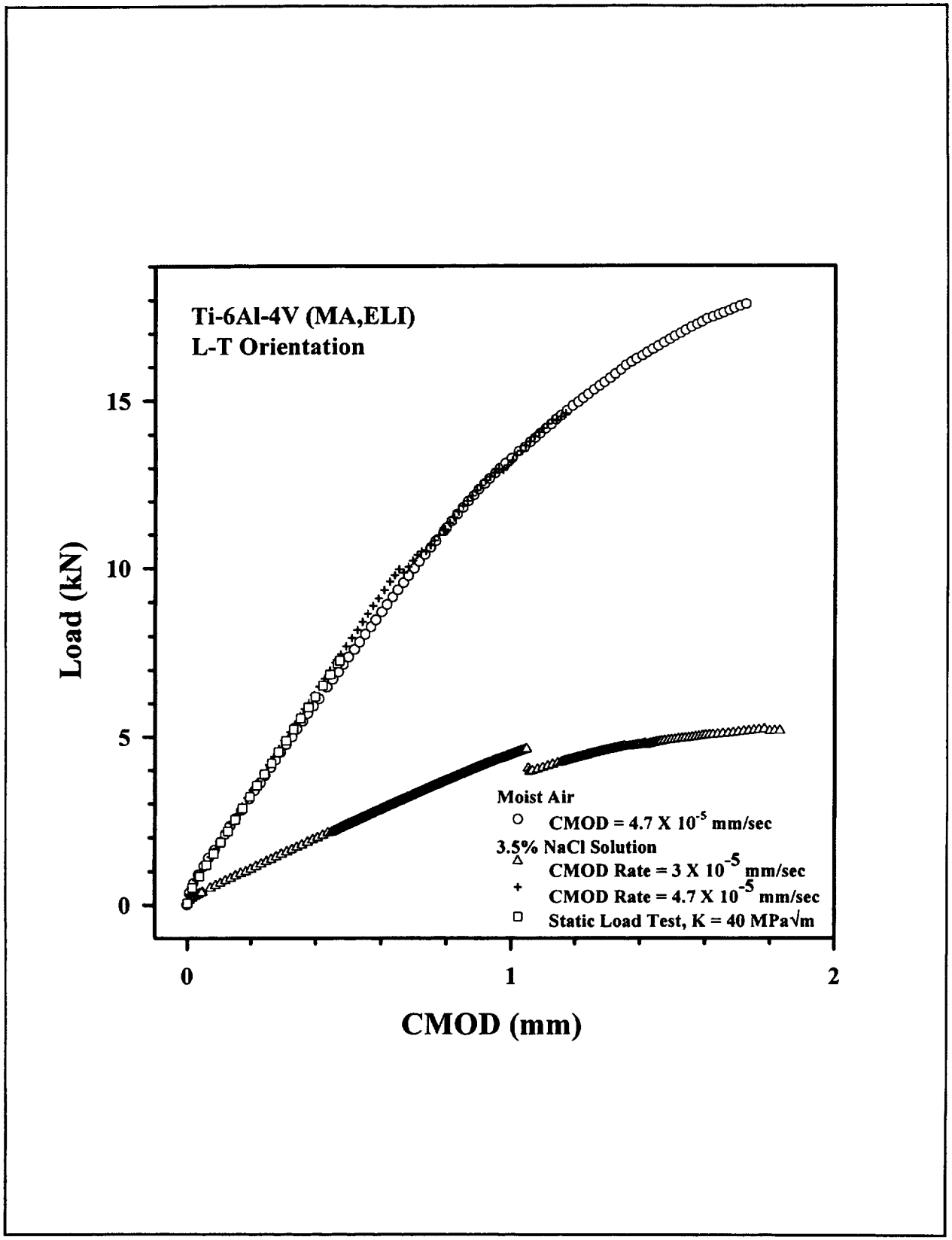

Figure 2: Summary of results for constant CMOD rate experiments with Ti-6Al-4V (MA,ELI) in moist air and 3.5% NaCl, along with results for a static load test conducted in 3.5% NaCl.

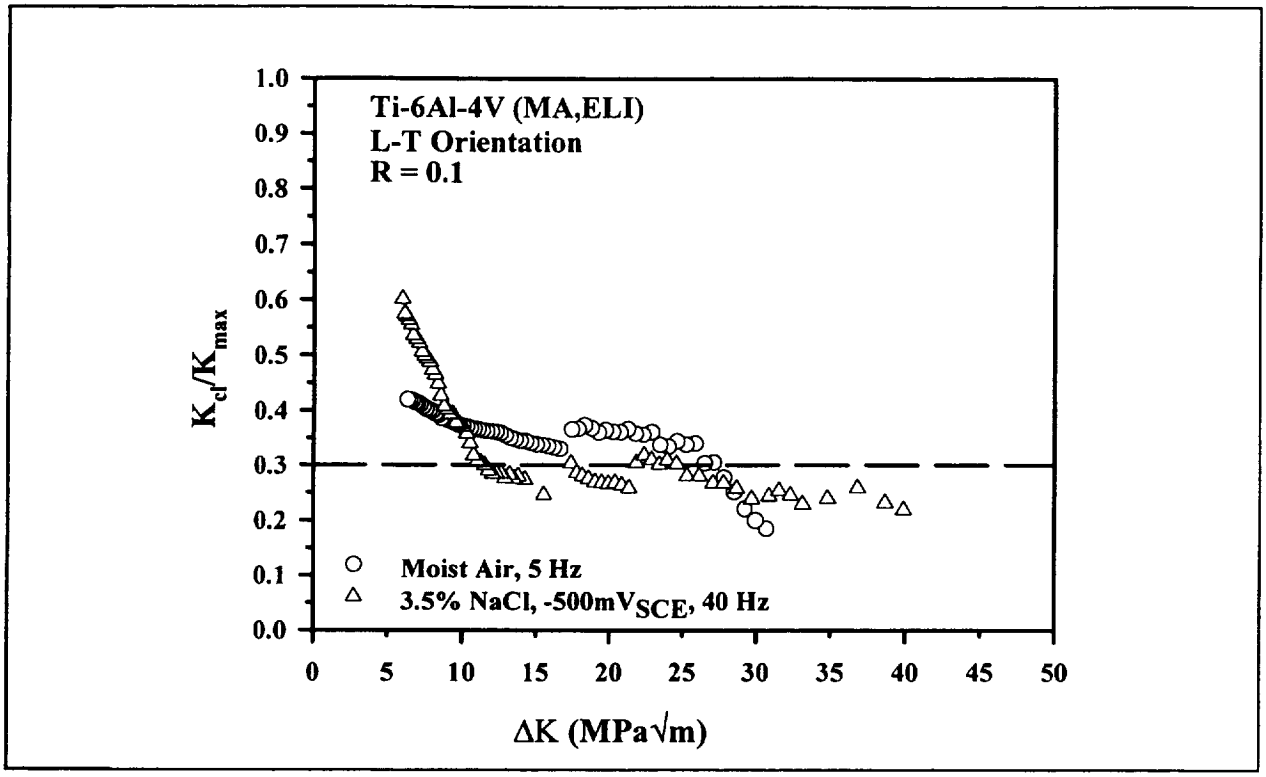

Figure 3: K_{cl}/K_{max} versus ΔK for Ti-6Al-4V (MA,ELI) in moist air and a 3.5% NaCl solution.

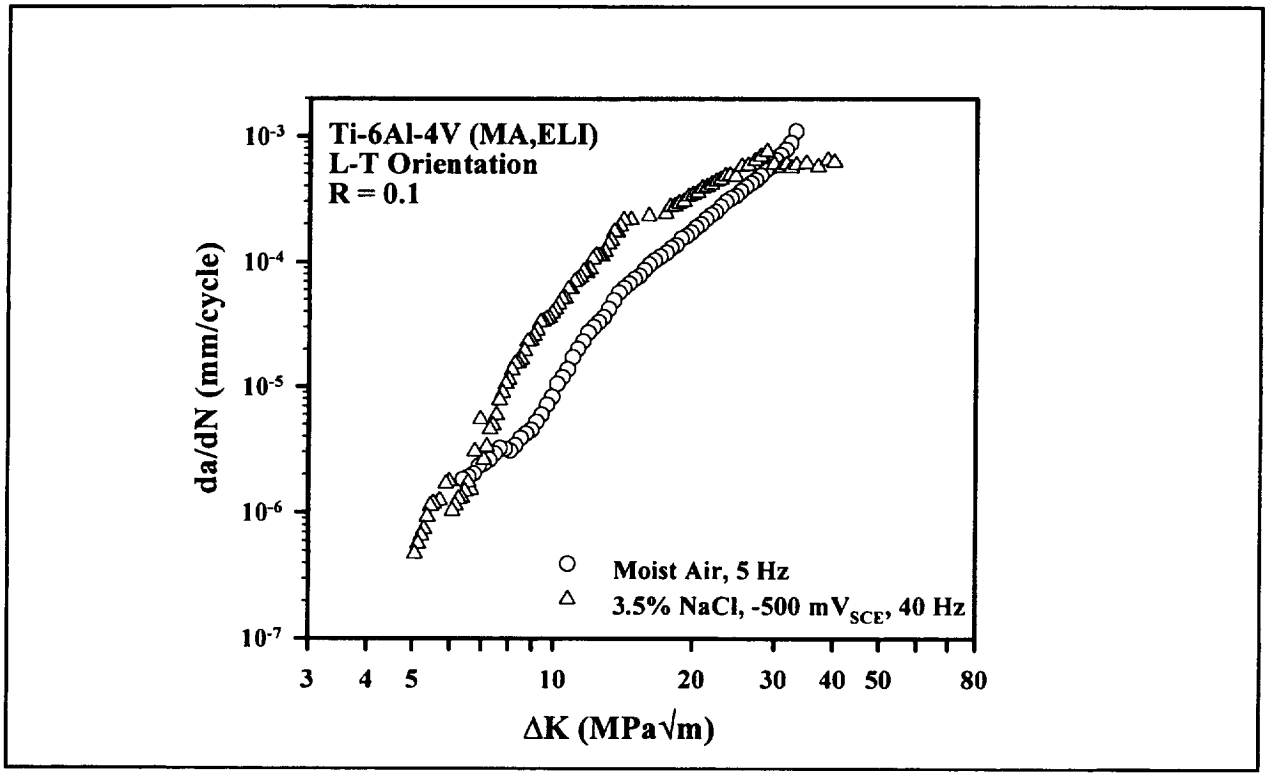

Figure 4: Da/dN versus ΔK for Ti-6Al-4V (MA,ELI) in moist air at 5 Hz and a 3.5% NaCl solution at a fixed electrode potential of -500 mV_{SCE}, and frequency of 40 Hz.

APPENDIX I: GRANT PUBLICATIONS (July 1 to December 31, 1994)

1. F.D. Wall and G.E. Stoner, "Critical Electrochemical Potentials Relating to the Rapid Environmentally Assisted Cracking of Advanced Aluminum Alloys", Proceedings of Aluminum-Lithium Alloys for Aerospace Applications Workshop, NASA George C. Marshall Space Flight Center, Huntsville, Alabama, May 1994, pp.122-131.

2. S.W. Smith and J.R. Scully, "Hydrogen Trapping and Its Correlation to the Hydrogen Embrittlement Susceptibility of Al-Li-Cu-Zr Alloys," In Proceedings of the 1994 TMS Conf. on Hydrogen Effects on Materials Behavior, eds. N. Moody and A.W. Thompson, Jackson, Wyoming (1994).

3. H.J. Koenigsmann and E.A. Starke, Jr., "Microstructural Stability and Fracture Behavior in Al-Si-Ge Alloys", Proceedings of the 4th International Conference on Aluminum Alloys - Their Physical and Mechanical Properties, T.H. Sanders, Jr. and E.A. Starke, Jr., eds., Atlanta, GA, Vol. II, pp. 24-31 (1994).

4. J. M. Duva, J. Aboudi, & C. T. Herakovich, "A Probabilistic Micromechanics Model for Damaged Composites", Damage Mechanics in Composites, D. H. Allen & J. W. Ju, eds., ASME, AMD-Vol. 185, pp. 1-20 (1994).

5. C. J. Lissenden, C. T. Herakovich, & M-J. Pindera, "Response of SiC/Ti Tubes Under Combined Loading - Part I: Theory and Experiment for Imperfect Bonding", J. Composite Materials, in press (1994).

6. C. J. Lissenden, C. T. Herakovich, & M-J. Pindera, "Response of SiC/Ti Tubes Under Combined Loading - Part II: Room Temperature Creep Effects", J. Composite Materials, in press (1994).

7. C. J. Lissenden, B. A. Lerch, & C. T. Herakovich, "Response of SiC/Ti Tubes Under Combined Loading - Part III: Microstructural Evaluation", J. Composite Materials, submitted for publication (1994).

8. C. J. Lissenden and C. T. Herakovich, "Numerical Modelling of Damage Development and Viscoplasticity in Metal Matrix Composites", Computer Methods in Applied Mechanics and Engineering, in press (1994).

9. C. J. Lissenden, C. T. Herakovich, & M-J. Pindera, "Inelastic Deformation of TMC Under Multiaxial Loading" in Life Prediction Methodology for Titanium Matrix Composites, W.S. Johnson, ed, ASTM STP, ASTM, Philadelphia, PA, to be published (1994).

10. C. J. Lissenden, and C. T. Herakovich, "Modelling Interfacial Debonding in Titanium Matrix Composites", Inelasticity and Micromechanics of Metal Matrix Composites, G. Z. Voyiadjis, ed., Proceedings, 12th U. S. National Congress of Applied Mechanics, Seattle, Elsevier Sciences, (1994).

11. C. J. Lissenden, C. T. Herakovich, and M-J. Pindera, "Damage Induced Room Temperature Creep of Titanium Matrix Composites", Durability of Composite Materials, R. C. Wetherhold, ed., ASME MD-Vol. 51, pp. 39-50 (1994),.

12. R. S. Piascik and R. P. Gangloff, "Modeling Environment-Enhanced Fatigue Crack Growth in Al-Li-Cu-Zr," in Hydrogen Effects on Material Behavior, N. R. Moody and A. W. Thompson, eds., TMS-AIME, Warrendale, PA, in press (1994).

13. M. E. Mason and R. P. Gangloff, "Modeling Time-Dependent Corrosion Fatigue Crack Propagation in 7000 Series Aluminum Alloys," in FAA/NASA International Symposium on Advanced Structural Integrity Methods for Airframe Durability and Damage Tolerance, C. E. Harris, ed., NASA Conference Publication 3274, Part 1, NASA-Langley Research Center, Hampton, VA, pp. 441-462 (1994).

14. S. T. Pride, J. R. Scully, and J. L. Hudgon, "Metastable Pitting of Aluminum and Criteria for the Transition to Stable Pit Growth," J. Electrochem. Soc., Vol. 141, No. 11, p. 3028 (1994).

APPENDIX II: GRANT PRESENTATIONS (July 1 to December 31, 1994)

1. F.D. Wall, G.E. Stoner, "Electrochemical Characterization and Occluded Environment Analysis of Localized Corrosion in Advanced Aluminum Alloys", Corrosion/94, Baltimore, MD, NACE, 1994.

2. R. P. Gangloff, R. S. Piascik and D. C. Slavik, "Hydrogen Environment-Enhanced Fatigue in Al-Li-Cu Alloys," 5th International Conference on the Effects of Hydrogen on Material Behavior, Jackson, WY, September, 1994 (Keynote).

3. E. Richey, III and R. P. Gangloff, "Time-Dependent Environmental Fatigue Crack Propagation in 7000 Series Aluminum Alloys," NASA Code Q Grant Review, Johnson Space Center, Houston, TX, November, 1994.

4. S.W. Smith, J.R. Scully, "Hydrogen Trapping and Its Correlation to the Hydrogen Embrittlement Susceptibility of Al-Li-Cu-Zr Alloys," 5th International Conference on the Effects of Hydrogen on Material Behavior, Jackson, WY, September, 1994.

5. S.W. Smith, J.R. Scully, "Hydrogen Trapping and Its Correlation to the Hydrogen Embrittlement Susceptibility of Al-Li-Cu-Zr Alloys," Poster Session, 5th International Conference on the Effects of Hydrogen on Material Behavior, Jackson, WY, September, 1994.

6. J.R. Scully, "Electrochemical, Chaos and Bond Percolation Analysis of Localized Corrosion," Physical Metallurgy Gordon Conf., Plymouth, NH, June, 1994.

7. J. M. Duva, J. Aboudi, and C. T. Herakovich, "A Probabilistic Micromechanics Model for Damaged Composites", Symposium on Damage Mechanics in Composites, ASME Int. Congress & Exposition, Chicago, November, 1994.

8. C. T. Herakovich, "High Temperature Composites", Symposium on Materials Technologies for the 21st Century, ASME Int. Congress & Exposition, Chicago, November, 1994.

9. C. J. Lissenden, C. T. Herakovich, and M-J. Pindera, "Damage Induced Room Temperature Creep of Titanium Matrix Composites", Symposium on Durability of Composite Materials, ASME Int. Congress & Exposition, Chicago, November, 1994.

10. J. D. McGee and C. T. Herakovich, "An Interfacial Damage Model for Fibrous Composites", Society of Engineering Science Annual Technical Meeting, Texas A & M, October, 1994.

11. H. J. Koenigsmann and E.A. Starke, Jr., "Microstructural Stability and Fracture Behavior in Al-Si-Ge Alloys", 4th International Conference on Aluminum Alloys, Atlanta, GA, September, 1994.

APPENDIX III: GRANT PROGRESS REPORTS (January, 1988 to December, 1994)

1. R.P. Gangloff, G.E. Stoner and R.E. Swanson, "Environment Assisted Degradation Mechanisms in Al-Li Alloys", University of Virginia, Report No. UVA/528266/MS88/101, January, 1988.

2. R.P. Gangloff, G.E. Stoner and R.E. Swanson, "Environment Assisted Degradation Mechanisms in Advanced Light Metals", University of Virginia, Report No. UVA/528266/MS88/102, June, 1988.

3. R.P. Gangloff, G.E. Stoner and R.E. Swanson, "Environment Assisted Degradation Mechanisms in Advanced Light Metals", University of Virginia, Report No. UVA/528266/MS89/103, January, 1989.

4. R.P. Gangloff, "NASA-UVa Light Aerospace Alloy and Structures Technology Program", UVa Report No. UVA/528266/MS90/104, August, 1989.

5. R.P. Gangloff, "NASA-UVa Light Aerospace Alloy and Structures Technology Program", UVa Report No. UVA/528266/MS90/105, December, 1989.

6. R.P. Gangloff, "NASA-UVa Light Aerospace Alloy and Structures Technology Program", UVa Report No. UVA/528266/MS90/106, June, 1990.

7. R.P. Gangloff, "NASA-UVa Light Aerospace Alloy and Structures Technology Program", UVa Report No. UVA/528266/MS91/107, January, 1991.

8. R.P. Gangloff, "NASA-UVa Light Aerospace Alloy and Structures Technology Program", UVa Report No. UVA/528266/MS91/108, July, 1991.

9. R.P. Gangloff, "NASA-UVa Light Aerospace Alloy and Structures Technology Program", UVa Report No. UVA/528266/MS92/109, January, 1992.

10. R.P. Gangloff, "NASA-UVa Light Aerospace Alloy and Structures Technology Program", UVa Report No. UVA/528266/MS93/111, July, 1992.

11. R.P. Gangloff, "NASA-UVa Light Aerospace Alloy and Structures Technology Program", UVa Report No. UVA/528266/MSE93/112, March, 1993.

12. R.P. Gangloff, "NASA-UVa Light Aerospace Alloy and Structures Technology Program", UVa Report No. UVA/528266/MSE93/113, July, 1993.

13. R.P. Gangloff, "NASA-UVa Light Aerospace Alloy and Structures Technology Program", UVa Report No. UVA/528266/MSE93/114, March, 1994.

14. R.P. Gangloff, "NASA-UVa Light Aerospace Alloy and Structures Technology Program", UVa Report No. UVA/528266/MSE94/116, July, 1994.

DISTRIBUTION LIST

1-4 Mr. D. L. Dicus
Contract Monitor
Metallic Materials Branch, MS 188A
NASA Langley Research Center
Hampton, VA 23681-0001

5-6* NASA Scientific and Technical Information Facility
P. O. Box 8757
Baltimore/Washington International Airport
Baltimore, MD 21240

7 Mr. Neil Price
Grants Officer, M/S 126
NASA Langley Research Center
Hampton, VA 23681-0001

8 Dr. Darrel R. Tenney
Materials Division
NASA Langley Research Center
Hampton, VA 23681-0001

9 Dr. Charles E. Harris
Mechanics of Materials Branch
NASA Langley Research Center
Hampton, VA 23681-0001

10 Mr. W. Barry Lisagor
Metallic Materials Branch
NASA Langley Research Center
Hampton, VA 23681-0001

11 Mr. T.W. Crooker
Code RM
NASA Headquarters
Washington, DC 20546

12 Dr. Robert S. Piascik
Mechanics of Materials Branch
NASA Langley Research Center
Hampton, VA 23681-0001

13 Mr. W. Brewer
Metallic Materials Branch, MS 188A
NASA Langley Research Center
Hampton, VA 23681-0001

14 Mr. Thomas T. Bales
Metallic Materials Branch, MS 188A
NASA Langley Research Center
Hampton, VA 23681-0001

15 Mr. John Wagner/Ms. Cynthia Lach
Metallic Materials Branch, MS 188A
NASA Langley Research Center
Hampton, VA 23681-0001

16 Dr. William F. Bates
Lockheed Aeronautical Systems Co.
86 South Cobb Drive
Marietta, GA 30063-0648

17 Dr. Alex Cho
Reynolds Metals Co.
4th and Canal Street
Richmond, VA 23261

18 Mr. E.A. Colvin
Alcoa Technical Center
Route 780, 7th Street Road
Alcoa Center, PA 15069

19 Dr. L.M. Karabin
Alcoa Technical Center
Route 780, 7th Street Road
Alcoa Center, PA 15069

20 Dr. Ravi Kahandal
McDonnell Douglas Aerospace
Mail Stop 36-90
3855 Lakewood Blvd.
Long Beach, CA 90846

21 Mr. Fred Casey
Space Transportation Systems Division
Rockwell International
Dept. 289 MC/AC56
12214 Lakewood Blvd.
Downey, CA 90241

22-23 E.A. Starke, Jr.; MS&E

24-25 R.P. Gangloff; MS&E

26 G. J. Shiflet; MS&E

27 G.E. Stoner; MS&E

28 J.A. Wert; MS&E

29 J.R. Scully; MS&E

30 C.T. Herakovich; CE and AM

31-32 S.S. Kerbel; Clark Hall

33 SEAS Preaward Administration Files

34 Mr. Gwyn Faile
Code ED 24
Marshall Space Flight Center
Huntsville, AL 35812

35 Mr. Brian McPherson
Code ED 24
Marshall Space Flight Center
Huntsville, AL 35812

36 Dr. William E. Quist
Boeing Aerospace and Electronics
Aerospace Group
Mail Stop GH-CJ
P.O. Box 3707
Seattle, WA 98124

37 Dr. Howard G. Nelson
NASA-Ames Research Center
EEM: 213-3
Moffett Field, CA 94035

38 Dr. R.G. Forman
Mail Code ES-5
NASA-L.B. Johnson Space Flight Center
Houston, TX 77058

39 Professor A.K. Noor
Center for Computational Structures Technology
NASA Langley Research Center
Hampton, VA 23681-0001

40 Prof. A.K. Ghosh
Department of Materials Science and Engineering
University of Michigan
2102 Dow Building
Ann Arbor, MI 48109-2136

41 Dr. D. Ferton
Pechiney Centre de Recherches
De Voreppe
B.P. 27 -- 38340 Voreppe
FRANCE

42 Dr. John Papazian
Grumman Aerospace & Electronics
Mail Stop A02-026
Bethpage, NY 11714-3582

43 Dr. Richard Lederich
McDonnell Douglas Aircraft Company
Mail Stop 111-1041
P.O. Box 516
St. Louis, MO 36166

44 Dr. Alan Hopkins
Senior Research Metallurgist
Research Institute
The University of Dayton
300 College Park
Dayton, OH 45469-0172

45 Dr. Frances Hurwitz
Ceramic Composites
NASA Lewis Research Center
21000 Brookpark Road
Cleveland, OH 44135

46 Dr. Malcolm Ozelton
Manager, Metallic & Ceramic Materials
B-2 Division
Northrop Corporation
8900 E. Washington Blvd.
T241/GK
Pico Rivera, CA 90660-3737

47 Dr. S. Sampath
Technical Center
Federal Aviation Administration
Atlantic City International Airport,
NJ 08405

48 Dr. James Staley
Alcoa Laboratories
Alcoa Center, PA 15069

49 Dr. Jeffrey Waldman
Code 6063
Naval Air Development Center
Warminster, PA 18974

*One reproducible copy Updated: March, 1995